A study of liquid crystals containing an atropisomeric 3,3'-dinitrobiphenyl core

by

Mark Moran

A thesis submitted to the Department of Chemistry
in conformity with the requirements
for the degree Master of Science

Queen's University
Kingston, Ontario, Canada
February, 2007

Your file Votre référence
ISBN: 978-0-494-26512-3
Our file Notre référence
ISBN: 978-0-494-26512-3

Abstract

Ferroelectric liquid crystals (FLCs) are attractive alternatives to nematic liquid crystals in display applications due to their lower energy requirements and fast switching times. Commercial FLCs are normally formed by mixtures of an achiral LC host and a chiral dopant, which induces a macroscopic polarization (P_s). Research in the Lemieux group has focused on the design of dopants with atropisomeric 3,3'-dinitrobiphenyl cores which exhibit large polarization powers in LC hosts with phenylpyrimidine cores such as **PhP1**. These dopants, however, cause a significant destabilization of the SmC phase at mole fractions greater than $\chi_d = 0.05$. This narrowing of the SmC phase has led to the development of liquid crystalline versions of these dopants, which should be more compatible with **PhP1**.

The first part of this thesis describes the structural modification of the carbon backbone of the side-chains of 4,4'[(4-alkyloxybenzoyl)oxy]-2,2',5,5'tetramethyl-3,3'-dinitrobiphenyls (**1.15**) with the goal of inducing liquid crystalline behaviour. Polycatenar derivatives (**2.6a-e**) were explored, but these compounds were found to be non-mesogenic and immiscible with **PhP1**. The replacement of one 4-alkyloxybenzoate group with the bulkier 4-pentylbicyclo[2.2.2.]octane-1-carboxylate group produced compounds with nematic mesophases (**2.8a-e**). These mesogens all show selective reflection properties and the helical pitch increases with increasing temperature. Compound **2.8d** has a lower polarization power than **1.15d** in **PhP1** and is consistent with a shift in the rotational distribution of the transverse dipole towards the tilt plane and reduced chirality transfer via core-core interactions.

The second part describes the use of oligomeric siloxanes (**3.2-3.4**) and semi-perfluorinated alkyl side-chains (**3.5**, **3.6** and **3.8**), to promote smectic phases in compounds containing the atropisomeric 3,3'-dinitrobiphenyl core via microphase segregation. Derivatives with one side-chain terminated with an oligomeric siloxane were employed as dopants but are immiscible with a siloxane-terminated analog of **PhP1**, **3.9**. Semi-perfluorinated alkyl chains were found to induce mesogenic behaviour and SmA* phases were observed for **3.8** and **3.9** while **3.11** forms N*, TGBA* and SmA* phases. Compound **3.11** shows selective reflection properties and the helical pitch decreases with increasing temperature. The δ_p of **3.8** and **3.11** is less than **1.15** and is consistent with a reduction in chirality transfer via core-core interactions.

Acknowledgements

I would like to thank Bob Lemieux for his support, patience, and guidance.

I would like to thank the talented group of chemists with whom I have worked over the past few years: Carl-Johan Carling, Qian "Rebecca" Cui, Jeremy Finden, Scott Hartley, Christa Huntley, Naohiko Ikuma, Li Li, Marcus Ohlin, Jeffery Roberts, Matthew Thompson, Eagranie "Eggy" Yuh, and Peng Zhang. These individuals, as well as summer and 4th year students, have made my time in the Lemieux group enjoyable and their insights have been appreciated. I would also like to thank the "adopted" members of the Lemieux lab Terry Koerner and Pedro Montoya for their scientific insight.

I would also like to thank the people who keep the department running smoothly. Françoise Sauriol in the NMR facility, Bernd Keller and Jie Sui in the mass spec lab, Ed Maracle and Robin Roberts in the electronics shop, Pam Brandy-Defoe and Susan Thompson-Lafosse in stores and Lindsay Hull and Tom Hunter for keeping instruments working. I would also like to thank Igor Kozin and Jason Vlahakis for help with the variable temperature UV-Vis spectroscopy and Gary Contant in the physics machine shop.

Finally, special thanks to my family, and in particular my parents Gordon and Margreat Ann, for all their love and support over the years.

Statement of originality

The experimental research presented in this thesis was conducted by the author under the supervision of Dr. R.P. Lemieux in the Department of Chemistry, Queen's University, unless otherwise noted.

Original work presented in this thesis includes: synthesis and physical characterization of chiral liquid crystals (*R*,*R*)-**3.4** and (*R*)-**3.5**; the synthesis and physical characterization of chiral dopants (*S*)-**3.2** and (*R*)-**3.3**; the measurement of their induced ferroelectric properties in the liquid crystal host **3.9**; the synthesis and physical characterization of chiral dopants (*R*)-**2.14a,** (*S*)-**2.14b**, (*R*)-**3.6** and (*S*)-**3.8**; the measurement of their induced ferroelectric properties in the liquid crystal host **PhP1**; the measurement of the helical pitch of (S)-3.8 in the nematic phase; The synthesis and physical characterization of chiral liquid crystals (*R*)-**2.16a-e**; the measurement of their helical pitch in the nematic phase; the induced ferroelectric properties of (*R*)-**2.16d** in liquid crystalline hosts **PhP1**, **DFT**, **NCB76**, and **PhB**; measurement of the induced electroclinic properties of (*R*)-**2.16d** in **PhP1**.

Table of contents

List of Tables

List of Figures

Abbreviations

α	Tilt susceptibility coefficient
ΔH	Heat of formation
δ	Chemical shift
δ_P	Polarization power
δ_{probe}	Polarization power of probe dopant
λ	Wavelength
λ_{max}	Wavelength of maximum absorption
θ	Tilt angle
$\mu_\perp$	Transverse dipole moment
χ_d	Mole fraction of dopant
AC	Alternating current
AM1	Austin model 1 semi-emperical method
aq.	Aqueous
B3LYP	Becke's three parameter hybrid functional using the Lee, Yang and Parr correlation function (density functional theory method)
Bu	Butyl
C	Electroclinic coupling constant
calc'd	Calculated
Col_h	Hexagonal Columnar liquid crystal phase
Col_r	Rectangular Columnar liquid crystal phase

Cr	Crystal
CTF	Chirality transfer feedback
DC	Direct current
DCC	1,3-Dicyclohexylcarbodiimide
DFT	2',3'-Difluoro-4"-heptyl-4-nonyl-[1,1';4',1"]terphenyl
DMAP	*N*,*N*-Dimethylaminopyridine
DMF	*N*,*N*-Dimethylformamide
e.e.	enantiomeric excess
e_c	electro clinic coefficient
E	Electric Field
EI	Electron impact ionization
ESI	Electrospray ionization
Et	Ethyl
Et_3N	Triethylamine
EtOAc	Ethyl acetate
EtOH	Ethanol
FLC	Ferroelectric liquid crystal
g	Glass
HPLC	High-pressure liquid chromatography
HRMS	High-resolution mass spectrometry
I	Isotropic
IPA	Isopropanol
ITO	Indium-tin oxide

LDI	Laser desorption ionization
MDW950	5-(2*S*,3*S*-difluorooctyloxy)-2-(4-octyloxyphenyl)pyridine
MHPOBC	4-[(1-methylheptyloxycarbonyl]phenyl 4'octyloxybiphenyl-4'-carboxylate
m.p.	Melting point
Me	Methyl
MS	Mass spectrometry
N	Nematic liquid crystal phase
N*	Chiral nematic liquid crystal phase (cholesteric phase)
n	Director
n	Side-chain length
NCB76	4-(4'-heptyl[1,1'-biphenyl]-4-yl)-1-hexylcyclohexanecarbonitrile
NMR	Nuclear magnetic resonance
p	Pitch
P_o	Reduced polarization
P_s	Spontaneous polarization
PhB	4-[(±)-(4-methylhexyl)oxy]phenyl 4-decyloxybenzoate
PhP1	2-(4-butyloxyphenyl)-5-(octyloxy)pyrimidine
PTFE	Polytetrafluoroethylene
SmA	Smectic A liquid crystal phase
SmA*	Chiral smectic A liquid crystal phase
SmB	Smectic B liquid crystal phase

SmC	Smectic C liquid crystal phase
SmC*	Chiral smectic C liquid crystal phase
SmC_A*	Anticlinic smectic C liquid crystal phase
SSFLC	Surface–stabilized ferroelectric liquid crystal
T	Temperature
T_C	Curie point
TGBA*	Twist grain boundary phase
THF	Tetrahydrofuran
TSiKN65	4-[3'-nitro-4'-((*R*)-1-methylhexyloxy)phenyl] phenyl 4-(6-heptylmethyltrisiloxyhexyloxy) benzoate
UV-Vis	Ultraviolet-visible
V_t	Threshold voltage to switching via Goldtone mode
z	Layer normal

Chapter 1. Introduction

Liquid Crystals (LCs) are intermediate between the well-ordered crystalline state and the highly disordered isotropic liquid state. Current research in Ferroelectric Liquid Crystals (FLCs) is focused on the synthesis of molecules that induce high polarization powers (*vide infra*) while maintaining a low viscosity. Most flat panel LC displays are based on twisted nematic mesogens and have refresh rates on the order of milliseconds. FLC displays are comprised of a small amount of chiral dopant in an achiral LC host that has desirable properties such as low viscosity and a broad temperature range. FLC displays also have faster response times, on the order of microseconds, and lower energy requirements than their twisted nematic predecessors. The research described herein focuses on modifying a class of non-mesogenic dopants previously synthesized in the Lemieux group to promote liquid crystalline properties and increase the miscibility in common liquid crystalline hosts.

1.1. Classification of liquid crystals

Lyotropic liquid crystals, normally formed by amphiphilic molecules such as detergents, require a solvent to display mesogenic behaviour and will not be discussed further in this dissertation. Thermotropic liquid crystals change their morphology, in the absence of solvent, as a function of temperature. There are four general types of thermotropic mesogens, which are classified by their shape and are depicted in Figure 1-1. Calamitic mesogens are rod-shaped, formed by a rigid (normally aromatic) core and flexible alkyl side-chain(s) at the periphery (**1.1**). Discotic mesogens are, as the name

suggests, disc-shaped with a flat polyaromatic core and multiple alkyl side chains (**1.2**). Polycatenar mesogens are a hybrid of calamitics and discotics, normally formed by a narrow rigid core and multiple alkyl side chains (**1.3**). Last are the bent-core, or banana-shaped, mesogens which have recently received a great deal of attention due to their unique chiral layered structure (**1.4**).[1]

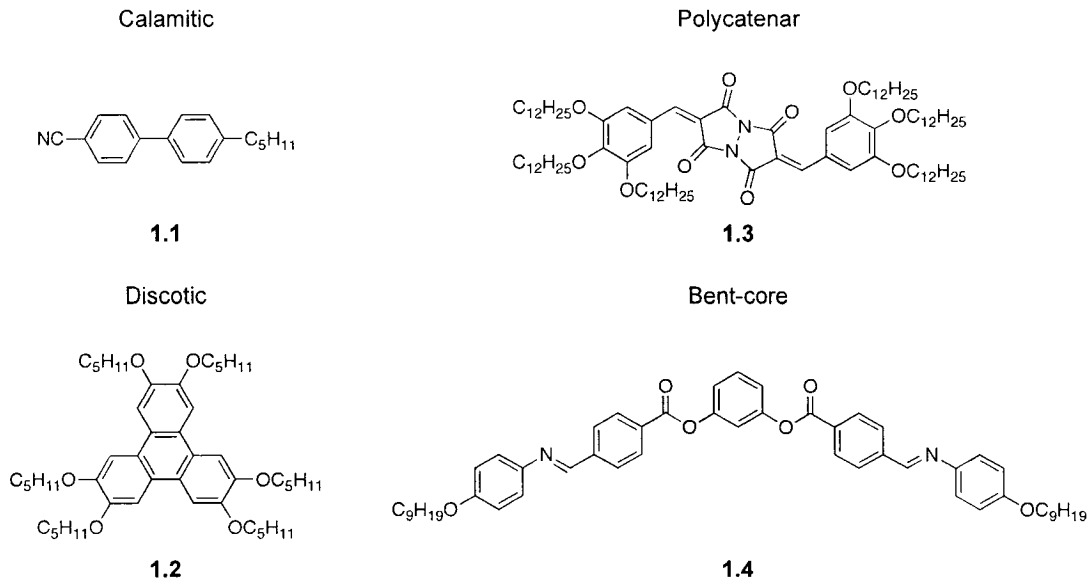

Figure 1-1. Examples of calamitic, discotic, polycatenar and bent-core liquid crystals.

1.2. Conventional phases of calamitic liquid crystals

The liquid crystal phases formed by calamitic mesogens are divided into two major subclasses. The first is the nematic phase (N) in which molecules exhibit only orientational order. The second class is the smectic phase in which molecules exhibit orientational order and are arranged in diffuse layers. There are several smectic phases, but only the smectic A (SmA) and the smectic C (SmC) will be discussed further.

1.2.1. The nematic phase

The nematic phase is characterized by molecular long axes aligned along a director **n** with no additional ordering, as shown in Figure 1-2. Molecules that tend to form nematic phases are characterized by large polarizability anisotropy and low lateral bulk. Factors that favour nematic phases over smectic phases are lateral substituents, dissymmetry, short alkyl chains and lack of polar groups, which tend to promote aggregation.

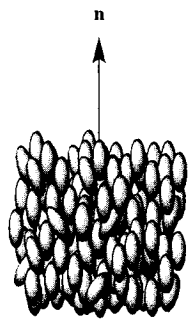

Figure 1-2. Schematic of the structure of the nematic mesophase.

1.2.2. The smectic A phase

The SmA phase can be described as a nematic phase which self-assembles into a layered structure, as shown in Figure 1-3. It is characterized by a diffuse layer structure in which the molecules are aligned along a director **n** that is parallel to the layer normal **z**. These molecules can rotate freely about their long axes. Molecules that have reduced lateral bulk, long alkyl side chains and substituents that promote micro-segregation, a concept which will be described later in this chapter, tend to form smectic phases.

1.2.3. The smectic C phase

The SmC phase, like the SmA phase, is characterized by a diffuse layer structure. The molecules align along a director **n**, which is tilted with respect to the layer normal **z,** as shown in Figure 1-3. The tilt angle θ between **n** and **z** is temperature dependant, and increases with decreasing temperature.

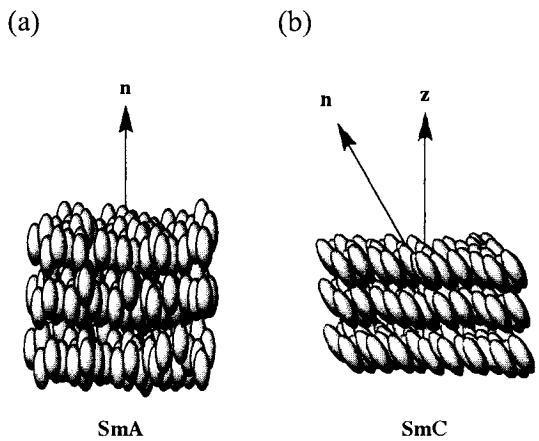

Figure 1-3. Schematic of the layered structures of (a) the smectic A and (b) the smectic C mesophases.

1.2.3.1. Molecular origins of tilt

As molecules cool from the SmA to the SmC phase, the degree of rotational freedom about **n** decreases, and lateral forces begin to play a more significant role in the order of the mesophase. Several models have been developed to describe the molecular tilt in the SmC phase. The McMillan model is based in part upon the observations that compound **1.5** forms a SmC phase while **1.6** does not, despite being isosteric and of similar length.[2] MacMillan proposed that, in order for molecules to form a SmC phase,

there must be polar functional groups such as ethers or esters linking the core to the side-chains.[3] As the rotational order increases, the coupling of these 'outboard dipoles' creates an induced torque that causes the tilt, as shown in Figure 1-4. The McMillan model also accounts for the temperature dependence of the tilt angle. This model, however, is not general, as there are known examples of molecules with outboard dipoles that do not form a SmC phase.

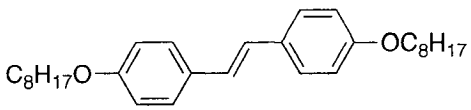

1.5: Cr (95 SmC) 112 I

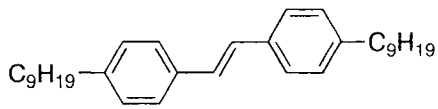

1.6: Cr 37 SmB 40 SmA 52

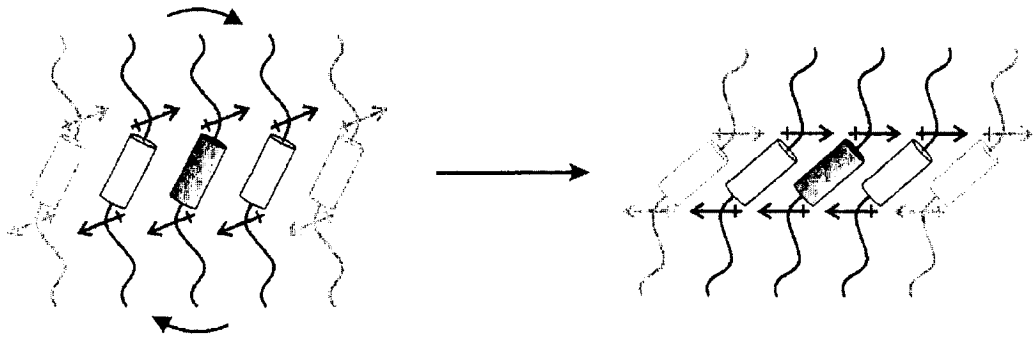

Figure 1-4. Illustration of the MacMillan model where coupled outboard dipoles create a torque that leads to the tilted structure of the SmC phase.

Wulf proposed that SmC formation is due to steric interactions and packing forces rather than the coupling of outboard dipoles.[4] He proposed that, in the SmA phase, molecules have rotational freedom about the long axis **n**, and have an overall cylindrical shape. Upon cooling, rotational freedom is lost, leading to an overall zigzag shape in the lowest energy conformation. The most efficient means of packing involves tilting the molecular long axes, as shown in Figure 1-5.

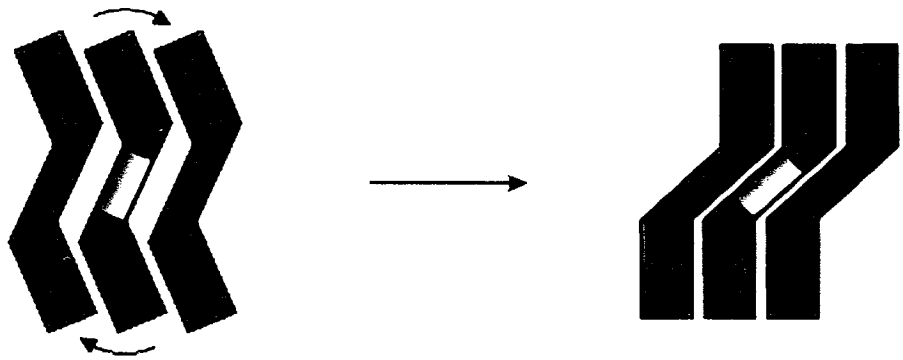

Figure 1-5. Schematic of the Wolf model where the zigzags pack closer when the core is more tilted than the side chains.

1.2.3.2. Chirality in the SmC phase

In 1976, Meyer predicted that a chiral SmC (SmC*) material should be ferroelectric and possess a spontaneous polarization (P_s).[5] This prediction was based upon a symmetry argument that introduction of chirality at the molecular level breaks reflection symmetry, reducing the symmetry of the phase from C_{2h} to C_2, which is inherently polar, as shown in Figure 1-6. Although polar order is intrinsic to each SmC* layer the SmC* a bulk SmC* material has a helical structure which is non-polar due to averaging of dipoles over a full helical pitch (helielectric), as shown in Figure 1-7.

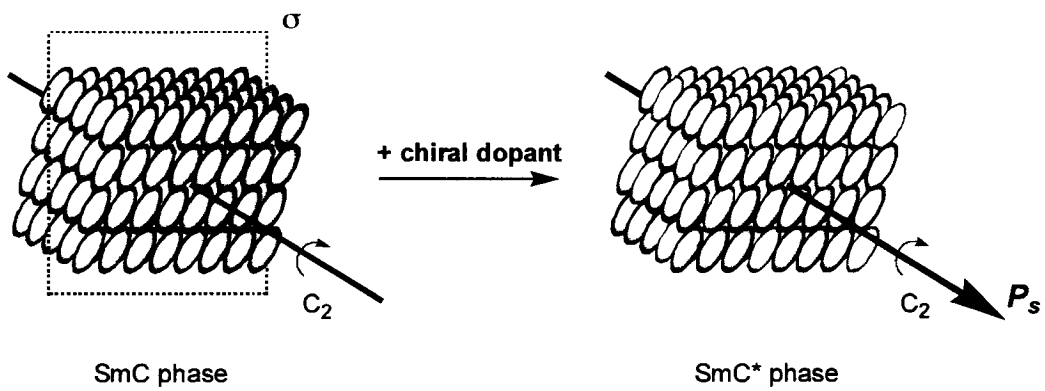

Figure 1-6. Symmetry elements of the SmC and SmC* phases.

The helical structure of the SmC* phase can be unwound when boundary conditions are imposed as shown by Clark and Lagerwall. The boundaries were rubbed polyimide conducting glass slides, which caused the helix to unwind and produce a surface-stabilized ferroelectric liquid crystal (SSFLC) with a net spontaneous polarization, P_s, as shown in Figure 1-7.[6] By application of an electric field across the SSFLC film the tilt orientation can be switched from $+\theta$ to $-\theta$ via precession of **n** about **z** by the coupling of P_s with the field, as shown in Figure 1-8. This is known as the Goldstone mode, which is a "hard" mode and no switching will occur until the applied field reaches the threshold voltage (V_t).

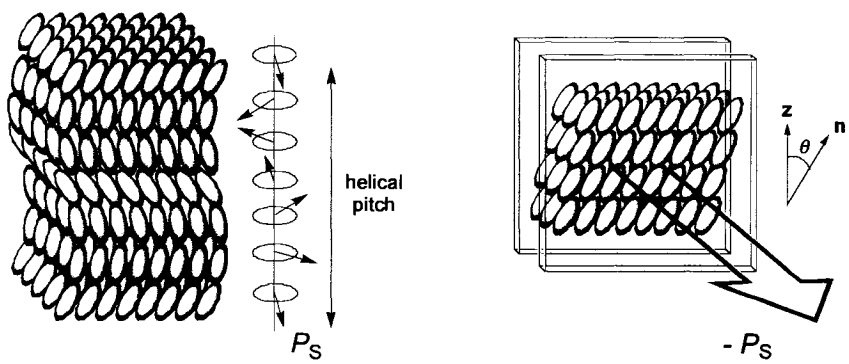

Figure 1-7. Unwinding of helical structure of the SmC* phase via boundary conditions. The sign of the spontaneous polarization is determined by the sign of (**z** × **n**), and in this case is negative according to the physics convention.

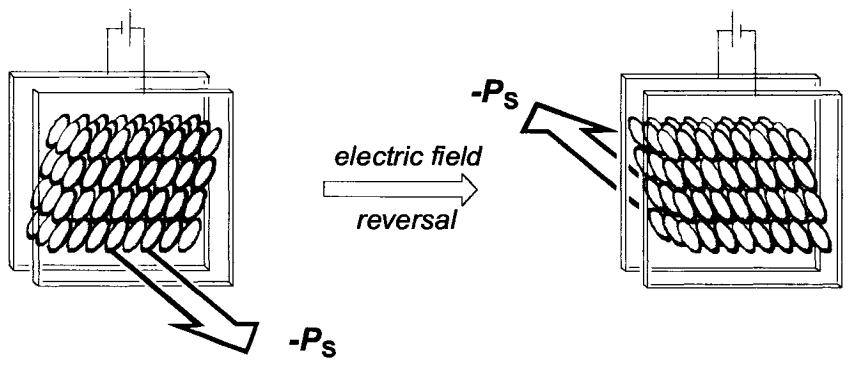

Figure 1-8. Switching between two degenerate SSFLC states by application of an electric field.

By virtue of the birefringence of the SSFLC, the switching between degenerate tilted states can be thought of as a molecular light shutter when the SSFLC film is positioned between crossed polarizers and **n** is oriented along one polarizer in one of the tilted states. Application of a field of one sign can lead to an "ON" state while application of the opposite field can lead to the "OFF" state.

Kuczyński and Stegemeyer demonstrated that a SmC* phase could be induced by the addition of a small amount of chiral material into an achiral SmC liquid crystal host.[7] This was an important finding since predicting empirically whether a molecule will form a SmC phase is often difficult. Neat SmC* materials are often very viscous and have high V_t to switching, which make them less desirable for device applications. The ability of a dopant to induce a spontaneous polarization in an achiral SmC host is expressed as the polarization power (eq. 1-1), where χ_d is the mole fraction of the dopant, P_o is the reduced polarization (eq. 1-2), which is a normalized form of P_s that accounts for variation in tilt angle from one host to the next.[7,8]

$$\delta_p = \frac{dP_o(\chi_d)}{d\chi_d} \qquad \text{(eq. 1-1)}$$

$$P_o = \frac{P_s}{\sin\theta} \qquad \text{(eq. 1-2)}$$

1.2.3.3. Type I and Type II Dopants

Stegemeyer made a distinction between chiral dopants based upon the location of the stereogenic center(s).[9] A Type I dopant, such as **MHPOBC**, has a stereogenic center located in one of the alkyl tails; such a dopant normally does not demonstrate a host dependence in terms of the value of δ_p.[9] However, a Type II dopant, such as **1.7** has the stereogenic center located in the core of the dopant; the polarization power of such a dopants normally shows a host dependence. Type II behaviour is attributed to steric interactions between host and dopant affecting the rotational distribution of the transverse dipole, $\mu_\perp$, with respect to the polar axis, as shown in Figure 1-9. Hence dopants with large polar ordering may induce a small polarization in one host, if $\mu_\perp$ is aligned near the tilt plane and large in another host if $\mu_\perp$ is oriented near the polar axis. This model treats the dopant as a "passive" guest, which adopts the conformation and rotational distribution that best fits in the binding site of host. Stegemeyer also proposed that the chirality of the dopant can be transferred to the host and cause polar ordering of the host.[9] This would align the transverse dipole of the host with that of the dopant and increase the polarization, which scales with the dipole of the host.[9] In this case the dopant is considered an "active" guest.

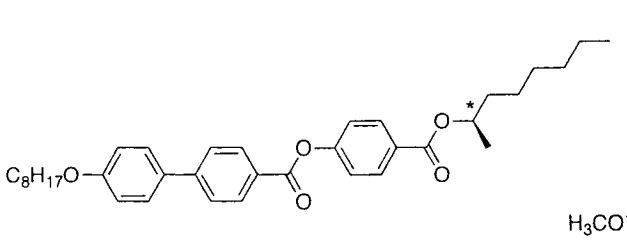

MHPOBC

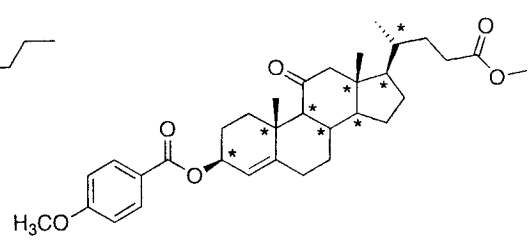

1.7

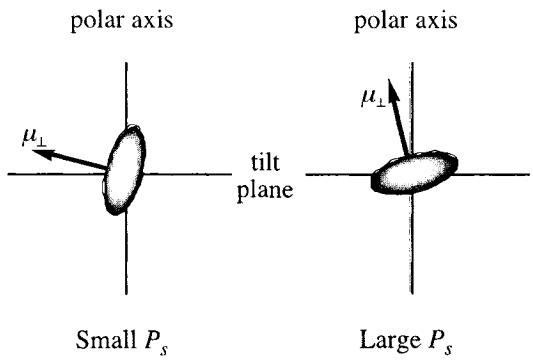

Figure 1-9. Representation of the rotational distribution of a Type II dopant and its transverse dipole ($\mu_\perp$) as viewed down the molecular long axes.

1.2.3.4. Molecular origins of P_s: The Boulder Model

A model for predicting the sign of polarization for a given SmC* mesogen was proposed by Walba and co-workers.[10,11] The Boulder model assumes that all molecules in the SmC phase assume the same time-averaged conformation and orientation. It is assumed that the molecules are in a zigzag shape with the side-chains fully extended in *anti* conformations. Deuterium NMR studies have shown that there is a preference for the 'all-*anti* conformation', particularly near the core, in liquid crystal phases.[12,13] X-ray diffraction experiments have also shown that the alkyl chains behave as if they were rigid and fully extended.[14]

In 1978, Durand and co-workers compared tilt angles measured by polarized optical microscopy (θ_{opt}) with those calculated by x-ray diffraction ($\theta_{x\text{-}ray}$).[15] The latter are derived by simple geometry and defines the molecular long axis as the vector connecting the two termini of the alkyl chains. The optical tilt depends on the

polarization anisotropy of the molecule and corresponds approximately to the tilt of the long axis of the aromatic core. There is normally a discrepancy between $\theta_{x\text{-ray}}$ and θ_{opt}, with $\theta_{opt} > \theta_{x\text{-ray}}$ which implies that the core is more tilted than the side-chains, as shown in Figure 1-10.

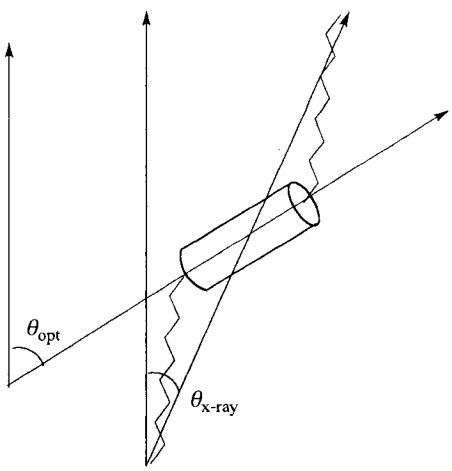

Figure 1-10. Schematic of the observed optical (θ_{opt}) and x-ray ($\theta_{x\text{-ray}}$) tilt angles showing that the core of SmC mesogens is more tilted than the side-chains.

The order imposed by the SmC phase is modeled by a mean field potential that has a bent cylindrical shape, as shown in Figure 1-11. This model can also be used for mixtures of achiral SmC hosts with chiral dopants. In the latter case, the host acts as a binding site with a bent cylinder shape, which constrains the dopant by analogy to host-guest chemistry. Once in the binding site, one dopant conformer should be preferred and the sign of P_s can be predicted by conformational analysis.

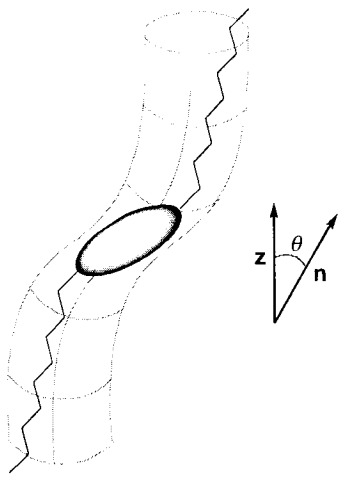

Figure 1-11. Representation of the binding site of SmC mesogens as described by the Boulder model.

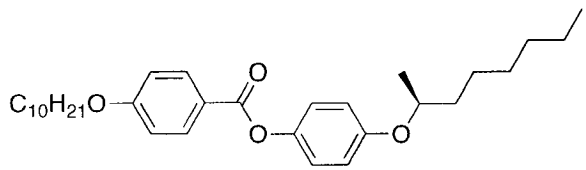

1.8

For example, to analyze the phenyl benzoate **1.8** according to the Boulder model, we assume that the molecule is positioned in the bent cylinder geometry with alky chains in the "all-*anti*" conformation, and identify the lowest energy conformation of the stereogenic center with respect to the core. While there are several polar functional groups in this molecule, a distinction must be made between those that are far from the stereogenic center (which will not contribute to P_s) and those which are sterically coupled to the stereogenic center (which contribute to P_s). In the case of **1.8**, both the decyloxy group and benzoate groups are remote from the 2-octyloxy group and should not contribute to P_s. The conformational analysis for rotation about the C2-C3 bond of the 2-octyloxy group reveals that the alkoxy group is coplanar with the phenyl ring and the

conformational distribution between two staggered conformations (a) and (b) dictate the sign of polarization. There is a third staggered conformation with the alkoxy dipole in the tilt plane, which does not contribute to P_s and is excluded from the conformational analysis. Conformation (a) (Figure 1-12) has the methyl group *anti* to the rest of the alkyl chain and corresponds to a negative sign of polarization ($-P_s$). Conformation (b), which corresponds to a positive sign of polarization ($+P_s$), has the methyl group *gauche* to the alkyl tail and is disfavoured compared to the *anti* conformation. The prediction is that this molecule, under the geometrical restrictions imposed by the binding site, will have $-P_s$, which is what is observed experimentally.[16]

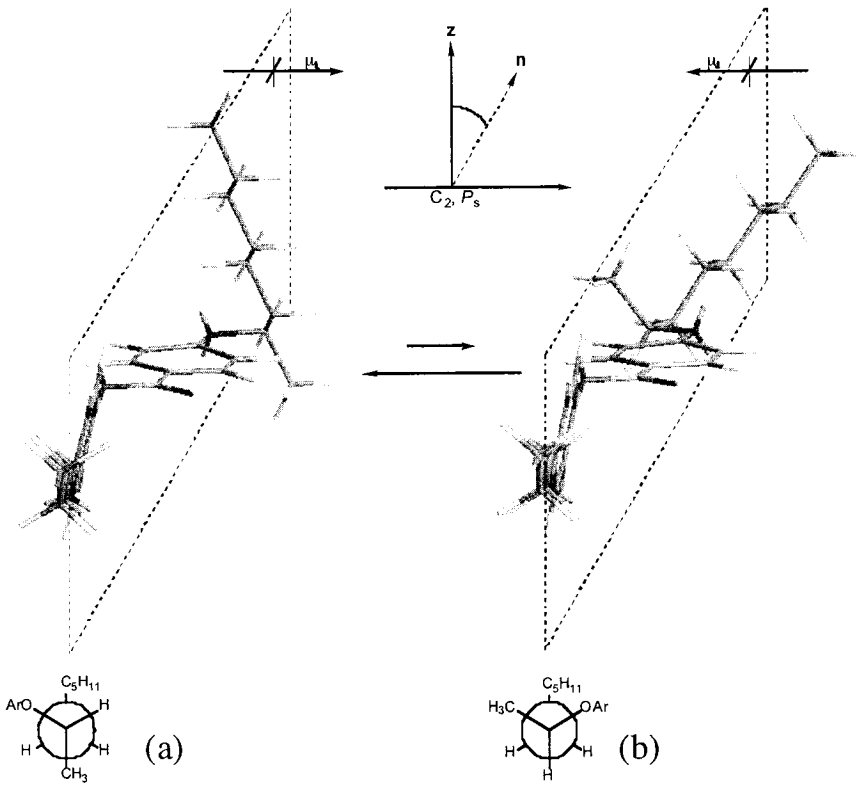

Figure 1-12. Rotational conformational analysis of the two orientations that give rise to P_s for **1.8**. Sign of polarization conforms with physics convention of dipoles from negative to positive.

However, the Boulder model does not account for all SmC* behaviour such as temperature dependant inversion of P_s.[17] Furthermore, it does not account for host dependence; the Boulder model assumes that the shape of the binding site is invariant with respect to the host. It assumes that a dopant is a passive guest, which does not affect the topography of the binding site.

1.2.4. Other Chiral Mesophases

The cholesteric, or chiral nematic (N*), phase has a helical structure (Figure 1-13) caused by the chirality of either the mesogenic structure or that of a dopant. The degree of twisting is characterized by the helical pitch (p), the distance required for one complete revolution, which is temperature dependant. Some nematogens display selective reflection upon irradiation with circularly polarized light of the same handedness of the screw sense of the nematic helix. If the helical pitch of the N* phase is the same magnitude of λ then the light is unable to propagate through material and hence is reflected. Because the pitch varies with temperature the property of selective reflection forms the basis of LC thermometers.[18]

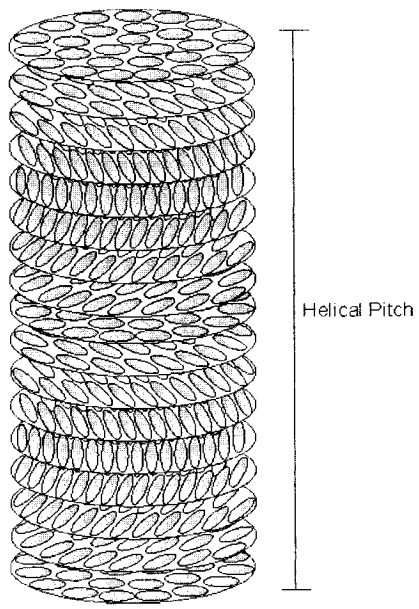

Figure 1-13. Representation of the helical twist induced by chirality in the nematic phase.

The chiral SmA (SmA*) phase is not ferroelectric but near the SmA*–SmC* transition there is a field-induced tilt, which breaks reflection symmetry. The loss of symmetry leads to a bias in the rotational distribution and hence one tilt direction is favoured over the other. This creates a net polarization and is known as the electroclinic effect. Since the tilt depends on the magnitude of the applied field, materials that display high electroclinic coefficients can be used for creating gray scale devices.[19]

A frustrated phase may exist between the SmA* and N* phases and is known as the twist grain boundary (TGB_A*) phase. It arises from a frustration between the propensity for molecules to form a helical structure and to form a lamellar structure, which cannot incorporate a helical twist. This frustration is accommodated by having

large smectic domains with screw dislocations perpendicular to the layer normal **n** with a helical pitch (p) (Figure 1-14).[20]

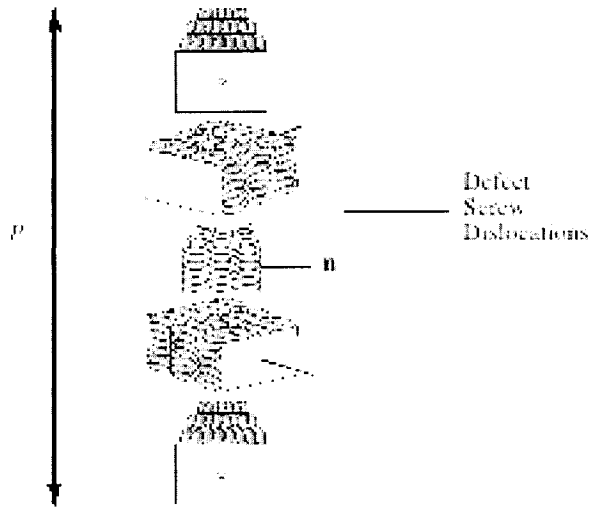

Figure 1-14. Twisted structure of the TGB_A* phase where the smectic layers are offset by screw dislocations.

1.3. Microphase Segregation

Liquid crystals form mesophases via microphase segregation. The self assembly of these molecules is based upon the inability of different molecular segments to interact favourably with one another. For conventional calamitic LCs, this segregation is between the aromatic cores and the aliphatic side-chains. Although it is difficult to predict whether a given molecule will possess the desired mesomorphic properties, one can bias smectic phases by using certain groups such as (semi)perfluorinated alkyl or an organosiloxane end-group, which have micro-segregating tendencies.

1.3.1. Organosiloxane groups

1.3.1.1. End-groups

The use of oligomeric siloxane end-groups in conventional calamitic liquid crystals has been shown to promote lamellar phases at the expense of nematic phases without greatly increasing the viscosity.[21] This is due to the incompatibility of the siloxane end-groups with both paraffinic and aromatic segments and their tendency to microphase segregate. Siloxanes can also be used as a means of increasing the miscibility of two incompatible molecules by forming a "virtual siloxane backbone", which is shown schematically in Figure 1-15.[22] For example, Coles demonstrated that the siloxane-terminated nitrostilbene **1.9** exhibits mesomorphic properties whereas the alkene-terminated precursor **1.10** is not liquid crystalline. Compound **1.9** was doped in two different siloxane hosts, (*R*)-**Br11Si3** and (*R,R*)-**Br-Si3-Br**. The phase diagrams of **1.9** in (*R*)-**Br11Si3** and (*R,R*)-**Br-Si3-Br** are shown in Figure 1-16 and Table 1-1, respectively and indicate that the siloxane derivatives are fully miscible and that the temperature ranges of the mesophases formed by the mixtures are greater than the temperature ranges of the individual components.[22,23] A similar study was performed with a heptamethyltrisiloxane-terminated azobenzene, **1.11**, which also showed increased stability of the smectic phases in mixtures with (*R*)-**Br11Si3**. The phase diagram of **1.11** in (*R*)-**Br11Si3** is shown in Figure 1-16.[23]

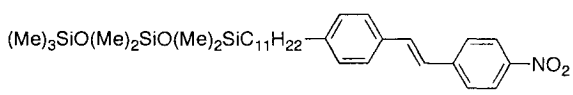

1.9: Cr 37 SmA 55 SmC 105 I

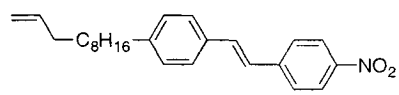

1.10

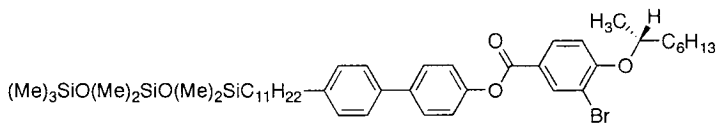

(*R*)-**Br11Si3**: Cr 42 SmC* 89 I

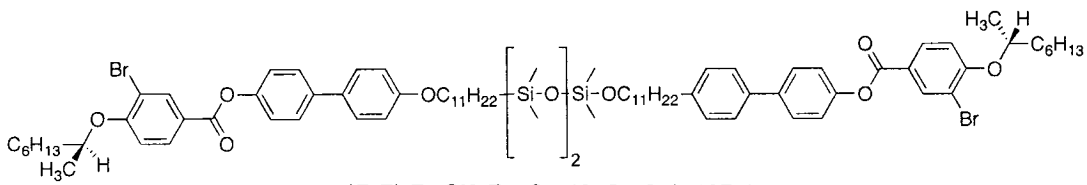

(*R,R*)-**Br-Si3-Br**: Cr 40 SmC_A* 107 I

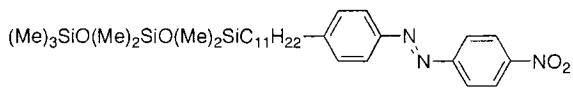

1.11: G 48 SmA 83 I

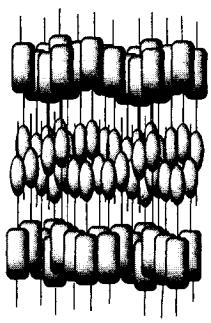

Figure 1-15. Representation of the segregation of siloxane groups (blocks) from the cores (ovals) and side chains (sticks).

(a)

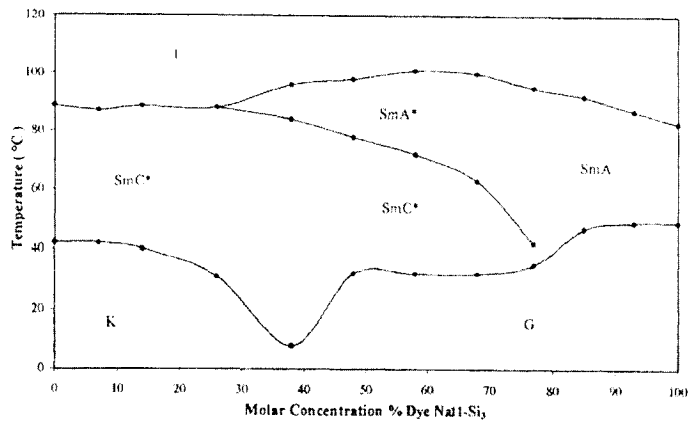

(b)

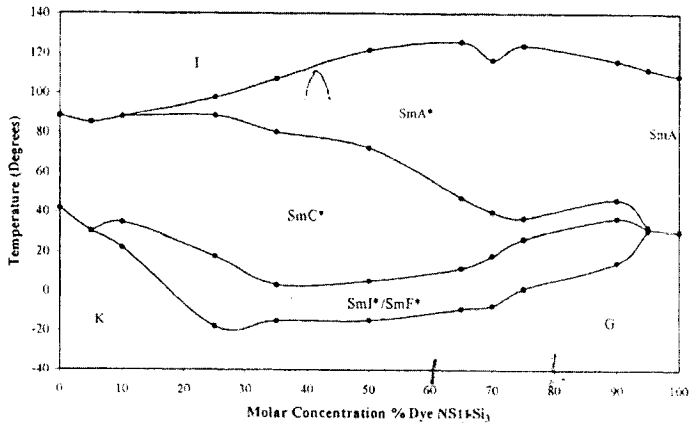

Figure 1-16. Phase diagrams for siloxane-terminated dopants (a) **1.9** and (b) **1.11** in the ferroelectric siloxane-terminated host (*R*)-**Br11Si3**. Taken from ref. 23.

Table 1-1. The phase sequence of **1.9** in the siloxane dimer (*R*,*R*)-**Br-Si3-Br**.

% **1.9** in (*R*,*R*)-**Br-Si3-Br** (w/w)	Phases sequence
100	Cr 37 SmC 55 SmA 105 I
50	Cr <20 SmC_A* 95 SmA 148 I
36	Cr <20 SmC_A* 112 SmA 138 I
0	Cr 50 SmC_A* 106 I

1.3.1.2. Central linking group

The use of oligomeric siloxanes as a bridge between two mesogenic compounds has also been explored as a means of promoting lamellar mesophases. Coles and co-workers showed that (*R*,*R*)-**Br-Si3-Br** forms an antiferroelectric SmC_A* phase.[24] This differs from the monomeric analogue, (*R*)-**Br11Si3**, which forms a ferroelectric SmC* phase. Antiferroelectric behaviour in compounds with an oligomeric siloxane group linking two known mesogens, also known as *mesogenic dimers*, has also been observed by Nishiyama and co-workers for compound (*S*,*S*)-**1.12**.[25] Guillon and co-workers have observed that the SmC* phase of (*R*,*R*)-**S-Si3-S** changes its polar order from antiferroelectric to ferroelectric on heating.[26] They describe the origins of the antiferroelectric ordering by first assembling the mesogens along their siloxane cores and then packing the molecules in a "V" shaped conformation, leading to an anticlinic interface. There is a competition, however, between the antiferroelectric "V" shape and the elongated conformation with ferroelectric polar order. This system was modeled by *ab initio* calculations which indicate that the two conformations are almost energetically equivalent.[26] A schematic of the two conformations is presented in Figure 1-17. Guillon rationalized that the propensity for the "V" shaped conformation is due to a greater biaxial polar ordering than the ferroelectric structure.[26]

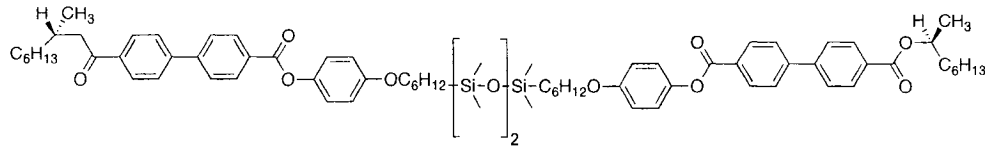

(*S*,*S*)-**1.12**: Cr 34 SmC_A^* 104 I

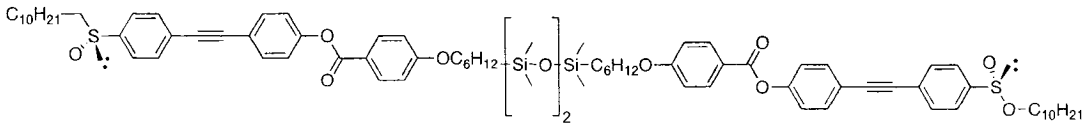

(*R*,*R*)-**S-Si3-S**: Cr 49 SmC_A^* 91 SmC* 97 I

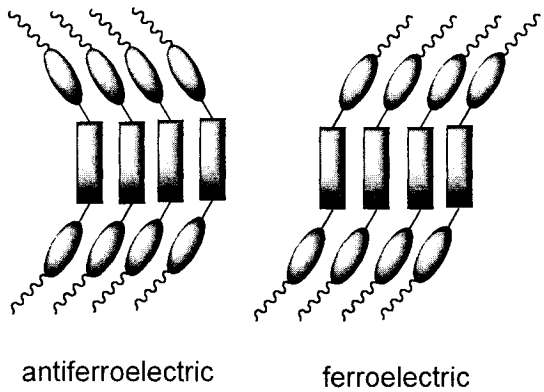

Figure 1-17. Schematic of the two packing arrangements of mesogenic dimers with oligomeric siloxane cores. The "V" orientation demonstrates antiferroelectric polar order while the elongated orientation exhibits ferroelectric polar order.

1.3.2. Perfluorinated alkyl groups

Semi-perfluorinated alkanes are arguably the simplest class of molecules known to form a lamellar mesophase. The use of (semi)-perfluorinated alkyl side chains has been shown to promote smectic phases due to the fluorophobic effect.[21] Perfluoroalkanes are also very chemically stable, which makes them attractive as component(s) in FLC mixtures since these molecules tend to have low viscosities.[21] The perfluorinated region

is very rigid and has a greater cross-section area (27-35 $Å^2$) than either its hydrocarbon equivalent (20 $Å^2$) or an aryl moiety (22 $Å^2$). Reiker demonstrated that, due to the large excluded volume of perfluorinated tails, these materials organize in an anti-parallel fashion, as shown in Figure 1-18. This offsets the lateral bulk associated with the core and allows for more efficient packing.[27]

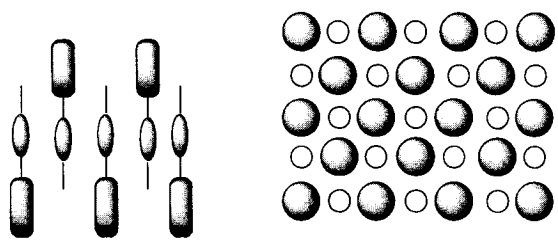

Figure 1-18. Representation of the antiparallel alignment of molecules with fluorinated alkyl side-chains. The cores (ovals) are aligned and the perfluorinated side-chains (blocks) invert orientation along smectic layer.

A study by Liu and Nohira demonstrated that the smectogenic properties of a homologous series of chiral phenylpyrimidines **1.13a-d** depends on the degree of perfluorination.[28] For a given number of perfluorinated carbons, the number of methylene spacers dictates the stability of the tilted smectic phase (SmC*) with the SmC* phase is destabilized to a greater extent with an increasing number of methylene spacers. The SmC* phase was also more stable, for a given chain length, when the extent of perfluorination increased.

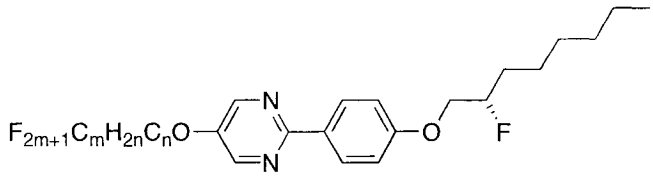

1.13a: m=3,n=4; Cr 81 SmC 110 SmA 113 I
1.13b: m=4,n=3; Cr 79 SmC 123 I
1.13c: m=4,n=4; Cr 84 SmC 117 SmA 121 I
1.13d: m=4,n=5; Cr 95 SmC 119 SmA 126 I

1.4. Atropisomeric biphenyl dopants

1.4.1. First generation

In 1996 Yang *et al.* demonstrated that non-mesogenic dopants with atropisomeric biphenyl cores could induce ferroelectricity in LC hosts.[29] Note that these dopants possess no stereogenic center but rather an axis of chirality due to restricted rotation about the central aryl-aryl bond. These dopants induce polarizations that depend on the host structure and are therefore considered to be Type II, according to Stegemeyer's classification.[9]

The atropisomer **1.14** shows particularly large host dependence. In the host **PhB** ferroelectric switching was observed but no polarization was detected for a mixture at $\chi_d = 0.05$ and the value of δ_p was determined to have an upper limit of 20 nC/cm^2.[30]. For liquid crystalline hosts **DFT**, **PhP1**, and **NCB76** the induced δ_p values were moderately large +63, +161 and +170 nC/cm^2 respectively. The observed polarizations were smaller than anticipated based upon the large magnitude of the transverse dipole. AM1

calculations suggest that there should be a very small bias for rotation of the core with respect to the side-chains in the binding site of the host (Figure 1-19). Conformations (c) and (d) do not give rise to polarization since the transverse dipole lies in the tilt plane. There is a small conformational bias towards (a), which corresponds to a positive sign of polarization for the (*S*) enantiomer of **1.14**. In order to design dopants capable of inducing large polarizations in SmC hosts, the conformational asymmetry should be coupled strongly to the transverse dipole moment. This idea was addressed in the second generation of atropisomeric biphenyl dopants.

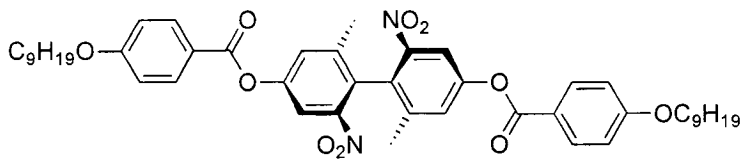

1.14

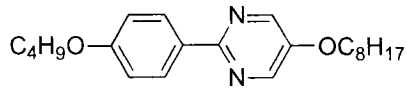

PhP1: Cr 58 SmC 85 SmA 95 N 98 I

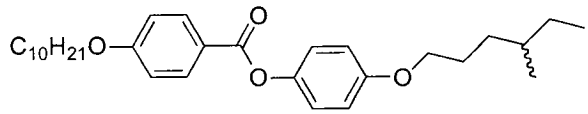

PhB: Cr 35 SmC 70.5 SmA 72 N 75 I

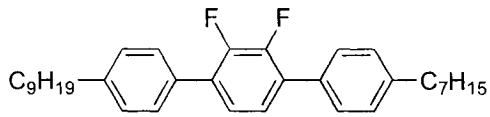

DFT: Cr 49 SmC 77 SmA 93 N 108 I

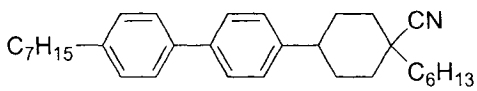

NCB76: Cr 66 (SmG 55) SmC 73 SmA 116 N 125 I

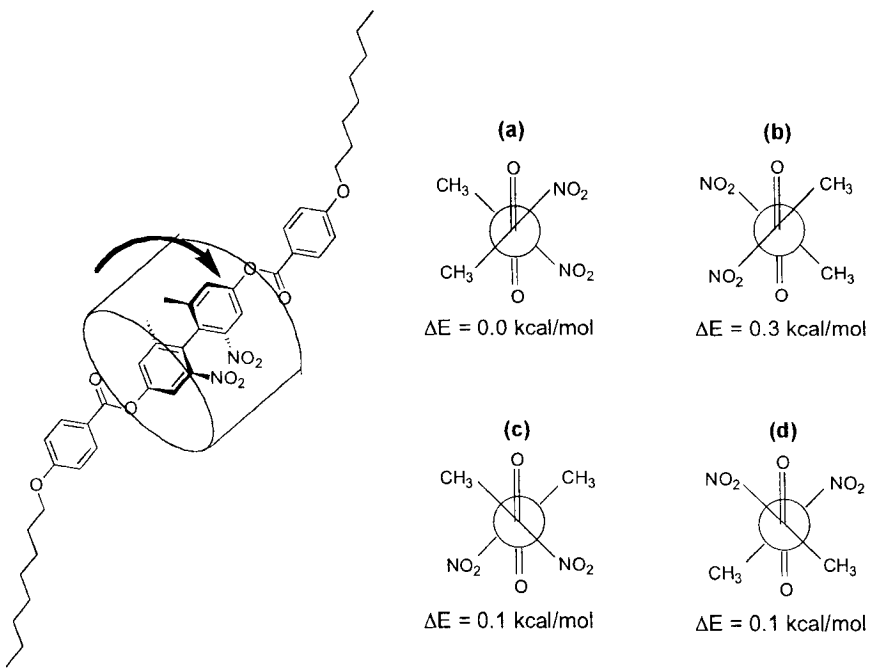

Figure 1-19. Relative energies produced by AM1 calculations of the four energy minima produced by rotating the core relative to the ester groups for **1.14.**

1.4.2. Second generation

A second generation of atropisomeric biphenyl dopants was developed with the symmetry breaking groups in the 3 and 3' positions.[30] An extensive structure property relation study was performed by varying the length of the alkyl tails of the 3,3'-dinitrobiphenyl core (**1.15a-j**) and altering the symmetry breaking group at the 3 and 3' positions (**1.16-1.19**). A summary of the δ_p value of these dopants in liquid crystalline hosts **PhP1**, **NCB76**, **PhB** and **DFT** is shown in (Table 1-2). It is evident that the 3,3'-dinitro dopant induces a larger polarization than the 2,2'-dinitro predecessor **1.14**. The 3,3'-dinitrobiphenyl system was modeled by *ab initio* calculations (B3LYP/631G(d)), which suggested that there is a significant increase in stereopolar coupling between the nitro groups and the ester linking groups (Figure 1-20).[31] This model also suggests that the (*R*) enantiomer of **1.15** should induce a negative polarization. This prediction was confirmed by correlating the sign of polarization to the absolute configuration of **1.15** by X-ray crystallographic analysis of the bis-(1*S*)-camphorsufonylamide derivative.[32]

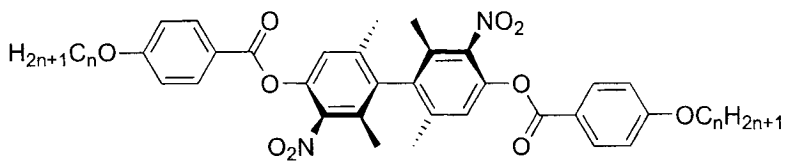

1.15a, n=1; **b**, n=4; **c**, n=6; **d**, n=8; **e**, n=9; **f**, n=12; **g**, n=14; **h**, n=16; **i**, n=18; **j**, n=20

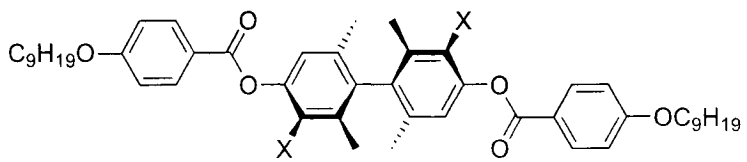

1.16, X = F; **1.17**, X = Cl; **1.18**, X = Br; **1.19**, X = CH_3

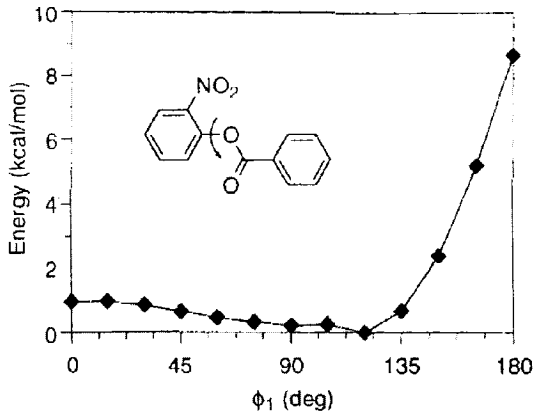

Figure 1-20. Relative energies of 2-nitrophenyl benzoate as a function of dihedral angle between C6, C1, O and C(O). Taken from ref. 31.

There is a large host dependence observed for both the 2,2'- and 3,3'-dinitrobiphenyl, with the 3,3' derivative **1.15d** in **PhP1** inducing the largest polarization power on record (1738 nC/cm^2). The low polarization induced by **1.15d** in **PhB** can be explained by the transverse dipole being oriented near the tilt plane, which is consistent with the sign reversal of the polarization. This alone, however could not account for the large polarization observed for mixtures of **1.15d** and **PhP1**. Although ordering of the transverse dipole of **PhP1** along the polar axis may be important, **PhP1** is not predicted to have the largest transverse dipole among the screened hosts.

Table 1-2. Polarization powers for dopants **1.15** – **1.19** in selected LC hosts.[30,31]

	δ_p (nC /cm^2)[a,b]			
dopant (X)	**PhP1**	**PhB**	**NCB76**	**DFT**
(*S*)-**1.15d** (NO_2)	1738 ± 95 (+)	<30 (-)	373 ± 54 (+)	124 (+)
(*R*)-**1.15e** (NO_2)	1555 ± 119 (-)	<34 (-)	514 ± 38 (-)	312 (-)
(*R*)-**1.16** (F)	255 ± 36 (-)	<40 (+)	94 ± 3 (-)	59 ± 6 (+)
(*S*)-**1.17** (Cl)	197 ± 28 (+)	<30 (+)	116 ± 7 (+)	60 ± 7 (+)
(*S*)-**1.18** (Br)	34 (+)	<20 (+)	83 ± 4 (+)	42 ± 1 (+)
(*S*)-**1.19** (Me)	46 ± 6 (-)	<26 (-)	<43 (-)	<60 (-)

[a] Uncertainties are ±1 standard deviation. [b] Sign of P_s indicated in parentheses.

1.4.3. The Chirality Transfer Feedback Model

In order to account for the large polarization power exhibited by **1.15d** in **PhP1**, the Chirality Transfer Feedback (CTF) model was developed. This was based, in part, on observations by Gottarelli and co-workers that atropisomeric dopants that have a good structural match with a nematic host induce tighter helical pitches than ones that have a poor structural match.[33] In a similar manner, it is thought that dopants that have a good structural match with the SmC host will transfer their chirality to the binding site to a greater extent than dopants that are not a good structural match, as shown in Figure 1-21. Once chirality is transferred, the binding site for hosts in proximity to the host/guest pair will be distorted, thereby favouring the binding of one conformation of the chiral dopant. This model is consistent with the Boulder model in that the chiral perturbation of the dopant will deform the bent cylinder into a chiral binding site and hence one diastereomeric pair will be favoured over the other, thereby increasing the polar order. Chirality transfer may also cause polar ordering of the host, as suggested by Stegemeyer.[9]

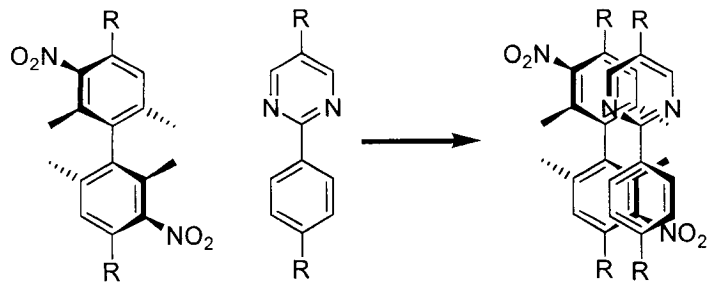

Figure 1-21. Representation of the chirality transfers between **1.15** and **PhP1** as an example of a host/dopant pair, which are structurally similar.

1.4.3.1. Indirect evidence of the CTF model

Initial evidence of the CTF model was based on the correlation of δ_p with the degree of core-core interactions between **1.15a-j** and **PhP1**. The δ_p increases with increasing chain-length and levels off for C8/C9. The positional order of the dopant should increase with increasing chain-length due to increased segregation between the side-chains and the cores. By increasing the positional order the degree of chirality transfer should also be increased.

Vizitiu and co-workers provided further evidence for the CTF model. Compound **1.20** is approximately the same length as **1.15d** but differs in that the 3,3'-dinitrobiphenyl core is offset with respect to the side-chains. The δ_p of **1.20** is 36% less than the symmetrical analog **1.15** (δ_p of 1101 nC/cm^2 vs. 1735 nC/cm^2).[30]

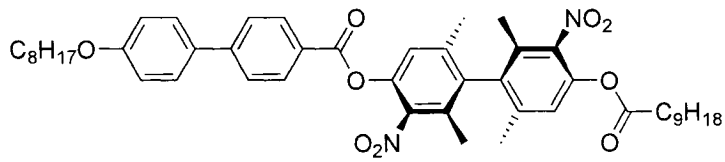

1.20

The induced pitch of the SmC* phase should correlate with the degree of chirality transfer. Figure 1-22 shows the inverse relationship between δ_p and pitch for mixtures of dopants of the type **1.15** in **PhP1** at $\chi_d = 0.02$. The concept of increased chirality transfer inducing a tighter helical pitch is consistent with observations by Gottarelli in chiral nematic systems (*vide supra*).[33]

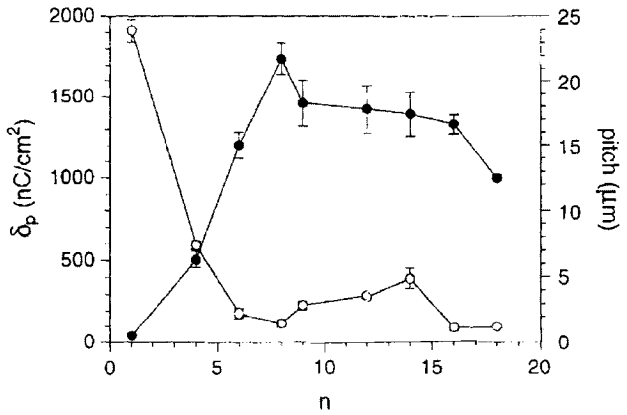

Figure 1-22. Dependence of chain-length (n) on the polarization power (●) and pitch (○) of dopants of the type **1.15** in **PhP1** at $\chi_{ll} = 0.02$. Taken from ref. 30

1.4.3.2. Direct evidence of the CTF model

In 2002, Hartley and co-workers performed a more extensive study in an attempt to find direct evidence for CTF. The experiments used mixtures of **1.15e** in either **PhP1** or **PhB** in the presence of a probe molecule.[34] The chiral probes **MDW950** and **1.21** were used to mimic the structure of **PhP1** and **PhB** respectively. The researchers hypothesized that if the perturbations exerted by **1.15e** were chiral in nature, then δ_p of these ternary mixtures in the presence of one enantiomer of **1.15e** will be different than δ_p in the presence of the other enantiomer. Alternatively, if δ_p was found to be invariant with respect to the configuration of **1.15e**, then the latter can be thought of as a passive guest.

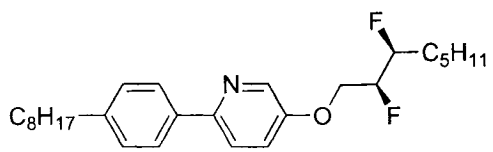

MDW950, δ_P = -435 nC/cm^2

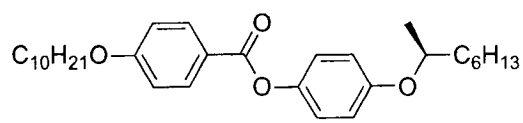

1.21, δ_P = -62 nC/cm^2

The polarization power of each probe was measured in their respective host; **MDW950** in **PhP1** has a δ_p value of -435 nC/cm^2 while **1.21** has a δ_p value of -62 nC/cm^2 in **PhB**.[34] In the presence of (+)-**1.15e** at constant mole fraction (χ_d) of 4% the δ_p value of **MDW950** in **PhP1** increases to -605 nC/cm^2, whereas in the presence of (-)-**1.15e**, at the same mole fraction, the δ_p decreased to -78 nC/cm^2. This reflects the diastereomeric relationship between dopant and probe and suggests that the perturbation is indeed chiral. For the case of **1.21** in **PhB**, there was no significant change in δ_p in the presence of either (+)- or (-)-**1.15e**, which suggests that the dopant is a passive guest in this system. These results are summarized in Figure 1-23.

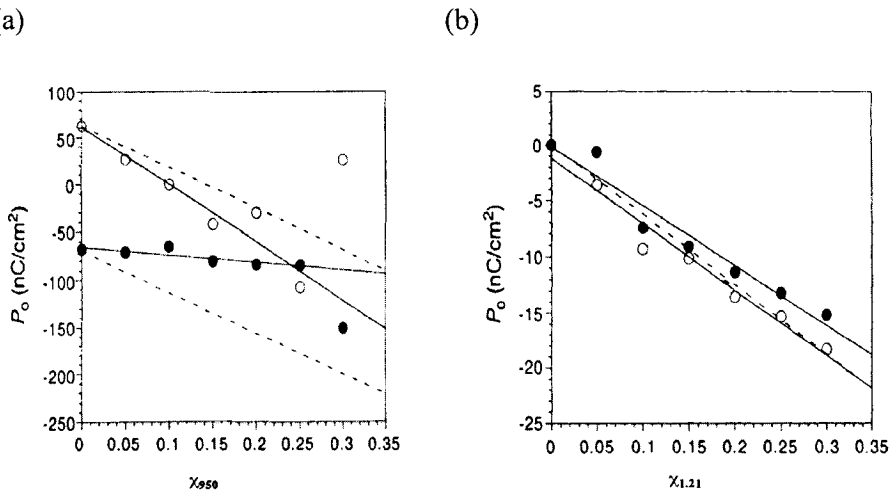

Figure 1-23. P_o measurements for (a) **MDW950** in the presence of (+)-**1.15d** (○) and (-)-**1.15d** (●) in **PhP1** and (b) **1.21** in the presence of (+)-**1.15d** (○) and (-)-**1.15d** (●) in **PhB**. Taken from ref. 34.

With the establishment that **1.15e** exerts chiral perturbations in **PhP1**, a second type of probe was employed to establish whether the "feedback" aspect of the CTF model was valid. These experiments employed a second atropisomer **1.19**, which shows very small δ_p (46 nC/cm^2) in **PhP1** (see Table 1-2). Dopants (+)-**1.19** and (-)-**1.19** were placed

in the presence of (+)-**1.15d** at $\chi_d = 0.04$. The results showed that δ_p of (+)-**1.19** was amplified 5.5 times to +256 nC/cm^2 while (-)-**1.19** showed a polarization sign inversion and a δ_p of +130 nC/cm^2 (Figure 1-24).[34] These results suggest that a chiral perturbation of the binding site of **PhP1** caused by (+)-**1.15e** is able to alter the rotational distribution of (-)-**1.19** to such an extent that it acts like (+)-**1.19**.

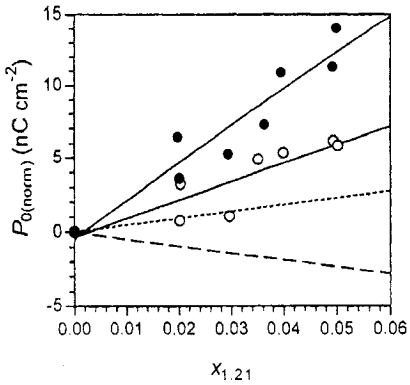

Figure 1-24. P_o plot for (+)-**1.19** (●) and (-)-**1.19** (○) in the presence of (+)-**1.15d** ($\chi_d = 0.04$) in **PhP1**. Short and long dashed lines indicate the δ_p of (+)-**1.19** and (-)-**1.19** in **PhP1**, respectively. Taken from ref. 34.

1.5. Project outline

The goal of this project was to expand upon the work of Vizitiu and Hartley and by designing molecules with the atropisomeric 3,3'-dinitrobiphenyl core that form liquid crystalline phases by using microphase segregation and increasing the lateral bulk of the side-chain(s). The non-mesogenic dopants of type **1.15** are very destabilizing to the SmC* of **PhP1** and the SmC* phase is not observed above a mole fraction of $\chi_d = \sim 0.17$. Stegemeyer showed that the introduction of mesogenic dopants into a liquid crystalline host can improve the compatibility of the mixture over a broader range of dopant mole

fractions.[9] By increasing the miscibility of dopant and host it would be possible to study cooperative effects of the dopant in the host **PhP1**.

The first section describes the synthesis of molecules with side-chains which match the lateral bulk of the 3,3'-dinitrobiphenyl core. This alteration makes the molecule more rod-shaped and should promote liquid crystalline phases. Two approaches were employed. The first was the design of polycatenar systems and the second uses a 4-pentylbicyclo[2.2.2.]octyl side-chain. Microphase segregation was also explored using organosiloxane-terminated and semiperfluorinated side-chains to stabilize smectic liquid crystalline phases.

1.6. References

(1) Link, D. R.; Natale, G.; Shao, R. Maclennan, J. E.; Clark, N. A., Körblova, E.; Walba, D. M. *Science.* **1997**, *278*, *1924.*

(2) Gray, G. W.; Goodby, J. W. G. Smectic Liquid Crystals: Textures and Structures; Leonard Hill: Glasgow, 1984.

(3) McMillan, W. L. *Physical Review A* **1973**, *8*, 1921.

(4) Wulf, A. *Physical Review A* **1975**, *11*, 365.

(5) Meyer, R. B.; Liebert, L.; Strzelecki, L.; Keller, P. *J. Phys. (Paris) Lett.* **1975**, *36*, L69.

(6) Clark, N. A.; Lagerwall, S. T. *Applied Physics Letters* **1980**, *36*, 899.

(7) Kuczyński , W.; Stegemeyer, H. *Chem. Phys. Lett.* **1980**, *70*, 123.

(8) Siemensmeyer, K.; Stegemeyer, H. *Chem. Phys. Lett.* **1988**, *148*, 409.

(9) Stegemeyer, H.; Meister, R.; Hoffmann, U.; Sprick, A.; Becker, A. *J. Mater. Chem.* **1995**, *5*, 2183.

(10) Walba, D. M.; Slater, S. C.; Thurmes, W. N.; Clark, N. A.; Handschy, M. A.; Supon, F. *J. Am. Chem. Soc.* **1986**, *108*, 5210.

(11) Walba, D. M. In *Advances in the Synthesis and Reactivity of Solids*; Mallouck, T. E., Ed.; JAI Press, Ltd.: Greenwich, CT, 1991; Vol. 1, p 173.

(12) Samulski, E. T.; Dong, R. Y. *J. Chem. Phys.* **1982**, *77*, 5090.

(13) Samulski, E. T. *Isr. J. Chem.* **1983**, *23*, 329.

(14) Bryan, R. F.; Leadbetter, A. J.; Mehta, A. I.; Tucker, P. A. *Mol. Cryst. Liq. Cryst.* **1984**, *104*, 257.

(15) Bartolino, R.; Doucet, J.; Durand, G. *Ann. Phys. (Paris)* **1978**, *3*, 389.

(16) Wand, M. D.; Vohra, R.; Walba, D. M.; Clark, N. A.; Shao, R. *Mol. Cryst. Liq. Cryst.* **1991**, *202*, 183.

(17) Terzis, A. F.; Photinos, D. J.; Samulski, E. T. *J. Chem. Phys.* **1997**, *107*, 4061.

(18) Gleeson, H. F. Thermography Using Liquid Crystals. In *Handbook of Liquid Crystals*; Demus, D., Goodby, J., Gray, G. W., Spiess, H.-W., Vill, V., Eds.; Wiley-VCH: Weinheim, 1998; Vol. 1, pp 823-838.

(19) Andersson, G.; Dahl, I.; Komitov, L.; Laggerwall, S. T.; Skarp, K.; Stebler, B. *J. Appl. Phys.* **1989**, *66*, 4983.

(20) Dierking, I. *Textures of Liquid Crystals*; Wiley-VCH; Weinheim, 2003.

(21) Tschierske, C. *J. Mater. Chem.* **1998**, *8*, 1485.

(22) Shoosmith; D., Carboni; C. Perkins, S.; Meyer, S.; Coles, H. J. *Mol. Cryst. Liq. Cryst.* **1999**, *331*, 181.

(23) Shoosmith, D. E.; Remnant, A.; Perkins, S. P.; Coles, H. J. *Ferroelectrics* **2000**, *243*, 75.

(24) Kloess, P.; McComb, J.; Coles, H. J.; Zentel, R. *Ferroelectrics* **1996**, *180*, 233.

(25) Nishiyama, I.; Yamamoto, J.; Yokoyama, H.; Méry, S.; Guillion, D.; Goodby, J. W. *Transactions of the Materials Research Society of Japan* **2004**, *29*, 785.

(26) Guillion, D.; Ospirov, M. A.; Méry, S., Siffert, M.; Nicoud, J.-F.; Bourgogne, C.; Sebastião, P. *J. Mater. Chem.* **2001**, *11*, 2700.

(27) Rieker, T. P.; Janulus, E. P. *Phys. Rev. E.* **1995**, *52*, 2688.

(28) Liu, H.; Nohira, H. *Liq. Cryst.* **1998**, *24*, 719.

(29) Yang, K.; Campbell, B.; Birch, G.; Williams, V. E.; Lemieux, R. P. *J. Am. Chem. Soc.* **1996**, *118*, 9557

(30) Vizitiu, D.; Lazar, C.; Halden, B. J.; Lemieux, R. P. *J. Am. Chem. Soc.* **1999**, *121*, 8229.

(31) Vizitiu, D.; Lazar, C.; Radke, J. P.; Hartley, C. S.; Glaser, M. A.; Lemieux, R. P. *Chem. Mater.* **2001**, *13*, 1692.

(32) Hartley, C. S.; Wang, R.; Lemieux, R. P. *Chem. Mater.* **2004**, *16*, 5297.

(33) Gottarelli, G.; Hilbert, M.; Samori, B.; Solladié, G.; Spada, G. P.; Zimmermann, R. *J. Am. Chem. Soc.* **1983**, *105*, 7318.

(34) Hartley, C. S.; Lazar, C.; Wand, M. D.; Lemieux, R. P. *J. Am. Chem. Soc.* **2002**, *124*, 13513.

Chapter 2. Use of steric bulk in alkyl side-chains to promote liquid crystalline behaviour in compounds containing an atropisomeric 3,3'dinitrobiphenyl core

It has been shown that dopants featuring an atropisomeric biphenyl core with nitro groups at the 3 and 3' positions have remarkably large polarization powers in liquid crystalline hosts with a phenylpyrimidine core, such as **PhP1**.[1] Stegemeyer demonstrated that non-mesogenic dopants normally cannot be doped beyond $\chi_d = 0.20$ in SmC liquid crystal hosts because the SmC phase is very prone to destabilization by impurities; however mesogenic dopants forming either N* or SmC* phases can be mixed in higher mole fractions.[2] Compound **1.15d** induces high polarizations in **PhP1**, but causes a narrowing of the SmC* phase temperature range and its disappearance beyond $\chi_d = 0.17$.[3] The destabilization is a reflection of the significant lateral bulk of the 3,3'-dinitrobiphenyl core, which precludes efficient packing into a layered structure formed by molecules with flat cores.

In order to produce more compatible dopants featuring the 3,3'-dinitrobiphenyl core, the synthesis of new derivatives designed to promote the formation of liquid crystal phases was undertaken. Two approaches were used to induce liquid crystalline behaviour based on extending the lateral bulk of the molecule beyond the core structure. The first focuses on increasing the number of alkyl tails to create a polycatenar structure.

Polycatenar molecules are hybrids between discotic liquid crystals and calamitic liquid crystals; the general structure is shown in Figure 2-1. These compounds display a rich polymorphism based upon the number of tails they possess, as well as their distribution at the periphery.[4] For hexacatenar materials, there have been very few examples of compounds with fewer than five rings in the core displaying mesogenic properties.[4] One such compound is **2.1**, in which the aryl core has a biphenyl ring with two tricatenar aryl rings linked by esters.[5] This compound possesses a monotropic hexagonal columnar phase.

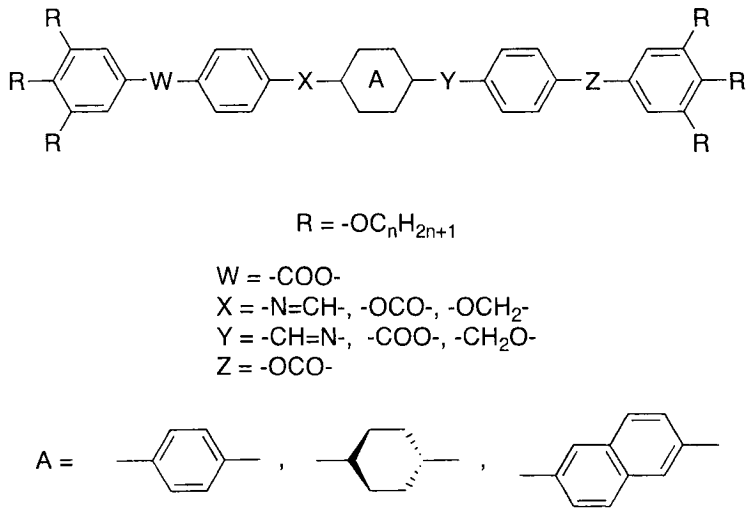

Figure 2-1. General structure of polycatenar molecules, showing common linking groups between the rings that make up the rigid core.

For tetracatenar systems, a minimum of four phenyl rings is normally required for any mesogenic properties to be observed. In symmetrical systems (*i.e.*, two identical biforked end-groups), 3,5-disubstitution (*e.g.* **2.2a** and **2.2b)** promotes columnar phases, while 3,4-disubstitution (*e.g.* **2.3a-c**) leads to a rich polymorphism including columnar

and calamitic mesophases.[4] Calamitic phases tend to be favoured with shorter alkyl chains while the columnar phases are observed with longer alkyl chains, as shown in series **2.3a-c**.[4]

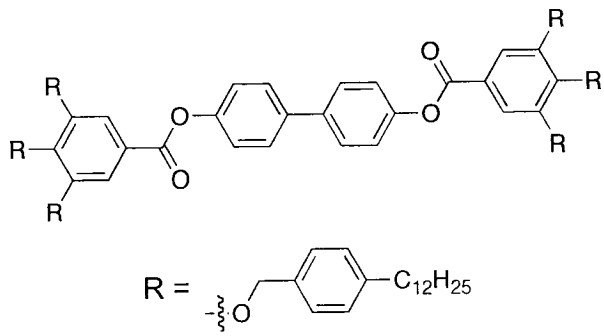

2.1: Cr (87 Col_h) 90 I

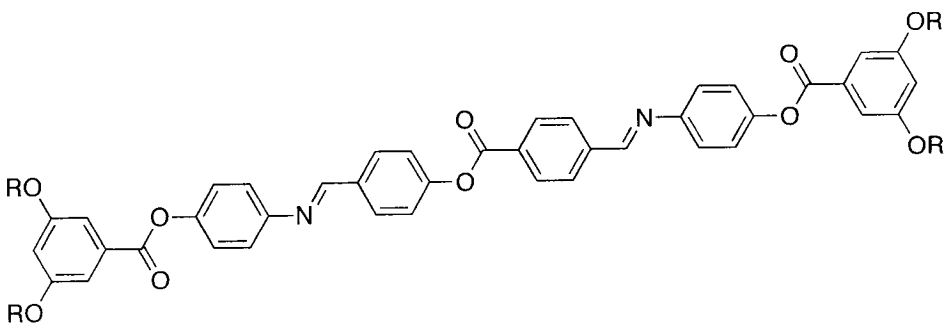

2.2

a: R = C_7H_{15}; Cr (110 Col_h) 104 I
b: R = $C_{10}H_{21}$; Cr 76 Col_h 110 I

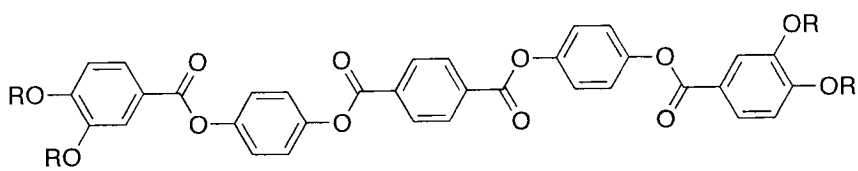

2.3

a: R = C_6H_{13}; Cr 195 N 217 I
b: R = $C_{10}H_{21}$; Cr 156 SmC 176 I
c: R = $C_{14}H_{29}$; Cr 142.5 Col_r 162 I

The second approach to induce liquid crystalline behaviour in compounds containing the 3,3'-dinitrobiphenyl core focuses on using a sterically bulky end-group, such as a 4-alkylbicyclo[2.2.2.]octyl side-chain. This laterally bulky segment has been shown to raise the clearing point of mesogens, as shown in Figure 2-2.[6] For example, consider the series of compounds:

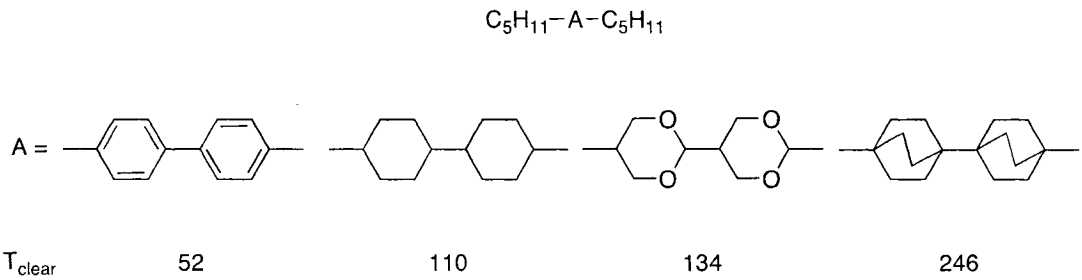

Figure 2-2. Clearing point of liquid crystals, with different cores containing two pentyl side-chains.

Work by Kaszynski and co-workers has focused on comparing of the mesogenic properties of molecules containing bicyclo[2.2.2.]octyl groups with those containing other common substituents, such as phenyl groups, and uncommon bulky groups such as carboranes.[7,8,9] They found that, compared to phenyl groups, the bicyclo[2.2.2.]octyl group promotes smectic phases, as shown by the rich smectic polymorphism of (*R*)-**2.4**.[8] A striking example of the increased stability of mesophases with the substitution of phenyl groups with bicyclo[2.2.2.]octyl groups is seen with 4,4'-dihexylbiphenyl (**2.5**) and 4,4'-dihexyl–bis-bicyclo[2.2.2]octane (**2.6**), where the clearing point is almost 200 K higher for **2.6** than for **2.5**.[7] In addition, the temperature range of the smectic phase of **2.6** is 166 K greater than for **2.5**.[7]

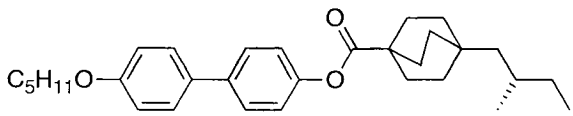

(*R*)-**2.4**: Cr 85 SmB* 91 SmC* 97 SmA* 133 N* 169 I

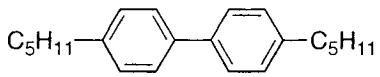

2.5: Cr 31 SmX 50 I

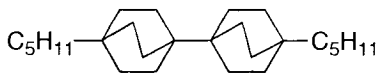

2.6: Cr 41 SmX 244 I

With these two motifs in mind we sought to synthesize derivatives of the 3,3'-dinitrobiphenyl core with polycatenar and bulky side-chains. The addition of extra tails or bicyclo[2.2.2.]octyl group(s) should match the lateral bulk of the 3,3'-dinitrobiphenyl core and therefore make the molecules more rod-shaped.

2.1. Synthesis and Resolution:

The synthesis of the common intermediate **2.13** (Scheme 2-1) was achieved following known procedures, and showed the expected physical and spectral properties.[10] 3,5-Dimethylanisole (**2.7**) was brominated to give **2.8**, which was coupled to give **2.9** by treatment with one equivalent of ^{n}BuLi followed by addition of half an equivalent CuCN and finally treatment with O_2. The resulting biphenyl was then nitrated with HNO_3 in the presence of H_2SO_4 and acetic acid to give (*RS*)-**2.10** as a racemic mixture. The enantiomers were resolved by two methods. Initially the resolution was achieved via classical means, and is now achieved more efficiently by preparative chiral phase HPLC (*vide infra*). The classical resolution was accomplished by reducing the nitro groups with stannous chloride to give (*RS*)-**2.11**, which was then treated with (*1S*)-(+)-

camphorsulfonyl chloride in the presence of triethylamine to give the diastereomers (*S*,*S*,*S*)-**2.12** and (*S*,*S*,*R*)-**2.12**. Resolution was achieved based on differences in the solubility of the two diastereomers in toluene and methanol. Toluene crystallizes the (*S*,*S*,*S*) diastereomer selectively, while methanol crystallizes the (*S*,*S*,*R*) diastereomer selectively. Removal of the camphor sulfonate chiral auxiliary was achieved by treatment with HBr in AcOH, regenerating the 3,3'-diaminobiphenyl (*R*)- and (*S*)-**2.11**, which were then oxidized with *m*CPBA to give (*R*)- and (*S*)-**2.10**. The methoxy groups were cleaved with BBr_3 to give (*R*)- and (*S*)-**2.13**. Analysis by chiral phase HPLC on a Daicel Chiralpak AS column was performed to determine the optical purity of the two enantiomers: the (*R*)- enantiomer was obtained in 75% e.e. and the (*S*)- enantiomer in 90% e.e. Normally the classical resolution would begin with 6.6 g of the mixture of diastereomers of (*S*,*S*,*R*) and (*S*,*S*,*S*)-**2.12** and yield 2.6 g of (*S*,*S*,*S*)-**2.12** (39% yield) and 2.2g of (*S*,*S*,*R*)-**2.12** (33% yield).

Scheme 2-1[a]

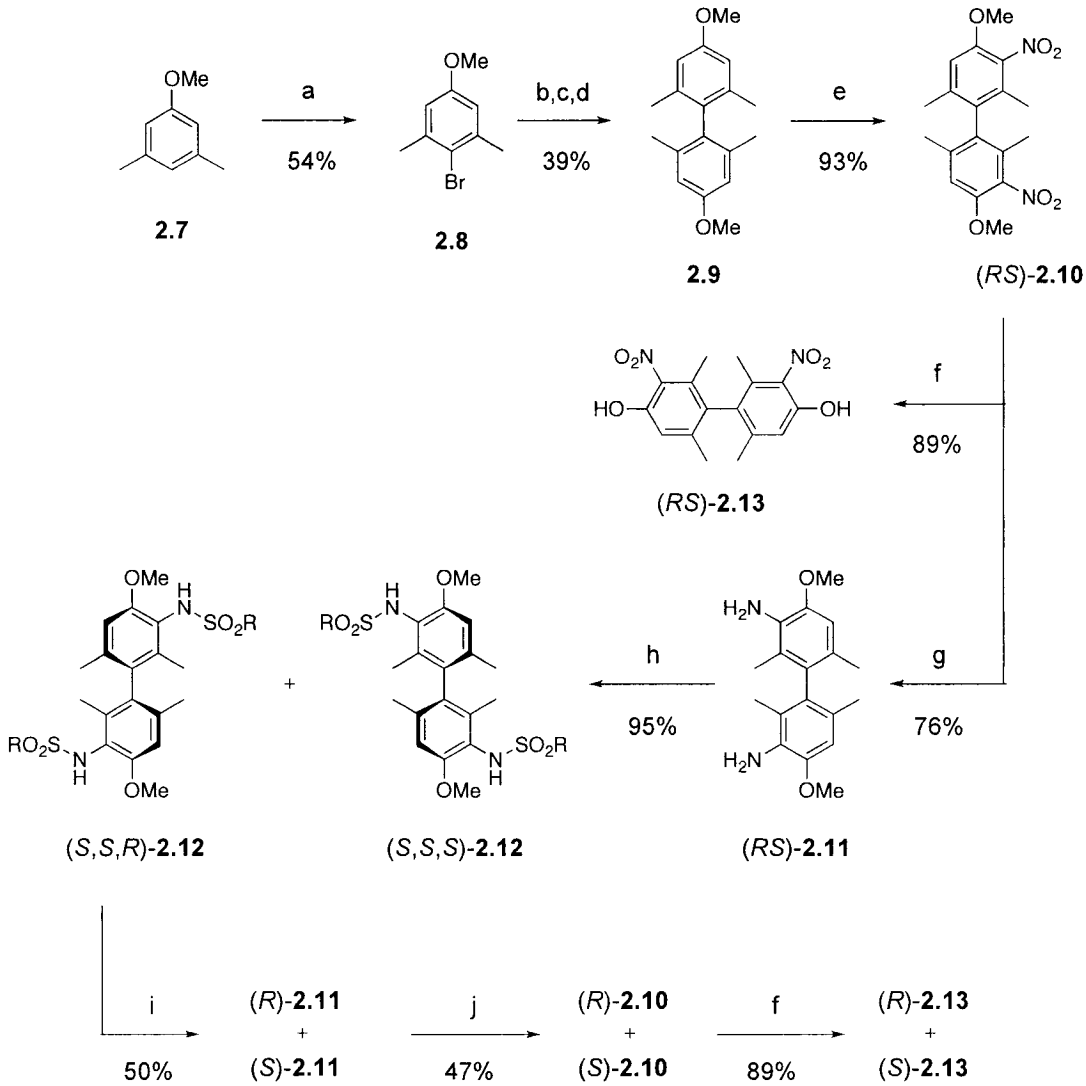

[a] (a) Br_2, $CHCl_3$, 5°C; (b) ^nBuLi, THF, -78°C; (c) CuCN; (d) O_2; (e) HNO_3, ACOH, H_2SO_4; (f) BBr_3, CH_2Cl_2; (g) $SnCl_2{\cdot}2H_2O$, EtOH, reflux; (h) (*1S*)-(+)-camphorsulfonyl chloride, $N(Et)_3$, CH_2Cl_2; (i) HBr, AcOH, reflux; (j) *m*CPBA, $CHCl_3$.

With the installation of a preparative Chiralpak AS HPLC column in 2005, we were able to resolve (*RS*)-**2.13** on a gram-scale more efficiently. The chiral HPLC resolution was achieved by first cleaving the methoxy groups of (*RS*)-**2.10** with BBr_3 and separating the enantiomers of **2.13** (1.0-1.4 grams per injection) using a mixture of 20%

EtOH in hexanes as eluant in approximately one hour. A representative HPLC chromatogram is shown in Figure 2-3. The resolved enantiomers were condensed with the appropriate di- or tri-alkoxybenzoic acid in the presence of DCC and DMAP to give the polycatenar derivatives **2.14a-e**, shown in Scheme 2-2. The unsymmetrical derivatives with a 4-pentylbicyclo[2.2.2.]octyl side-chain, (*R*)-**2.16a-e**, were synthesized by treatment of (*R*)-**2.13** with 1.05 equivalents 4-pentylbicyclo[2.2.2.]octane-1-carboxylic acid in the presence of DCC and DMAP to give (*R*)-**2.15**, followed by condensation with the required 4-alkoxybenzoic acid in the presence of DCC and DMAP, to give (*R*)-**2.16a-e**, as shown in Scheme 2-3.

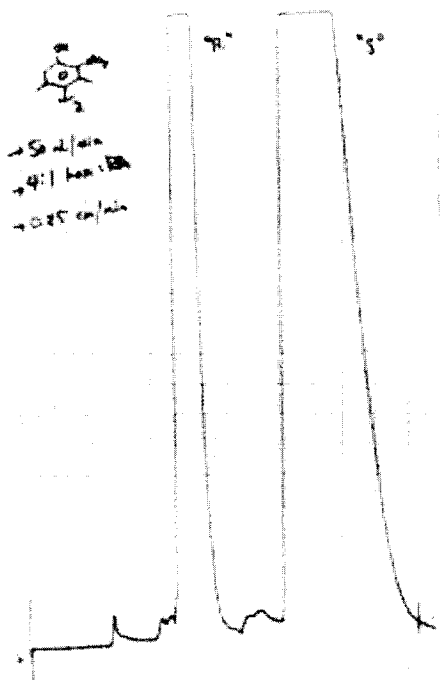

Figure 2-3. Chromatogram for the resolution of (*R*)- and (*S*)-**2.13** with 20% EtOH in hexanes as eluant.

Scheme 2-2[a]

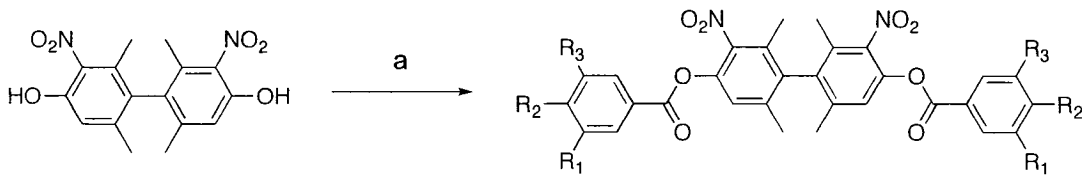

(*R*)- and (*S*)-**2.13**

(*R*)-**2.14a**: $R_1 = R_2 = OC_{10}H_{21}$, $R_3 = H$, 72%
(*S*)-**2.14b**: $R_1 = R_2 = OC_{12}H_{25}$, $R_3 = H$, 66%
(*R*)-**2.14c**: $R_1 = R_3 = OC_{10}H_{21}$, $R_2 = H$, 54 %
(*S*)-**2.14d**: $R_1 = R_3 = OC_{12}H_{25}$, $R_2 = H$, 55 %
(*S*)-**2.14e**: $R_1 = R_2 = R_3 = OC_{10}H_{21}$, 64 %

[a] (a) DCC, DMAP, CH_2Cl_2 **a:** 3,4-bis-decyloxybenzoic acid; **b:** 3,4-bis-dodecyloxybenzoic acid; **c:** 3,5-bis-decyloxybenzoic acid; **d:** 3,5-bis-dodecyloxybenzoic acid; **e:** 3,4,5-tris-decyloxybenzoic acid.

Scheme 2-3[a]

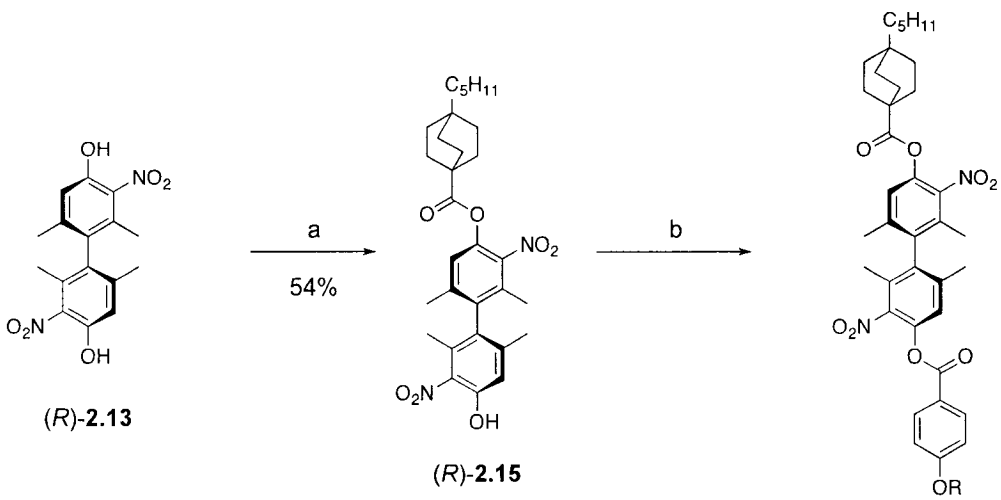

(*R*)-**2.13**

(*R*)-**2.15**

(*R*)-**2.16a**: R = OC_6H_{13}, 74 %
(*R*)-**2.16b**: R = OC_8H_{17}, 54 %
(*R*)-**2.16c**: R = $OC_{10}H_{21}$, 78 %
(*R*)-**2.16d**: R = $OC_{12}H_{25}$, 83 %
(*R*)-**2.16e**: R = $OC_{14}H_{29}$, 88 %

[a] (a) DCC, DMAP, CH_2Cl_2, 4-pentylbicyclo[2.2.2.]octane-1-carboxylic acid; b) DCC, DMAP, CH_2Cl_2, **a:** 4-hexyloxybenzoic acid; **b:** 4-octyloxybenzoic acid; **c:** 4-decyloxybenzoic acid; **d:** 4-hdodecyloxybenzoic acid; **e:** 4-tetradecyloxybenzoic acid.

2.2. Results and Discussion:

2.2.1. Polycatenar molecules

In order to promote mesogenic behaviour in molecules with the atropisomeric 3,3'-dinitrobiphenyl core the series of polycatenar derivatives **2.14a-e** were synthesized. Tetracatenar compounds (*R*)-**2.14a** and (*S*)-**2.14b** are solids at room temperature, but have no mesogenic properties. Both (*R*)-**2.14a** and (*S*)-**2.14b** are immiscible with the liquid crystalline host **PhP1** at $\chi_d \geq 0.05$; large isotropic regions were evident by polarized microscopy, indicating an incompatibility between polycatenar dopant and phenylpyrimidine host. The isotropic domains diminish on cooling, but are persistent just above the crystallization point. Such incompatibilities are likely the result of the lateral chain destabilizing the lamellar structure by inhibiting the close packing of **PhP1**.

The phase transition temperatures for mixtures of (*R*)-**2.14a** and (*S*)-**2.14b** in **PhP1** at $\chi_d = 0.05$ were determined by polarized microscopy (Table 2-1). Even though persistent isotropic domains were apparent, polarization measurements were conducted in the SmC* phase; the biphasic textures at 5 K below the Curie point ($T-T_C = -5$ K) are shown in Figure 2-4. At $T-T_C = -5$ K, the mixture of (*R*)-**2.14a** in **PhP1** has a spontaneous polarization (P_s) value of -0.97 nC/cm^2 with a tilt angle of 17°, which corresponds to a reduced polarization (P_o) of -3.2 nC/cm^2. A mixture of (*S*)-**2.14b** in **PhP1** has a P_s value of +1.99 nC/cm^2 and a tilt angle of 9°, which corresponds to a P_o of +13.4 nC/cm^2. The signs of polarization for (*R*)-**2.14a** and (*S*)-**2.14b** in **PhP1** are consistent with those observed for other 3,3'-dinitrobiphenyls of the same handedness in

PhP1. At the same reduced temperature and dopant mole fraction the P_o of (*R*)-**1.15d** is -86.2 nC/cm^2.[1] However, due to poor compatibility of the two polycatenar dopants in **PhP1** one cannot draw any conclusions from this comparison.

Table 2-1. Phase transitions (°C) for mixtures of (*R*)-**2.14a** and (*S*)-**2.14b** in host **PhP1** at χ_d = 0.05.

dopant	I	I+N	I+SmA	I+SmC	Cr
(*R*)-**2.14a**	92.5	95	79.7	42.3	
(*S*)-**2.14b**	-	90.7	76	40.8	

Consistent with literature observations, hexacatenar compound (*S*)-**2.14e** was obtained as an oily liquid and did not crystallize at temperatures as low as -78°C.[4] Hexacatenar compounds normally have very low clearing points and are solids at room temperature when they have at least five or more rings in the core. Compound (*S*)-**2.14e** features only 4 aryl rings and is likely too short to be mesogenic. Both (*R*)-**2.14c** and (*S*)-**2.14d** were obtained as oily liquids and, like their hexacatenar analogue, did not form a crystalline phase at temperatures as low as -78°C. Considering that these materials are oils, and the incompatibility of (*R*)-**2.14a** and (*S*)-**2.14b** in **PhP1**, no further doping experiments were performed.

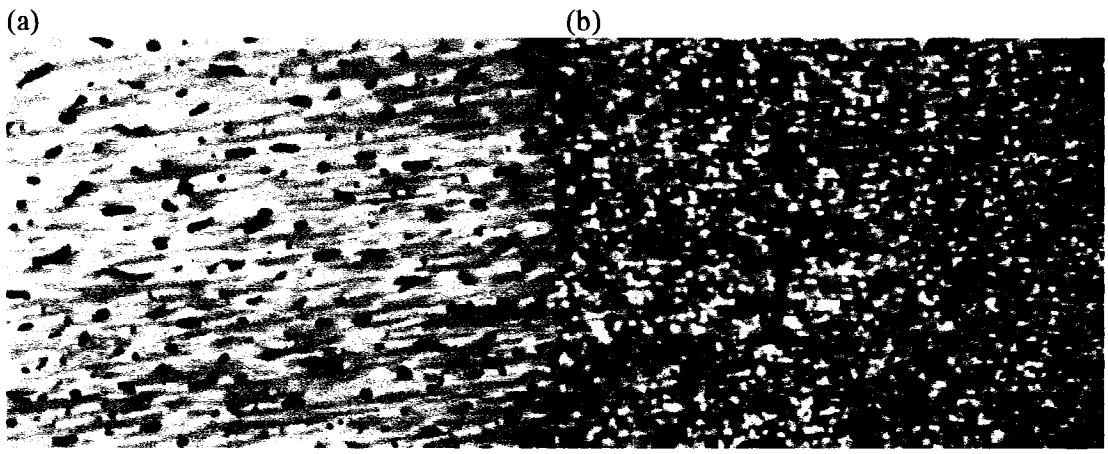

Figure 2-4. Texture of the SmC* phase for mixtures of (a) (*R*)-**2.14a** and (b) (*S*)-**2.14b** in **PhP1** 400X (χ_d = 0.05) at T-T_C = -5 K.

2.2.2. Unsymmetrical bicyclo[2.2.2.]octyl derivatives

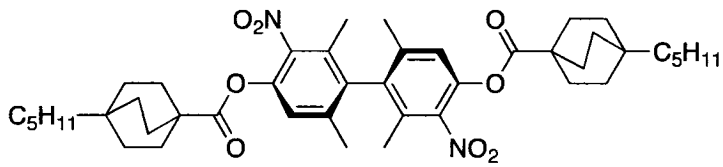

(*R*)-**2.17**

It has been shown previously in the Lemieux group that a derivative of the 3,3'-dinitrobiphenyl core with two 4-pentylbicyclo[2.2.2]octyl side-chains (*R*)-**2.17** forms an enantiotropic chiral nematic phase from 175 to 250 °C.[11] However, when used as a dopant, the polarization induced by (*R*)-**2.17** in **PhP1** at χ_d = 0.04 was below the detection limit. This was attributed to the bulky bicyclo[2.2.2]octyl groups preventing core-core interactions between the dopant and liquid crystal host.[11] As a compromise aimed at balancing the mesogenic properties and polarization, a homologous series of unsymmetrical derivatives with one bicyclo[2.2.2.]octyl side-chain and one 4-alkoxybenzoate side-chain (**2.16a-e**), were synthesized.

2.2.2.1. Mesogenic Properties

Compounds (*R*)-**2.16a-e** form chiral nematic phases with clearing points that decrease with increasing length of the alkoxy side-chain. On cooling the N* phase persists down to room temperature due to supercooling. The texture of the N* phase is shown in Figure 2-5. Representative Differential Scanning Calorimetery (DSC) traces for the first and second heating/cooling cycles are shown in Figure 2-6. The temperatures and enthalpies of transitions for the five derivatives are given in Table 2-2. Importantly, samples of (*R*)-**2.16a** and (*R*)-**2.16b** prepared for texture analysis exhibited selective reflection at room temperature, which is characteristic of a helical pitch on the order of the wavelength of visible light.

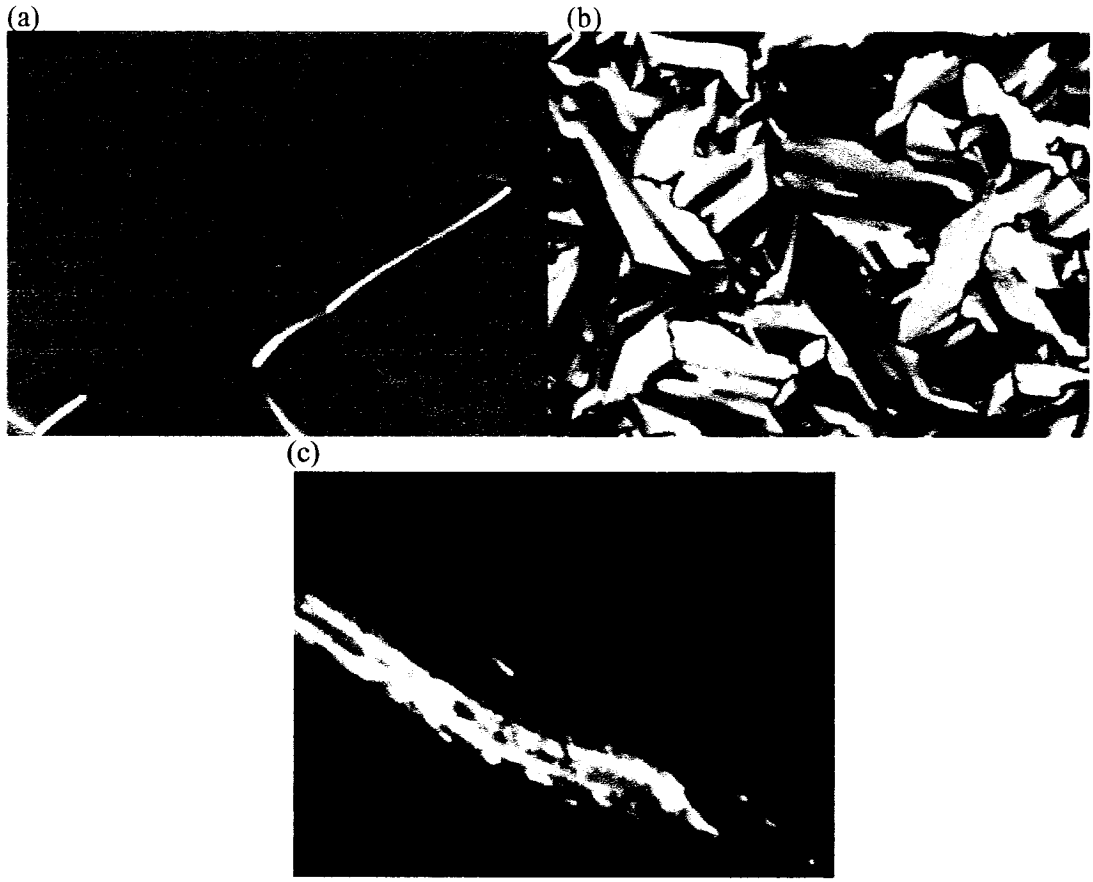

Figure 2-5. Texture of the N* phase of (*R*)-**2.16e** 400X (a) in a 4 mm rubbed polyimide coated cell (b) on a glass slide fitted with a cover slip on cooling, and (c) on the same glass slide after shearing the cover slip. All images were recorded at 145 °C and selective reflection in the red region of the visible spectrum is evident in (a) and (c).

Table 2-2. Phase transition temperatures (°C) and enthalpies of transition (in parentheses) of (*R*)-**2.16a-e** measured by DSC on heating.

compound	ΔH (J/g)	
	Cr	N I
(*R*)-**2.16a**	112.8 (33.4)	206.4 (2.3)
(*R*)-**2.16b**	95.6 (25.0)	183.1 (2.8)
(*R*)-**2.16c**	105.3 (45.0)	168.6 (2.2)
(*R*)-**2.16d**	107.9 (37.5)	157.8 (1.9)
(*R*)-**2.16e**	106.3 (52.3)	148.8 (1.4)

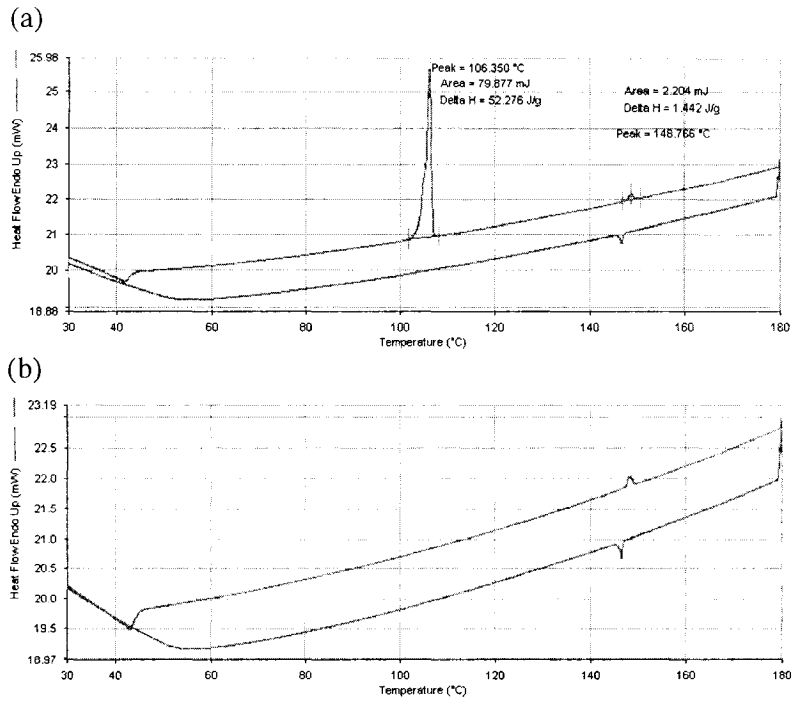

Figure 2-6. DSC trace of (a) first and (b) second heating/cooling cycles for (*R*)-**2.16e**.

2.2.2.2. Pitch measurements

The N* helical pitches of (*R*)-**2.16a-e** were measured as λ_{max} of selective reflection by UV-Vis spectroscopy. Samples were loaded into Grandjean-Cano wedge cells and placed on a vertically orientated hot stage. A deuterium-tungsten lamp was focused through the sample and the reflection spectrum was recorded (as absorbance) by an Ocean Optics photodetector interfaced to a computer. The pitch measurements were obtained on heating and Table 2-3 shows the helical pitch calculated 10 K below the N*-I transition. The slopes of the pitch vs. temperature plots, which give excellent least squares fits ($R^2 > 0.99$), are also shown in Table 2-3. A representative example of a

reflection spectrum and a plot of λ_{max} vs. reduced temperature are shown in Figure 2-7 and Figure 2-8 respectively.

Table 2-3. Pitch measurements, at $T-T_{NI} = -10$ K, and the slope of the pitch vs. reduced temperature plot for nematogens (*R*)-**2.16a-e**.

Mesogen	Pitch at $T-T_{NI} = -10$ K (nm)[a]	Slope (nm/K)
(*R*)-**2.16a**	1252 ± 12	3.4 ± 0.1
(*R*)-**2.16b**	1028 ± 18	4.6 ± 0.2
(*R*)-**2.16c**	786 ± 12	4.2 ± 0.2
(*R*)-**2.16d**	640 ± 5	4.7 ± 0.1
(*R*)-**2.16e**	585 ± 7	4.8 ± 0.2

[a] The pitch is calculated based on the regression line of the pitch vs. temperature plot. The error in the pitch and slope are ± 1 standard error.

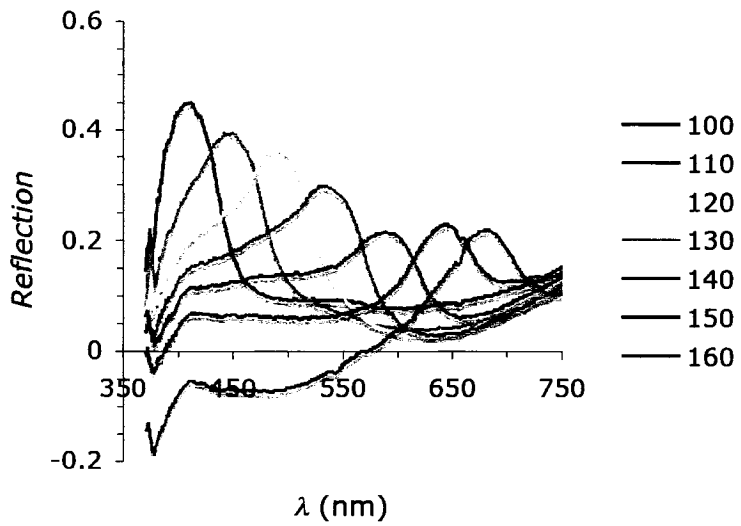

Figure 2-7. Reflection spectrum of (*R*)-**2.16d** at temperatures ranging from 100–160°C.

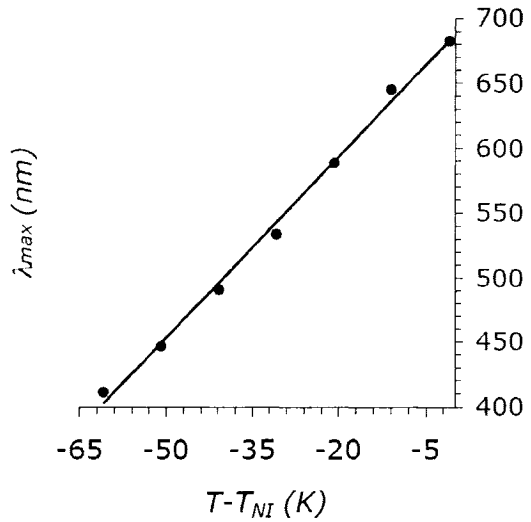

Figure 2-8. Plot of the pitch of (*R*)-**2.16d** vs. reduced temperature. Solid line indicates least squares best fit.

Except for **2.16a**, the slope values are more or less the same, which suggests that compounds **2.16b-e** have similar thermal expansion coefficients. The pitch at $T-T_{IN} = -10$ K decreases with increasing alkoxy chain length, which can be rationalized by considering the excluded volume of the tail, which increases with increasing chain length. An increase in excluded volume at one end makes the molecule more wedge-shaped. The wedge is cone-shaped due to the zigzag shape of the tail, which can rotate freely about the Ar-O bond (Figure 2-9). By virtue of the form chirality of the N* phase, these wedges are offset from one layer to the next, the magnitude of the offset should increase with increasing excluded volume. Assuming similar thermal expansion coefficients, an increase in angular offset, requires fewer molecules to achieve a full helical twist, thus resulting in a shorter pitch (Figure 2-10).[12]

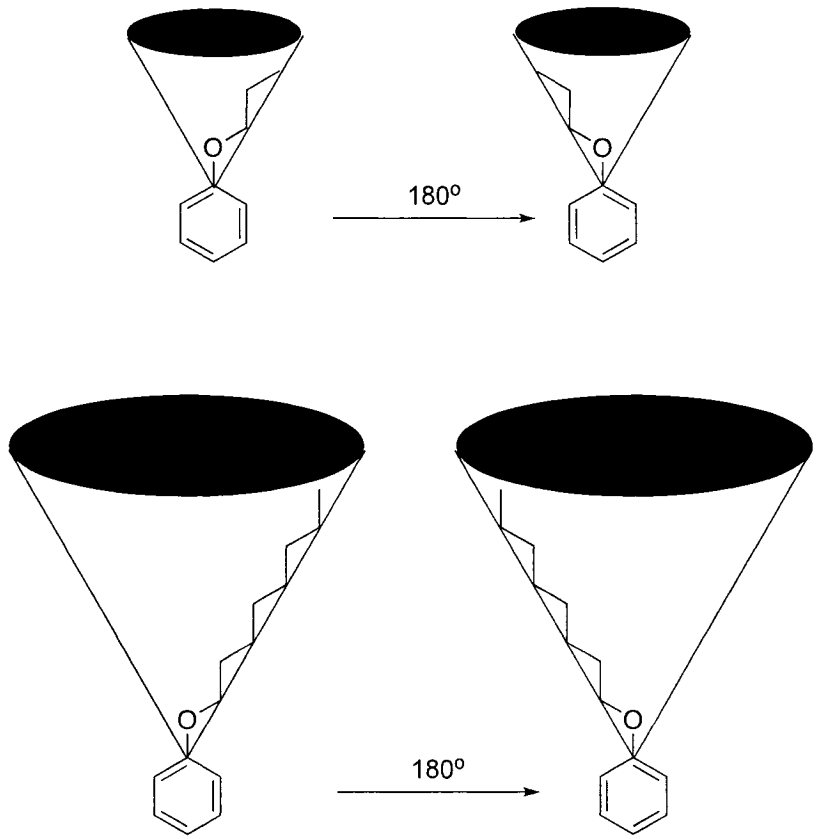

Figure 2-9. Cone shape of the alkoxy tail, which defines the excluded volume.

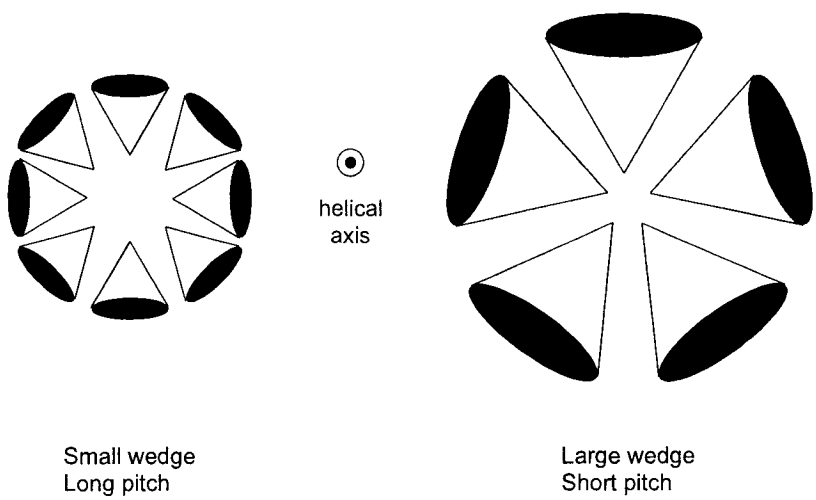

Figure 2-10. Schematic of the packing of wedge shapes in the N* phase looking down the helical axis.

The helical pitch of (*R*)-**2.16a-e** increases with increasing temperature instead of the more commonly observed decrease in pitch; such temperature dependence of the pitch is extremely rare for pure nematic materials, but is more commonly observed in induced N* systems.[13] Durand reported the first example of this type of temperature dependence in 1967 for the cholesterol derivative **2.17**.[14] Compound **2.18** is another cholesterol derivative that exhibits this unusual temperature dependent-pitch.[15] These two cholesterol derivatives do not have an underlying SmA* phase. Apart from the cholesterol core, a common structural feature of these mesogens is a branching element at the end of one side-chain; a methyl group at the 5-position in **2.17** and a methyl ester group in **2.18**. These branching elements decrease the aspect ratio and, more importantly, increase the excluded volume at one end relative to the other, which is a feature also found in **2.16a-e**.

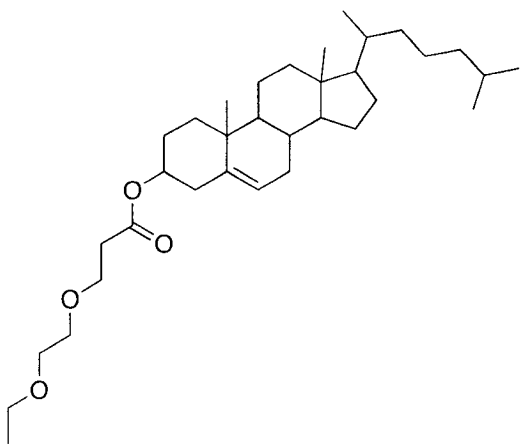

2.17; Cr 15 N* 31 I
(from ref. 15)

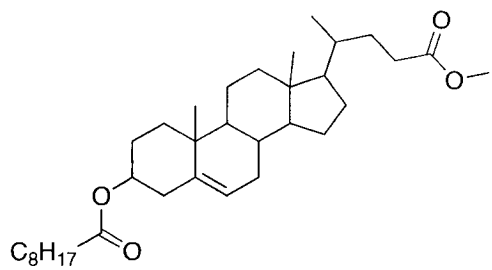

2.18; Cr 63 N* 79 I

There are two competing intrinsic properties, which will affect the temperature dependence of the helical pitch of a chiral nematic phase.[12] The first is the thermal expansion coefficient which controls the intermolecular separation of mesogens in the N* phase along the helical axis. With heating, the intermolecular separation increases, causing the pitch to increase. The second property is the increase in helical twist with increasing temperature due to a decrease in the twist elastic constant (k_{22}).[12] The twist elastic constant is the force required to return an achiral nematic mesogen back to the director after an external stimulus. In the case of cholesteric materials k_{22} is an intrinsic property by virtue of the form chirality of the N* phase. Most N* materials show a decrease in pitch with increasing temperature due to the decrease in k_{22} being a stronger force than thermal expansion.[12] These two competing factors are shown schematically in Figure 2-11. Since the helical pitch values for (*R*)-**2.16a-e** increase with increasing temperature suggests the changes in pitch associated with thermal expansion is greater than the change associated with a decrease in k_{22}.

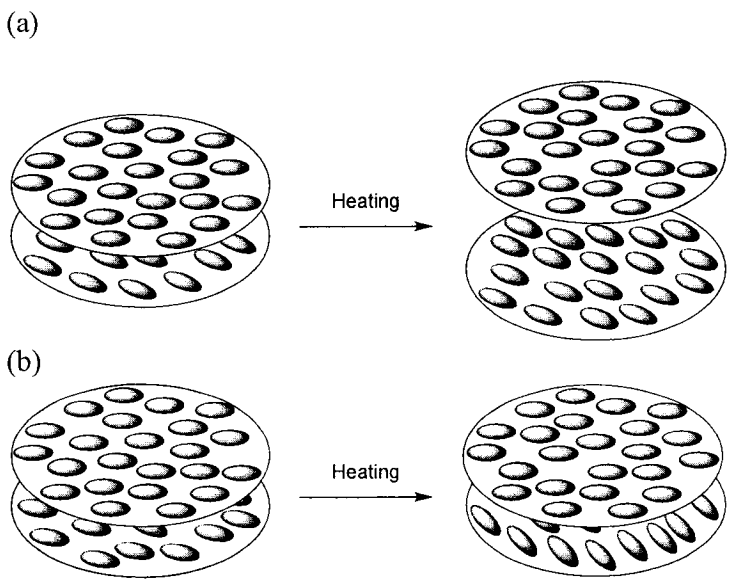

Figure 2-11. Schematic representation of (a) the thermal expansion of the N* phase on heating and (b) the increase in helical twist due to a decrease in k_{22} on layer to the next.

*2.2.2.3. Polarization measurements of (R)-***2.16d** *in* **PhB**, **DFT** *and* **NCB76**

As a representative of the series (*R*)-**2.16a-e**, compound (*R*)-**2.16d** was used to measure the induced polarization in four liquid crystalline hosts (**PhB**, **DFT**, **NCB76** and **PhP1**). This compound was chosen because its length (41.4 Å) is similar to that of the atropisomeric 3,3'-dinitrobiphenyl with 4-nonyloxybenzoate side-chains, (*R*)-**1.15e** (45.4 Å) according to molecular modeling at the AM1 level.[16] Reduced polarizations, P_o, were measured for mixtures of (*R*)-**2.16d** in **PhB**, **DFT** and **NCB76** at $\chi_d = 0.05$ and are listed in Table 2-4 along with the corresponding P_o values for mixtures of (*R*)-**1.15d** in these hosts at $\chi_d = 0.05$. The sign of polarization is consistent with that induced by (*R*)-**1.15d** in the same hosts.[1]

Table 2-4. P_o values, measured at $T-T_C = -5$ K for mixtures of (*R*)-**1.15e** and (*R*)-**2.16d** in the hosts **PhB**, **DFT** and **NCB76** at $\chi_d = 0.05$.

dopant	P_o (nC/cm^2)[a]		
	PhB	**DFT**	**NCB76**
(*R*)-**1.15e**	+1.7	-15.6	-25.7
(*R*)-**2.16d**	+9.8	-0.4	-5.1

[a] P_o values of (*R*)-**1.15e** are derived from δ_p values in reference 1.

A common trend of P_o values for mixtures of (*R*)-**2.16d** and (*R*)-**1.15e** in **DFT**, **PhB**, and **NCB76**, is a shift towards less negative (more positive) values going from (*R*)-**1.15e** to (*R*)-**2.16d**. Considering that the magnitude of the transverse dipole, $\mu_\perp$, of both (*R*)-**2.16d** and (*R*)-**1.15e** should be approximately the same, this trend may be explained by a shift in rotational distribution of the dopant in the binding site of each host in the same sense. In the two cases with a negative reduced polarization the shift in rotational

distribution would be towards the tilt plane; in the case with positive reduced polarization the shift would be toward the polar axis (Figure 2-12).

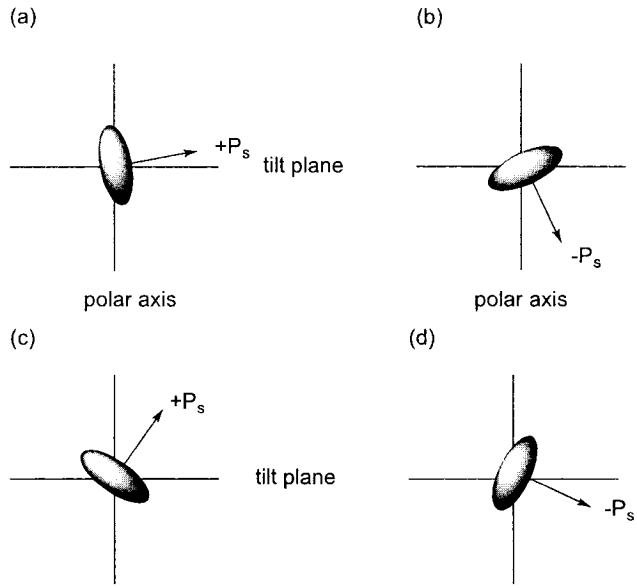

Figure 2-12. Schematic of the orientation of the transverse dipole of (*R*)-**1.15e** in (a) **PhB** and (b) **NCB76** and **DFT**; (*R*)-**2.16d** in (c) **PhB** and (d) **NCB76** and **DFT.**

*2.2.2.4. Doping experiments of (R)-***2.16d** *in* **PhP1**

2.2.2.4.1. Solubility

A phase diagram for (*R*)-**2.16d** in **PhP1** was constructed to assess the compatibility of the mesogenic dopant relative to its non-mesogenic analogues, such as (*R*)-**1.15e**. As shown in Figure 2-13, the temperature range of the N* and SmA* phases are broadened with increasing χ_d of (*R*)-**2.16d** at the expense of the SmC* phase. This is consistent with the higher degree of out-of-layer fluctuations in the orthogonal SmA* phase, which can accommodate the lateral bulk of the atropisomeric core by decreasing core-core interactions with host molecules.

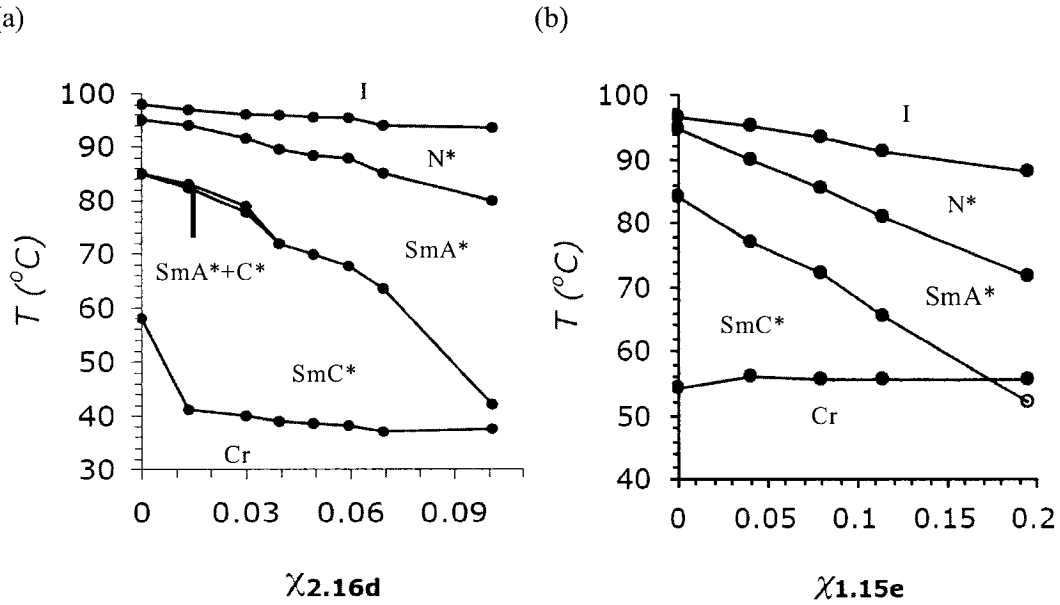

Figure 2-13. Phase diagram of (a) (*R*)-**2.16d** in **PhP1** on cooling and (b) (*R*)-**1.15e** in **PhP1** on heating. The SmC* of the χ_d = 0.20 mixture is monotropic (○). The phase diagram is regenerated from ref. 10.

The dopant (*R*)-**2.16d** causes a more pronounced destabilization of the SmC* phase of **PhP1** than its non-mesogenic analogue, (*R*)-**1.15e**. It is important to note, however, that these two phase diagrams are not directly comparable since the data for (*R*)-**2.16d** was obtained on cooling while the data for (*R*)-**1.15e** was obtained on heating.[3] There is a discrepancy between the observed SmC*-Cr transition temperature because the mixture of (*R*)-**2.16d** in **PhP1** undergoes supercooling. This phenomenon was also observed with mixtures of (*R*)-**1.15e** in **PhP1**: a sample with χ_d = 0.02 crystallized at 40 °C, whereas pure **PhP1** crystallized at 58 °C.[1] The mixture of (*R*)-**2.16d** in **PhP1** at χ_d = 0.10, however, does not show a spontaneous polarization on heating in a 4 μm cell with an applied voltage of 6 V/μm, thus indicating the absence of a SmC* phase. These results suggest that (*R*)-**2.16d** destabilizes the SmC* of **PhP1** to a greater extent than (*R*)-

1.15e. This may be due to the fact that, unlike (*R*)-**1.15e**, the lateral bulk of (*R*)-**2.16d** extends beyond the 3,3'-dinitrobiphenyl core.

2.2.2.4.2. Polarization Measurements

Compound (*R*)-**2.16d** was doped into the liquid crystalline host **PhP1** up to χ_d = 0.10 and gave good alignment of the SmC* phase in 4 μm rubbed polyimide ITO cells. A plot of P_o vs. χ_d at $T-T_C$ = -5 K gave a good linear fit (R^2 = 0.94) corresponding to a δ_p value of -976 ± 104 nC/cm^2 (Figure 2-14). The value of δ_p is approximately 50% of that reported for (*R*)-**1.15d** in **PhP1** (1738 ± 95 nC/cm^2)[1], but is much greater than that reported for the symmetrical bicyclo[2.2.2.]octyl derivative, which is less than 30 nC/cm^2.[11] The reduced δ_p value observed for (*R*)-**2.16d**, compared to (*R*)-**1.15d** can be explained, in part, by a shift in the rotational distribution of the dopant in the binding site of the host towards the tilt plane. The laterally bulky bicyclo[2.2.2.]octyl group of (*R*)-**2.16d** may also reduce the degree of chirality transfer, with respect to (*R*)-**1.15d**, in **PhP1** by reducing the degree of core-core interaction. This reduction of chirality transfer could decrease the δ_p based on the CFT model and was listed as the primary factor for the very low polarization power of (*R*)-**2.17** in **PhP1**.[11]

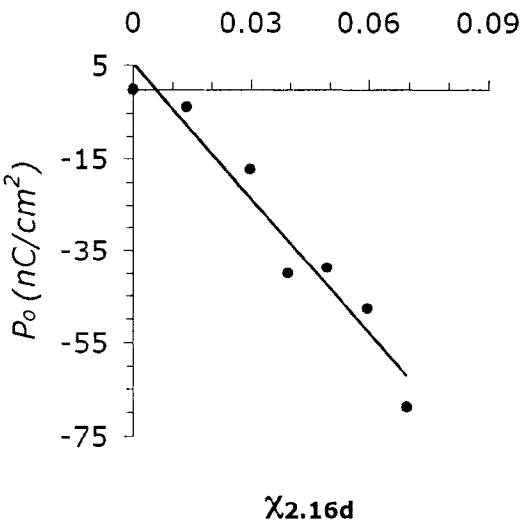

Figure 2-14. Plot of P_o vs. χ_d for (*R*)-**2.16d** in **PhP1** at T-T_C = -5 K. Solid line indicates least squares best fit.

2.2.2.4.3. Electroclinic Measurements

Upon investigation of the spontaneous polarization induced by (*R*)-**2.16d** in the liquid crystalline host **PhP1,** a polarization could be measured above the SmA*-SmC* transition which is consistent with an electroclinic effect. The largest observed electroclinic polarization was approximately 9 nC/cm^2 with an applied field of 6 V/μm at a χ_d = 0.10. The electroclinic polarization is closely related to the spontaneous polarization observed in SmC* materials and is described by the same symmetry argument developed by Meyer (see section 1.2.3.2). The electroclinic effect is derived from Landau theory which predicts θ is directly proportional to the applied field strength E (at low field) by the following relationships[17]:

$$\theta = e_c E \qquad (2.1)$$

$$e_c = \frac{c}{\alpha(T - T_C)} \qquad (2.2)$$

where α is a non-chiral parameter known as the tilt susceptibility coefficient, which describes the torque taking the director back to the layer normal. The term c is a chiral parameter describing the coupling between the P_s and the tilt in the SmC* phase.

Compound (*R*)-**1.15e**, which induces very large spontaneous polarizations in **PhP1**, also induces a very strong electroclinic effect in mixtures with the same host. Inspired by the large polarizations observed in the SmA* phase for (*R*)-**2.16d** in **PhP1**, we sought to measure the electroclinic coefficient, e_c, for mixtures of (*R*)-**2.16d** in **PhP1** at χ_d = 0.06, 0.07 and 0.10. The induced tilt angles, θ, were determined by application of an AC square wave, with applied voltages ranging from 0 - 13.5 V/μm, at a frequency of 0.1 Hz. The tilt angles were measured as half the angle between the two extinction states observed by polarized microscopy. Relative temperatures of $T\text{-}T_C$ = +4, +2.5, +1.5 K were used to evaluate e_c. Measurements of electroclinic effect induced by chiral dopants on achiral hosts are sparse due to the inability of most dopants to induce a strong electroclinic response.

The induced tilt angles measured for mixtures of (*R*)-**2.16d** in **PhP1** increase with increasing E and show linear behaviour in samples with mole fractions of χ_d = 0.06 and 0.07 (R^2>0.95) except for the χ_d = 0.06 sample at $T\text{-}T_C$ = +2.5 K. The mixture of (*R*)-**2.16d** with a χ_d = 0.10 in **PhP1** shows nonlinear behaviour with E > 1 V/μm. For this mixture, tilt angles used for determining e_c were measured near 0 V to obtain linear fits

(R^2>0.90) which pass through the origin. The plots of θ vs. E are shown in Figure 2-15 and the values of e_c are shown in

Table 2-5.

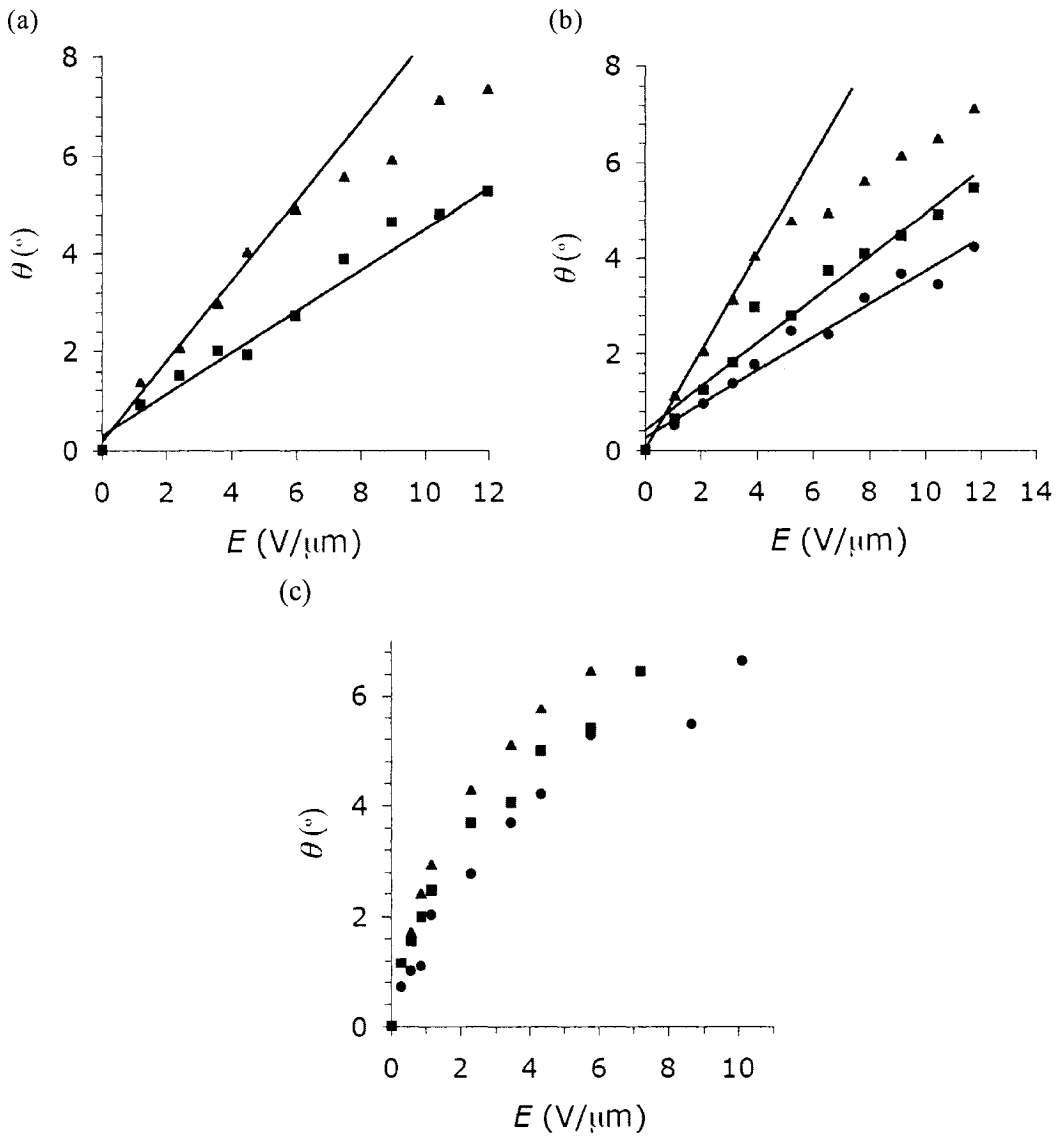

Figure 2-15. Induced tilt vs. applied voltage, E, for mixtures of (*R*)-**2.16d** in **PhP1** at (a) χ_d = 0.06, (b) χ_d = 0.07 and (c) χ_d = 0.10: T-T_C = +4 K as (●), T-T_C = +2.5 K as (◆) and T-T_C = +1.5 K as (■). The solid lines represent the least-squares fit used to determine e_c, except for (c) where lines of best fit are excluded for clarity. The e_c values were obtained by least-squares analysis on points from E = 0 – 1.2 V/μm.

Table 2-5. Electroclinic coefficients of (*R*)-**2.16d** in **PhP1**. Errors are ± 1 standard error.

	e_c (° μm/V)		
$T-T_{AC}$ (K)	χ_d 0.06	χ_d 0.07	χ_d 0.10
+4		0.46 ± 0.01	1.54 ± 0.26
+2.5	0.42 ± 0.05	0.53 ± 0.05	2.01 ± 0.28
+1.5	0.82 ± 0.04	1.01 ± 0.02	2.70 ± 0.23

The value of e_c for (*R*)-**2.16d** in **PhP1** (0.46 ° μm/V at $T-T_C$ = +4 K) at a mole fraction of χ_d = 0.07 is approximately twice the e_c observed for a mixture (*R*)-**1.15e** in **PhP1** (0.21 ° μm/V at $T-T_C$ = +5 K) at the same mole fraction, despite the fact the polarization power is approximately half in the same host. The value of e_c for (*R*)-**2.16d** can be extrapolated to 6.7 ° μm/V for χ_d = 1. This value is of the same order of magnitude as the mesogen with the largest electroclinic coefficient in the literature, **TSiKN6**, (e_c of 6-7 ° μm/V at $T-T_C$ = +5).[18] Previous research in the Lemieux group has determined that CTF is not a significant factor in the SmA* phase.[3] Mesogens that comprise the SmA* phase tilt as rigid rods under an applied field, and do not conform to the bent cylinder shape of the SmC* phase. For the dopant (*R*)-**1.15e**, the chiral parameter *c* did not change dramatically from host to host, but rather the tilt susceptibility, α, was the primary contributor to the e_c value. By virtue of similar stereopolar units, the value of *c* for (R)-**2.16d** and (*R*)-**1.15e** is expected to be very similar, and so any differences in e_c may be attributed to differences in α.

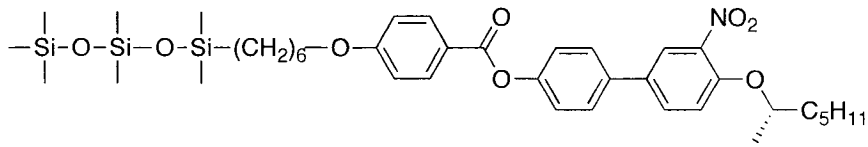

TSiKN65: SmC* 25 SmA* 56 I

2.3. References

(1) Vizitiu, D.; Lazar, C.; Halden, B. J.; Lemieux, R. P. *J. Am. Chem. Soc.* **1999**, *121*, 8229.

(2) Stegemeyer, H.; Meister, R.; Hoffmann, U.; Sprick, A.; Becker, A. *J. Mater. Chem.* **1995**, *5*, 2183.

(3) Hartley, C. S.; Kapernaum, N.; Roberts, J. C.; Giesselmann, F.; Lemieux, R. P. *J. Mater. Chem.* **2006**, *16*, 2329.

(4) Nguyen, H.-T.; Destrade, C.; Malthête, J. Phasmids and Polycatenar Mesogens. In *Handbook of Liquid Crystals*; Demus, D., Goodby, J., Gray, G. W., Spiess, H.-W., Vill, V., Eds.; Wiley-VCH: Weinheim, 1998; Vol. 2B, pp 865-885.

(5) Malthete, J.; Nguyen, H. G.; Levelut, A.-M. *J. Chem. Soc., Chem. Commun.* **1986**, *20*, 1548.

(6) Petrov, V. F.; Torgova, S. I.; Karamysheva, L. A.; Takenaka, S. *Liq. Cryst.* **1999**, *26*, 1141.

(7) Piecek, W.; Kaufman, J. M.; Kaszynski, P. *Liq. Cryst.* **2003**, *30*, 39.

(8) Januszko, A.; Kaszynski, P.; Drzewinski, W. *J. Mater. Chem.* **2005**, 5, 452.

(9) Januszko, A.; Glab, K. L.; Kaszynski, P.; Lewis, R.A.; Mehl, G. H.; Wand. M. D. *J. Mater. Chem.* **2006**, *16*, 3183.

(10) Hartley, C. S. Ph. D. Thesis, Queen's University, Kingston, 2005.

(11) Lazar, C. Ph.D. Thesis, Queen's University, Kingston, 2001.

(12) Gleeson, H. F. Thermography Using Liquid Crystals. In *Handbook of Liquid Crystals*; Demus, D., Goodby, J., Gray, G. W., Spiess, H.-W., Vill, V., Eds.; Wiley-VCH: Weinheim, 1998; Vol. 1, pp 823-838.

(13) Tamaoki, N. *Adv. Mater.* **2001**, *13*, 1135.

(14) Agócs, P. M.; Bata, L. *Mol. Cryst. Liq. Cryst.* **1984**, *107*, 391.

(15) Harada, T.; Crooker; P. *Mol Cryst. Liq. Cryst.* **1975**, *30*, 79.

(16) Vizitiu, D. Ph. D. Thesis, Queen's University, Kingston, 1999.

(17) Abdulhalim, I.; Moddel, G. *Liq. Cryst.* **1991**, *9*, 493.

(18) Spector, M. S.; Heiney, P. A.; Naciri, J.; Weslowski, B. T.; Holt, D. B.; Shashidhar, R. *Phys. Rev. E* **2000**, *61*, 1579.

Chapter 3. Use of microphase segregation to promote liquid crystalline behaviour in compounds containing an atropisomeric 3,3'dinitrobiphenyl core

Having established that a calamitic molecule with an atropisomeric 3,3'-dinitrobiphenyl core can form a nematic liquid crystal phase by the inclusion of one or two bulky 4-pentylbicyclo[2.2.2.]octyl group(s), we sought to harness microphase segregation to further promote smectic phases using semiperfluorinated alkanes and organosiloxane groups. Hence, the 3,3'-dinitrobiphenyl core was fitted with alkoxysiloxane, alkoxysiloxane benzoate and semiperfluorinated alkoxybenzoate side-chains as the means of promoting microphase segregation.

3.1. Synthesis and resolution

The atropisomeric 4,4'-dihydroxy-2,2',5,5'-tetramethyl-3,3'-dinitrobiphenyl core (**2.13**) was synthesized as described in Chapter 2 (Scheme 2-1). Both (*R*)- and (*S*)-**2.13** were coupled to 6-(1,1,3,3,5,5,5-heptamethyltrisiloxyl)-hexan-1-ol using the Mitsunobu reaction to give (*R*)- and (*S*)-**3.1**.[1] Reaction of (*R*)-**3.1** with 1-bromooctane and Cs_2CO_3 gave (*R*)-**3.2**; condensation of (*S*)-**3.1** with 4-octyloxybenzoic acid in the presence of DCC and DMAP gave (*S*)-**3.3** (Scheme 3-1). The central unit for (*R*,*R*)-**3.4**, 4-[6-(1,1,3,3,5,5 hexamethyl trisiloxanyl)-bis-hexyloxy]benzoic acid, was synthesized by

adapted literature procedures[2] and then condensed with (*R*)-**2.15** in the presence of DCC and DMAP to give (*R*,*R*)-**3.4** (Scheme 3-2).

Scheme 3-1[a]

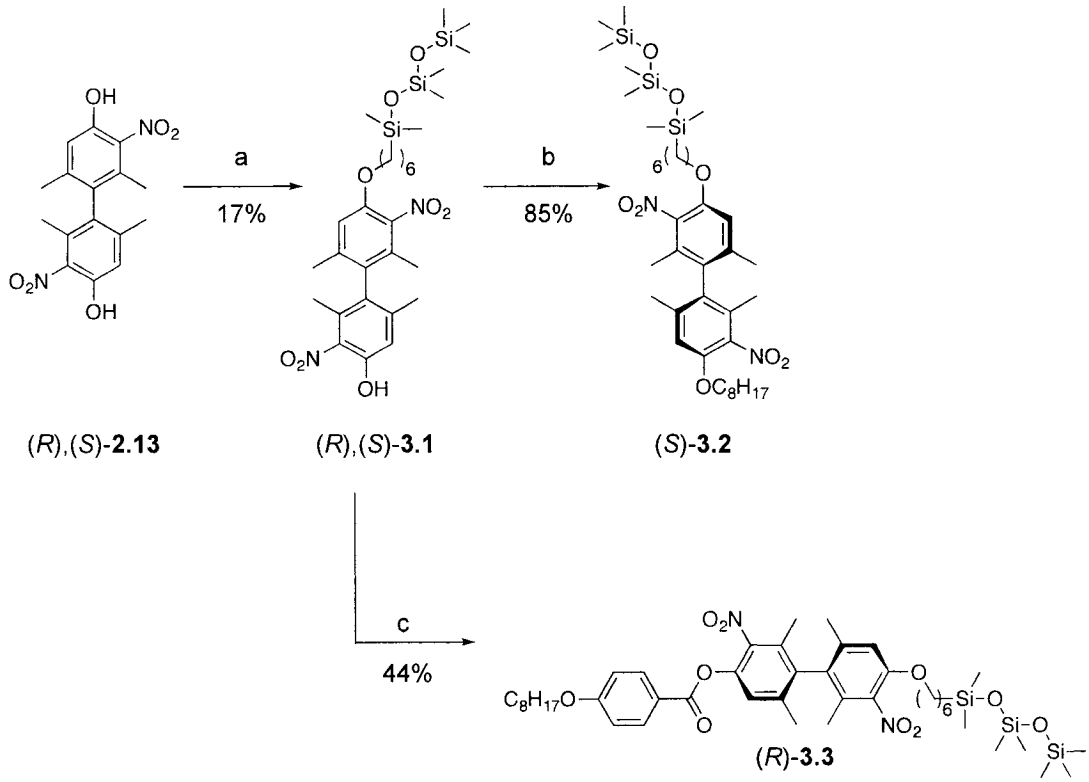

(*R*),(*S*)-**2.13** (*R*),(*S*)-**3.1** (*S*)-**3.2** (*R*)-**3.3**

[a] *Reagents and conditions*: (a) PPh_3, DIAD, 6-(1,1,3,3,5,5,5-heptamethylsiloxanyl)hexan-1-ol, CH_2Cl_2, Ar; (b) Cs_2CO_3, 1-bromooctane, CH_2Cl_2, Ar; (c) DCC, DMAP, 4-octyloxybenzoic acid, CH_2Cl_2, Ar.

Scheme 3-2[a]

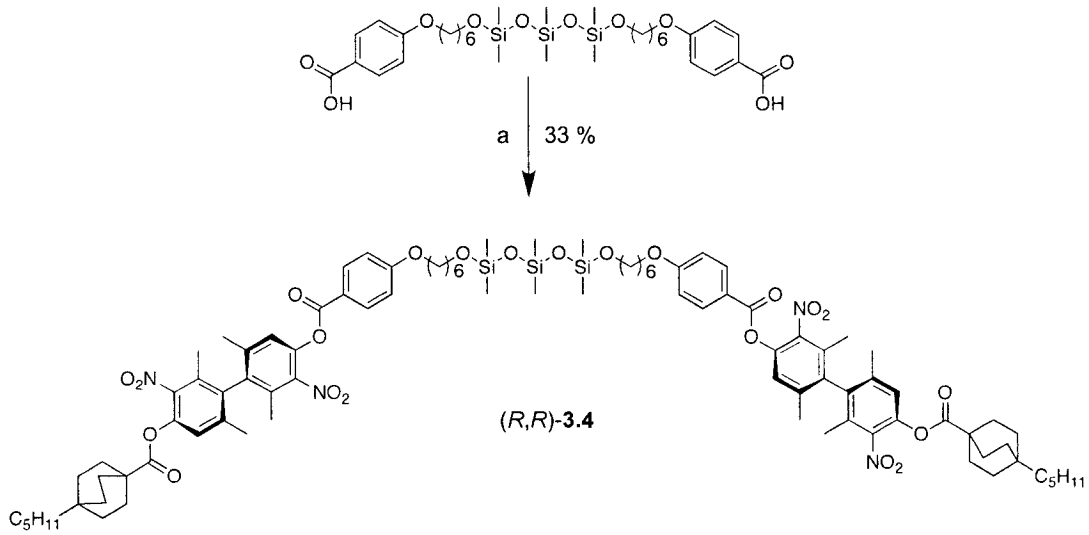

[a] *Reagents and conditions*: (a) DCC, DMAP, (*R*)-4-hydroxy-2,2',6,6'-tetramethyl-4'-[(4-pentylbicyclo[2.2.2]octan-1-oyl)oxy]-3,3'dinitrobiphenyl, CH_2Cl_2, Ar.

Semiperfluorinated derivatives with a 4-pentylbicyclo[2.2.2.]octyl side-chain were synthesized by condensation of (*R*)-**2.15** with 4-(3,3,4,4,5,5,6,6,7,7,8,8,9,9,10,10,10-heptadecafluoro)decyloxybenzoic acid or 4-(5,5,6,6,7,7,8,8,9,9,10,10,10-tridecafluoro)decyloxybenzoic acid in the presence of DCC and DMAP to give to give (*R*)-**3.5** and (*S*)-**3.6** respectively (Scheme 3-3). The 4-octyloxybenzoate analogue (*S*)-**3.8** was synthesized by first condensing (*S*)-**2.13** with 1.05 equivalents of 4-octyloxybenzoic acid in the presence of DCC and DMAP to give (*S*)-**3.7,** followed by coupling with 4-(5,5,6,6,7,7,8,8,9,9,10,10,10-tridecafluoro)decyloxybenzoic acid in the presence of DCC and DMAP (Scheme 3-4).

Scheme 3-3[a]

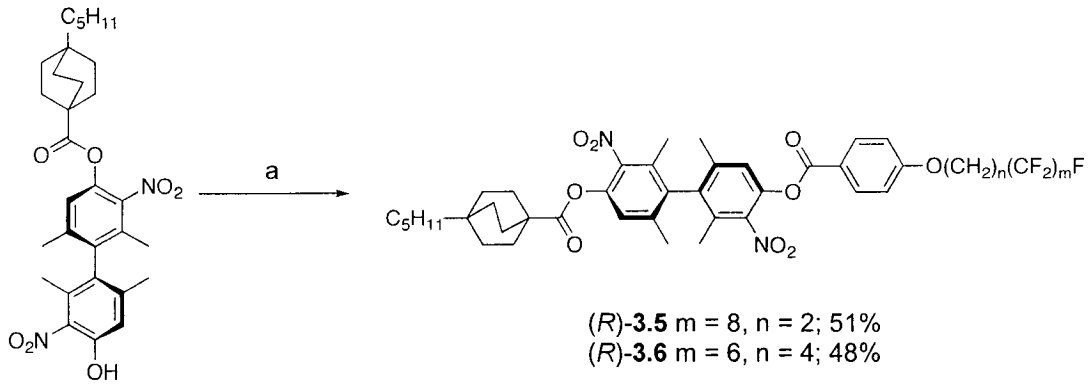

(*R*)-**2.15**

[a] *Reagents and conditions*: (a) DCC, DMAP, CH_2Cl_2, Ar; (**3.5**) 4-(5,5,6,6,7,7,8,8,9,9,10,10,10-tridecafluoro)decyloxybenzoic acid; (**3.6**) 4-(3,3,4,4,5,5,6,6,7,7,8,8,9,9,10,10,10-heptadecafluoro)decyloxybenzoic acid.

Scheme 3-4[a]

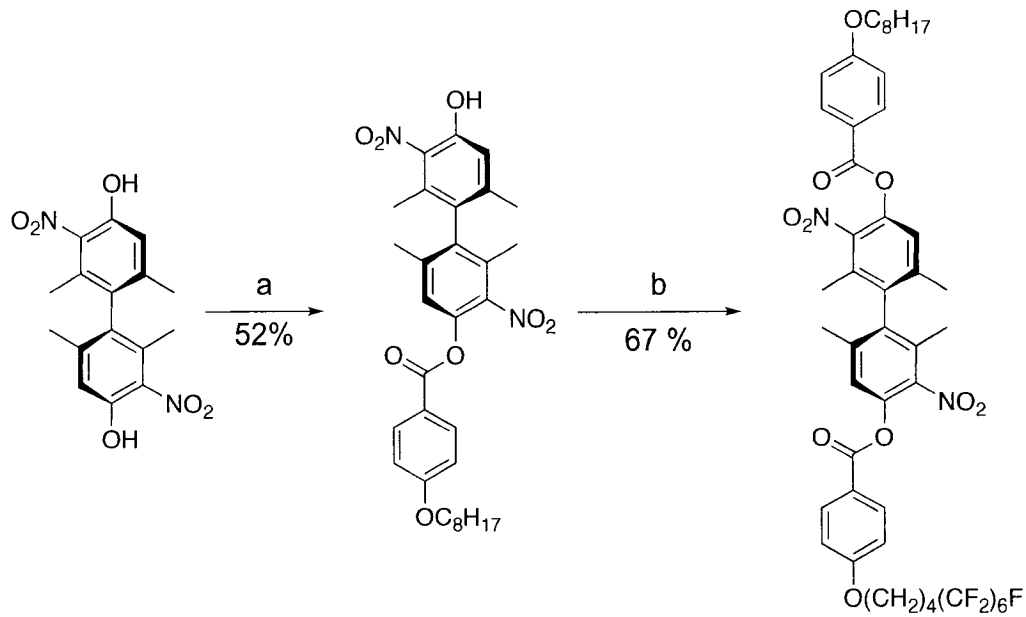

(*S*)-**2.13** (*S*)-**3.7** (*S*)-**3.8**

[a] Reagents and conditions: (a) DCC, DMAP, 4-octyloxybenzoic acid, CH_2Cl_2, Ar; (b) DCC, DMAP, 4-(5,5,6,6,7,7,8,8,9,9,10,10,10-tridecafluoro)decyloxybenzoic acid, CH_2Cl_2, Ar.

3.2. Organosiloxane groups

3.2.1. Siloxane-terminated atropisomers as dopants in a siloxane terminated host

The addition of oligomeric siloxane end-groups to the atropisomeric 3,3'-dinitrobiphenyl core was undertaken for two reasons. First, we sought to increase the solubility of the dopant in a SmC siloxane host without disrupting the lamellar ordering. Secondly, microphase segregation would allow for better control of the degree of core-core interaction between host and dopant by varying the length of the tether linking the core to the siloxane end-group. Two types of dopants were synthesized: (*R*)-**3.2**, with one trisiloxane-terminated alkoxy side chain and one octyloxy side-chain, and (*S*)-**3.3** with a trisiloxane-terminated alkoxy side-chain and a 4-octyloxybenzoate side-chain. These two compounds are both oils at temperatures as low as -78 °C. Each was doped into a trisiloxane-terminated phenylpyrimidine **3.9**, which was synthesized by members of the Lemieux lab. Compound **3.9** is analogous to the liquid crystalline host **PhP1**, and polarization measurements were carried out.

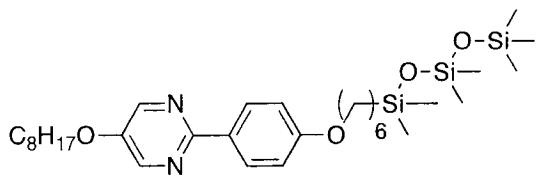

3.9: Cr 26 SmC 75 SmA 77 I

The bis-alkoxy derivative (*S*)-**3.2** is immiscible with **3.9** at mole fractions of $\chi_d \geq 0.05$, as indicated by polarized microscopic analysis showing persistent isotropic/SmC*

biphasic textures at temperatures as low as 20 °C. A spontaneous polarization value of +0.14 nC/cm^2 and a tilt angle of 11° were measured at T-T_C = -5 K for a mixture of (*S*)-**3.2** in **3.9** at χ_d = 0.05. This corresponds to a P_o value of +0.80 nC/cm^2. The sign of polarization is consistent with that induced by the symmetrical 3,3'-dinitrobiphenyl derivatives (*S*)-**1.15** in **PhP1**. The P_o value of (*S*)-**3.2** in **3.9** is significantly lower than that induced by (*S*)-**1.15d** in **PhP1** at the same mole fraction (+86.9 nC/cm^2)[3], which is likely due to an effective mole fraction that is far less than χ_d = 0.05, as evidenced by the persistent isotropic domains in the SmC* phase (Figure 3-1).

The derivative (*R*)-**3.3** is also immiscible with **3.9** at $\chi_d \geq 0.05$. The SmC* phase and isotropic domains (Figure 3-1) coexist down to 20 °C. F or a χ_d = 0.05 mixture of (*R*)-**3.3** in **3.9** at T-T_C = -5 K the value of P_s is –0.75 nC/cm^2 with a tilt angle of 14°. This corresponds to a P_o value of –3.2 nC/cm^2, which is significantly lower than that induced by (*R*)-**1.15d** in **PhP1** at the same mole fraction (-86.9 nC/cm^2)[3]. The sign of polarization is consistent with the 3,3'-dinitrobiphenyl derivative (*R*)-**1.15d** in **PhP1**. This is due to an effective mole fraction of (*R*)-**3.2** in **3.9** that is also less than χ_d = 0.05. The presence of isotropic domains suggests that the 3,3'-dinitrobiphenyl core fitted with a siloxane-terminated alkoxy group ((*S*)-**3.2** and (*R*)-**3.3**) do not form a suitable host/guest pair with the siloxane-terminated phenylpyrimidine **3.9**.

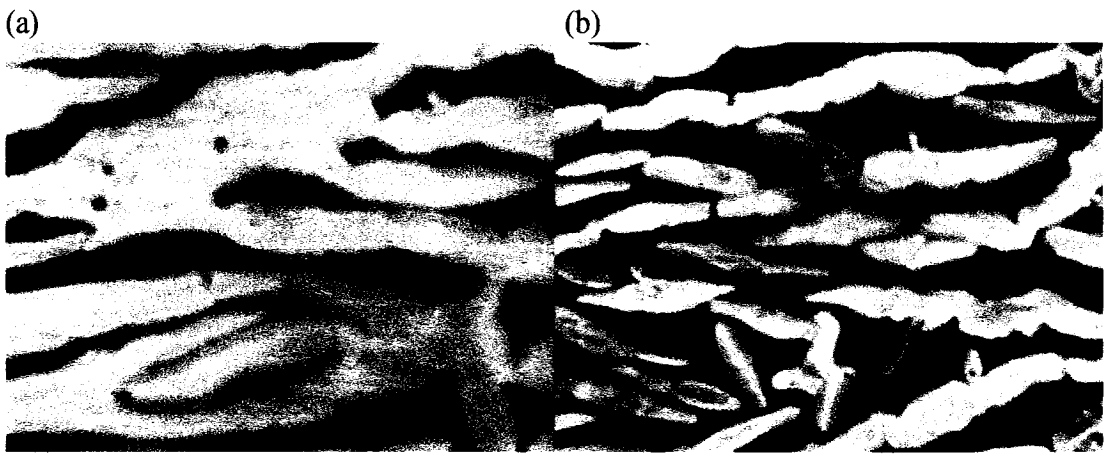

Figure 3-1. SmC* textures of (a) (*S*)-**3.2** and (b) (*R*)-**3.3** in the siloxane-terminated phenylpyrimidine host **3.9** 400X at a mole fraction of $\chi_d = 0.05$ observed at $T\text{-}T_C = -5$ K.

3.2.2. Oligomeric siloxanes as central a linking group

Despite the fact that mesogenic dimers linked by oligomeric siloxane groups tend to form antiferroelectric SmC_A* phases[2,4,5], the linking group used by Guillon[2] in (*R,R*)-**S-Si$_3$-S** was employed to tether two 3,3'-dinitrobiphenyl cores with a 4-pentylbicyclo[2.2.2.]octyl carboxylate group, resulting in compund (*R,R*)-**3.4**. This particular moiety was chosen since the bicyclo[2.2.2.]octyl side-chain promotes liquid crystalline properties in compounds containing the 3,3'-dinitrobiphenyl core.

Unlike the first class of 3,3'-dinitrobiphenyl derivatives with siloxane-terminated alkyl groups ((*S*)-**3.2** and (*R*)-**3.3**), compound (*R,R*)-**3.4** is a solid at room temperature and forms a chiral nematic phase between 149 and 165 °C. As with the unsymmetrical alkoxybenzoate series with a bicyclo[2.2.2.]octyl group, **2.16a-e**, the N* phase of (*R,R*)-**3.4** supercools down to temperatures as low as 20 °C. Identification of the N* phase by texture analysis was achieved by shearing the sample between the glass slide and cover

slip to obtain an oily streak texture commonly observed for the N* phase (Figure 3-2). The formation of the N* phase may be attributed to the presence of the short pentyl side-chains at each end which disfavours smectic phases. Because of their large lateral bulk, the bicyclo[2.2.2.]octyl groups as well as the 3,3'-dinitrobiphenyl core are likely to prevent the close packing of siloxane units. Although rare, there are other examples of compounds with oligomeric siloxane units that form a nematic phase. Examples include **3.10a-c**, which features oligomeric di-, tri- and tetrasiloxane groups on a lateral chain that is capped with a bulky tribenzosilatrane unit. The tribenzosilatrane group, although much closer to the siloxane functionality than the 3,3'-dinitrobiphenyl core in (*R,R*)-**3.4**, effectively prevents the self-assembly of the siloxane units.[6] The effectiveness of the suppression of microphase segregation is further demonstrated by the low enthalpies of the N-I transition for **3.10a-c** of 0.40, 0.17 and 0.16 J/g respectively, which suggests that the degree of disorder in the nematic phase is particularly high.

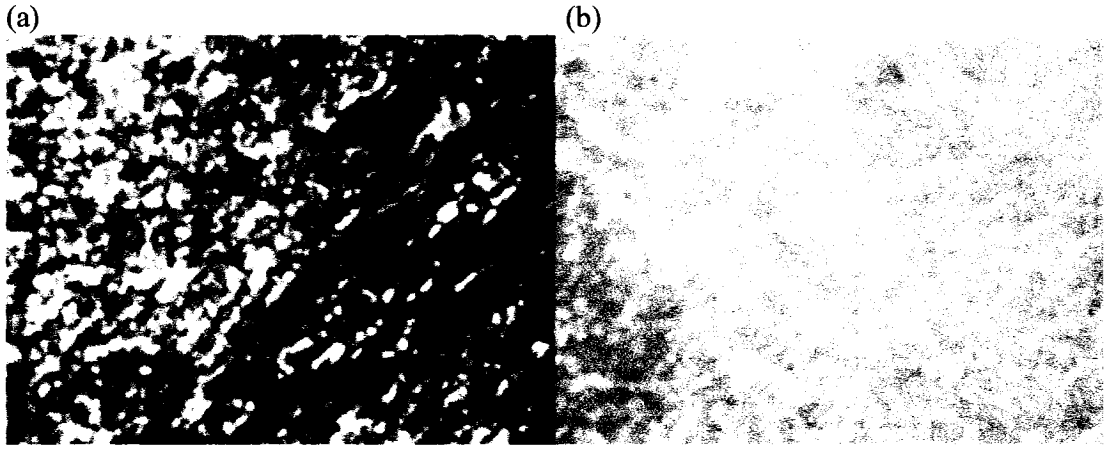

Figure 3-2. Texture of the nematic phase of (*R,R*)-**3.4** 400X at 154 °C on heating (a) before and (b) after shearing the cover slip.

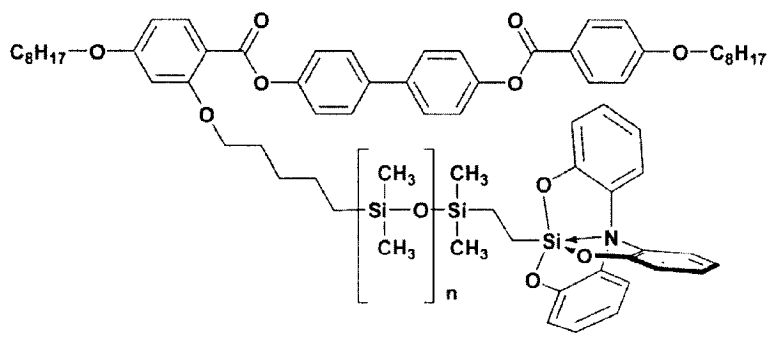

3.10

a: n = 1; g 12 N 57 I
b: n = 2; g 5 N 53 I
c: n = 3; g -4 N 51 I

Taken from ref. 6.

We sought to synthesize the bis-alkoxybenzoate analogue **3.11** as the reduced bulk at the periphery and longer aliphatic side-chains should promote smectic phases to a greater extent than for (*R*,*R*)-**3.4**. However, despite several attempts using **3.7** and DCC/DMAP coupling or synthesis by coupling the acid chloride of the siloxane core with **3.7** in CH_2Cl_2 with $N(Et)_3$ as a base, compound **3.11** could not be isolated. One identified product of this reaction was the bis-octyloxybenzoate **1.15e**, which suggests the ester linkage is cleaved and the newly formed carboxylic acid is free to react with an aryl hydroxy group.

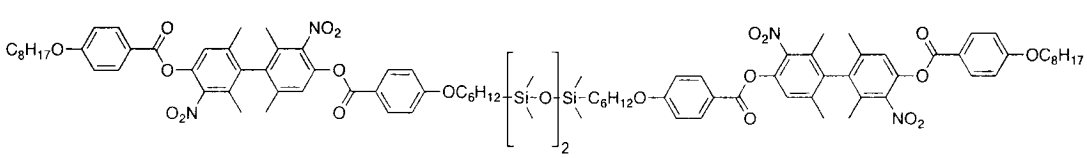

3.11

3.3. Semiperfluorinated groups

3.3.1. Compounds with a bicyclo[2.2.2.]octyl side-chain

3.3.1.1. Phase sequence

Semiperfluorinated alkyl tails were introduced to promote smectic phases in derivatives containing the 3,3'-dinitrobiphenyl core by harnessing the fluorophobic effect, which describes the incompatibility of highly fluorinated segments and hydrocarbon segments.[7]

Compound (*R*)-**3.5** was chosen as prototype based on the previous observation that one bicyclo[2.2.2.]octyl side-chain promotes mesogenic properties in compounds containing the 3,3'-dinitrobiphenyl core. According to DSC and polarized microscopic analysis, compound (*R*)-**3.5** forms a chiral SmA* phase from 185 to 225 °C on heating, and supercooling is evident in a 4 μm polyimide coated cell down to 128 °C. The SmA* and crystalline textures observed on cooling in a 4 μm polyimide coated cell without an applied field are shown in Figure 3-3.

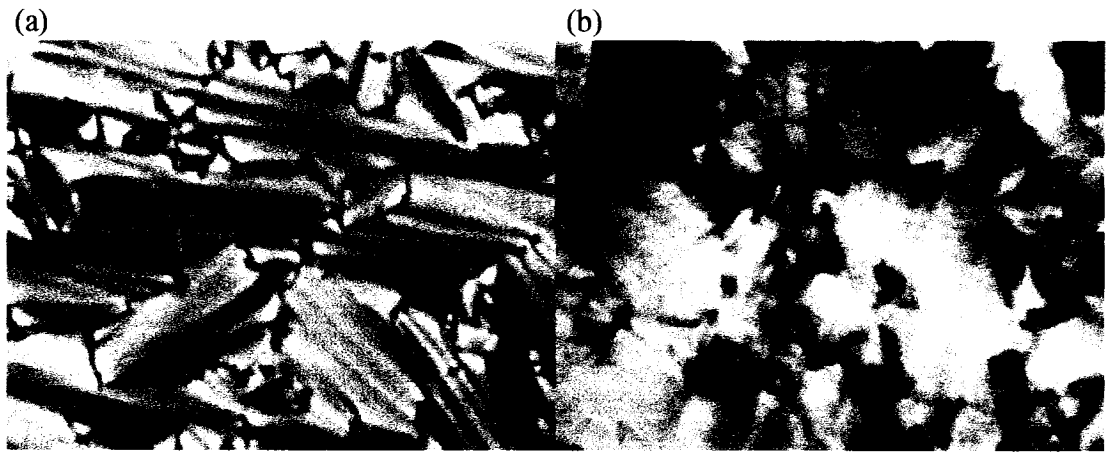

Figure 3-3. (a) SmA* and (b) crystalline textures of (*R*)-**3.5** 400X at (a) 200 °C and (b) 128 °C, observed by polarized microscopy in a 4 μm polyimide coated cell in the absence of an applied field.

Compound (*R*)-**3.5** was not explored as a dopant in the complementary host **PhP1** due to its chemical instability. As a solution in $CDCl_3$, a change in colour was observed from colourless to a yellow solution with a cloudy precipitate over the course of several days. (*R*)-**3.5** also decomposes at high temperature; after two heating/cooling cycles, the material from the DSC pan degrades into a yellow oil. Three heating/cooling cycles of the DSC are shown in Figure 3-4. It is evident that thermal decomposition occurs based on a decrease in clearing point and a decrease in the enthalpy of the transitions from one cycle to the next. The decomposed product was not characterized. Furthermore, the synthesis using 3,3,4,4,5,5,6,6,7,7,8,8,9,9,10,10,10-heptadecafluoro-1-iododecane gives a poor yield under standard alkylating conditions (Cs_2CO_3 in dry DMF) due to the competing elimination reaction that is inherent with this substrate.[8] With these problems identified, the structure was modified and the number of fluorinated carbons on the alkyl chain was reduced.

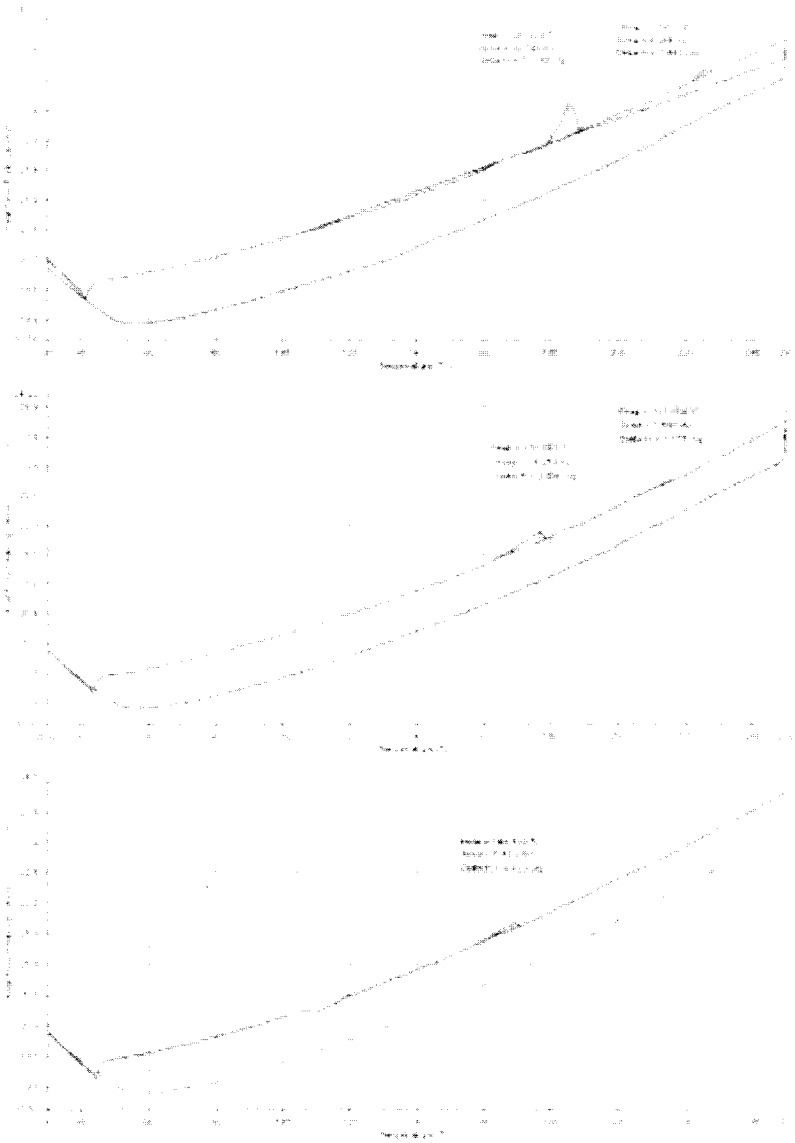

Figure 3-4. DSC trace of successive heating/cooling cycles of (R)-**3.5.**

We switched to a more commonly used semiperfluorinated alkyl side-chain that has a C4 alkyl spacer as opposed to a C2, thus reducing the likelihood of elimination. Like its predecessor (*R*)-**3.5**, (R)-3.6 forms only a SmA* phase from 148 to 192 °C ($\Delta H_{Cr\text{-}SmA}$ = 15.7 J/g, $\Delta H_{SmA\text{-}I}$ = 3.7 J/g); the texture of the SmA* phase is shown in Figure 3-5. The temperature range of the SmA* phase is reduced from 54 K for (*R*)-**3.5** to 44 K for

(*R*)-**3.6**, and the clearing point of (*R*)-**3.6** is 36 K degrees lower than that of (*R*)-**3.5**. The third heating/cooling cycle of the DSC for (*R*)-**3.6** (Figure 3-6) shows evidence of supercooling of the SmA* phase beyond -30 °C. Recrystallization occurs during the heating cycle at approximately 120 °C. Unlike (*R*)-**3.5** the heating and cooling cycle is fully reproducible over at least 3 cycles, which suggests that (*R*)-**3.6** is thermally stable. The decrease in temperature range of the smectic phase and clearing point from (*R*)-**3.5** to (*R*)-**3.6** is consistent with observations by Liu and Nohira who demonstrated that the temperature range of the smectic phases increases with the degree of fluorination for the homologous series **1.10a-d**.[9]

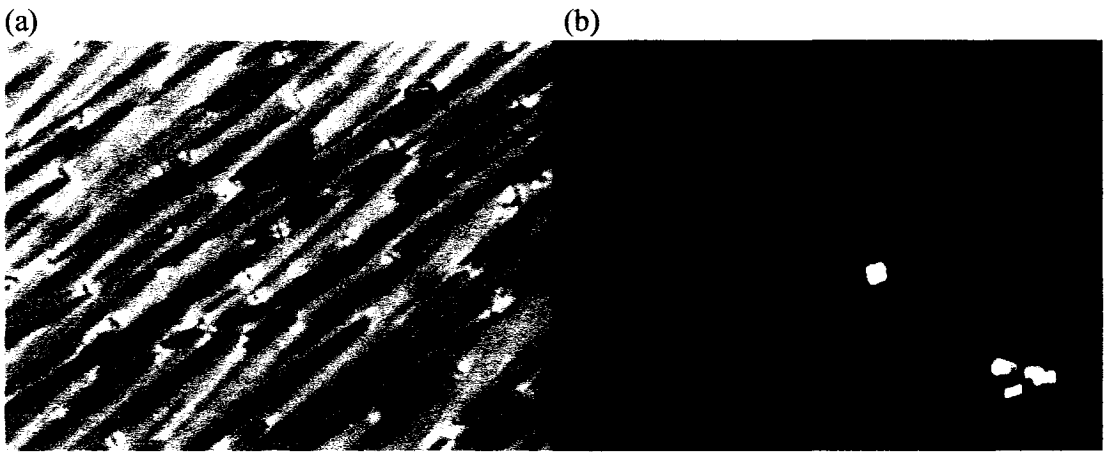

Figure 3-5. Texture of the SmA* of (*R*)-**3.6** 400X (a) in a polyimide-coated 4 μm cell without an applied field and (b) on a glass slide fitted with cover slip exhibiting homeotropic alignment.

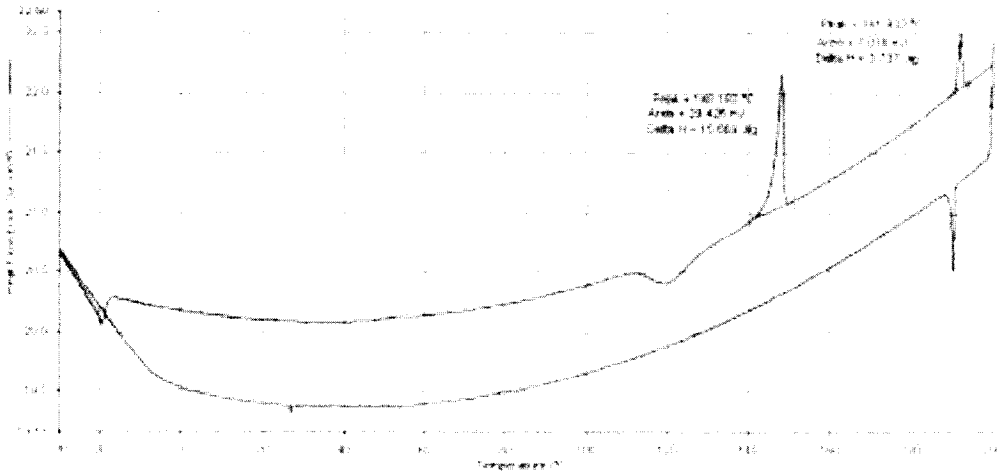

Figure 3-6. DSC trace of (*R*)-**3.6** on the third heating/cooling cycle.

3.3.1.2. Polarization measurements

The semiperfluorinated compound (*R*)-**3.6** was doped into the phenylpyrimidine host **PhP1** at a mole fraction of $\chi_d = 0.03$ to compare the induced polarization value with that of its hydrocarbon analogue with a dodecyloxy benzoate tail, (*R*)-**2.16d**. The transition temperatures of the mixture on cooling are I 98 N* 93 SmA* 82 SmC* 41 Cr; by comparison the transition temperatures on cooling for a $\chi_d = 0.03$ mixture of (*R*)-**2.16d** in **PhP1** is I 96 N* 92 SmA* 79 SmA*+SmC* 78 SmC* 40 Cr. Thus, it is evident that the SmC* phase of the host **PhP1** is destabilized to a lesser extent with the semiperfluorinated dopant, (*R*)-**3.6**, than with a hydrocarbon analog (*R*)-**2.16d**, at the same mole fraction.

The reduced polarization of a $\chi_d = 0.03$ mixture of (*R*)-**3.6** in **PhP1** is -10.4 nC/cm^2. The sign of polarization is consistent with that of other atropisomeric 3,3'-

dinitrobiphenyl dopants with the *R* configuration, such as (*R*)-**1.15d**, in **PhP1**.[3] This value is approximately 60% that of the P_o induced by (*R*)-**2.16d** (-17.1 nC/cm^2) in **PhP1**. The decrease in polarization observed for (*R*)-**3.6** may be attributed to the change in the rotational distribution of the transverse dipole of the dopant in the binding site of the **PhP1** host. Furthermore, by virtue of the increased excluded volume associated with the perfluorinated side-chain there may be a reduction in chirality transfer through core-core interactions. The fluorophobic segregation due to the presence of the fluorinated side-chain may also influence the positional order of the dopants in the binding site and consequently the degree of core-core interaction between dopant and host.

3.3.2. Compound with a benzoate side-chain

3.3.2.1. Phase sequence

In order to enable molecules to pack more efficiently, and improve core-core interactions, the bulky bicyclo[2.2.2.]octyl side-chain was substituted for an octyloxy benzoate group. The resulting compound (*S*)-**3.8**, forms an N*, twist grain boundary (TGBA*) and SmA* phases on cooling only (monotropic) and are observable on a glass slide fitted with a cover slip. The transition from I to N* is occurs at 127 °C and the texture of the chiral nematic phase exhibits selective reflection properties (Figure 3-7). Upon further cooling, the N* forms a TGB_A* phase at 107 °C, which is observable for approximately 1 K before the SmA* is formed. Textures of these two mesophases on a glass slide fitted with a cover slip are shown in Figure 3-8.

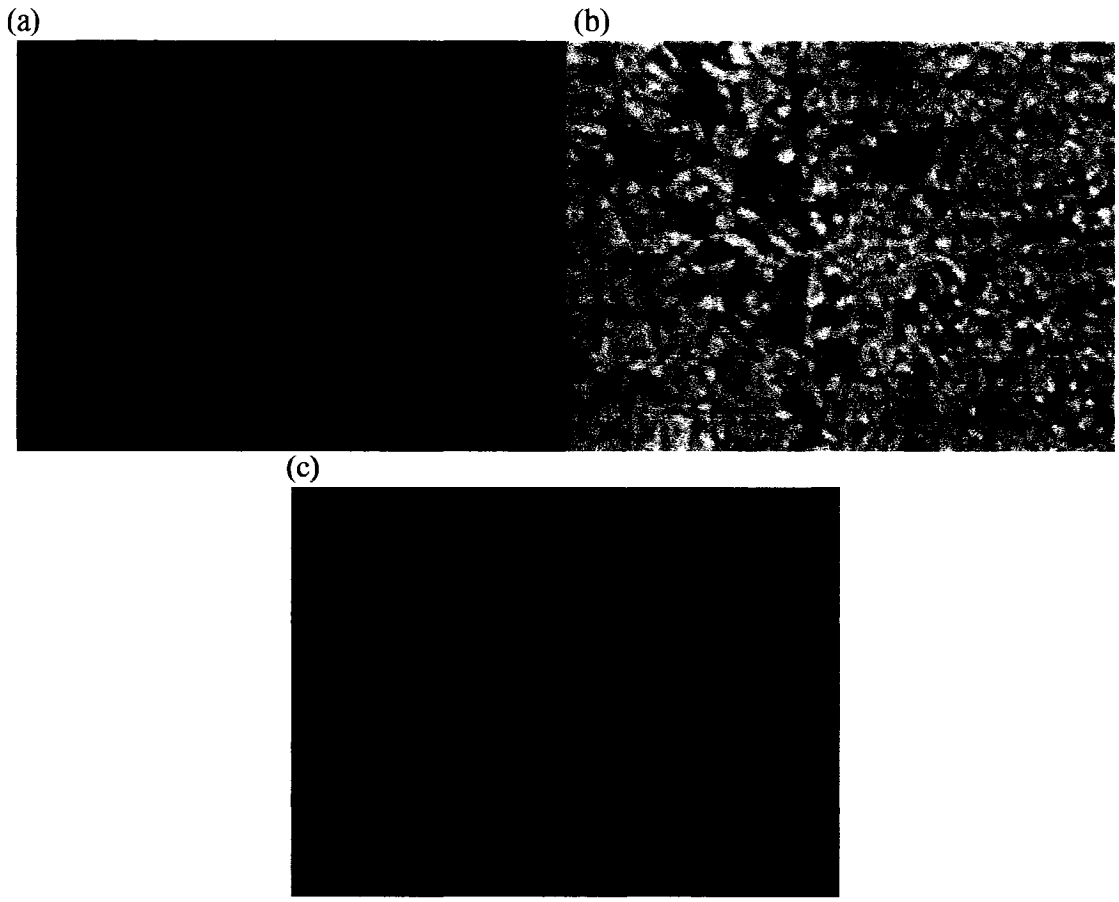

Figure 3-7. Texture of the nematic phase of (*S*)-**3.8** 400X, obtained in a polyimide coated 4 μm cell at 6 V/μm, showing selective reflection. The temperatures at which these phases are observed are (a) 114 °C, (b) 112 °C and (c) 110 °C.

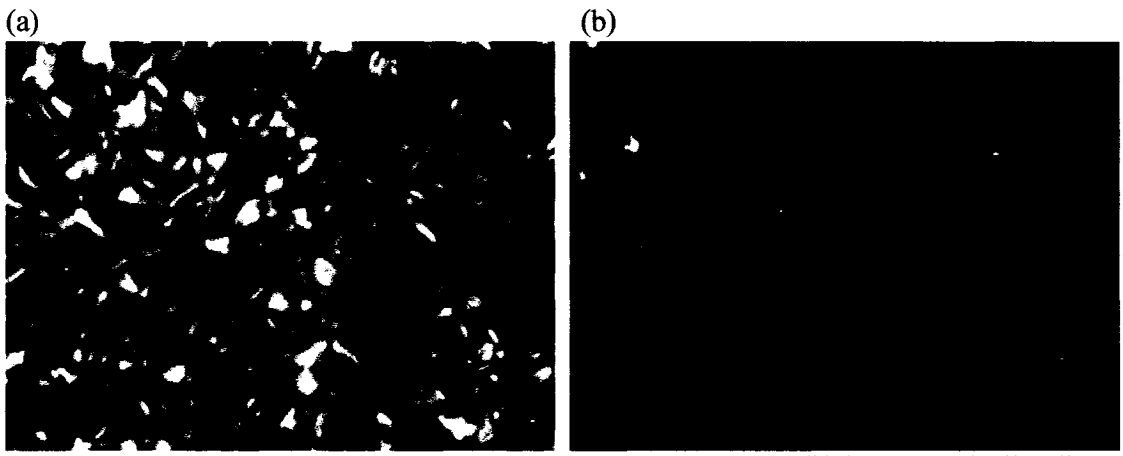

Figure 3-8. Texture of (a) the twist grain boundary (TGB_A*) and (b) homeotropically aligned SmA* phase of (*S*)-**3.8** 400X, obtained by polarized microscopy on a glass slide fitted with a cover slip at 107 °C and 100 °C, respectively.

The TGB_A* phase of (*S*)-**3.8** exhibits the filament texture which is normally observed for samples with homeotropic anchoring conditions, which was confirmed by the dark texture of the underlying SmA* phase (Figure 3-8). The TGB_A* phase, when observed in neat materials, usually has a very narrow temperature range on the order of ~1 K, which is consistent with our observation. Since compounds forming N* phase with semi-perfluorinated side-chains are rare, no examples of mesogens forming a TGB_A* phase with a perfluorinated tail could be found in the literature. Compounds (*S*)-**3.12** and (*R*)-**3.13** are examples of mesogens that form a TGB_A* phase.[10]

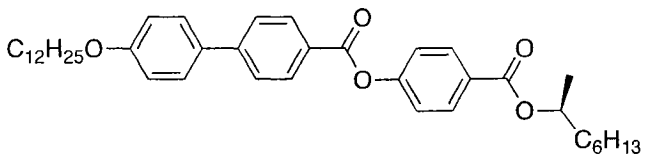

(*S*)-**3.12**

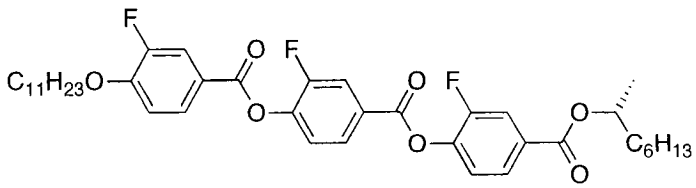

(*R*)-**3.13**

Compound (*S*)-**3.8** supercools into the SmA* with the observed crystallization occurring very slowly at 84 °C. Compound (*S*)-**3.8** also exhibits electroclinic switching, as well as induced polarizations as high as 6 nC/cm^2 at 6 V/μm, beginning at 91 °C. However, electroclinic measurements were not rigorously performed due to the instability of the SmA* phase at temperatures below 95 °C.

The DSC trace of (*S*)-**3.8** (Figure 3-9) shows only one peak on heating, which corresponds to a Cr to I transition; the enthalpy (Δ_H = 34.4 J/g) is too large to be an N* to I transition. This was confirmed by polarized optical microscopy, which showed that there are no observable mesophases on heating in a polyimide-coated ITO cell. On cooling, the I to N* transition has a significantly lower enthalpy than the melting peak and there are two broad negative enthalpy peaks at approximately 80 °C on cooling and another at 70 °C on heating. It is interesting to note that (*S*)-**3.8**, with only one group promoting liquid crystalline properties forms monotropic mesophases and (*R*)-**3.6**, with two liquid crystal promoting groups, forms enantiotropic mesophases.

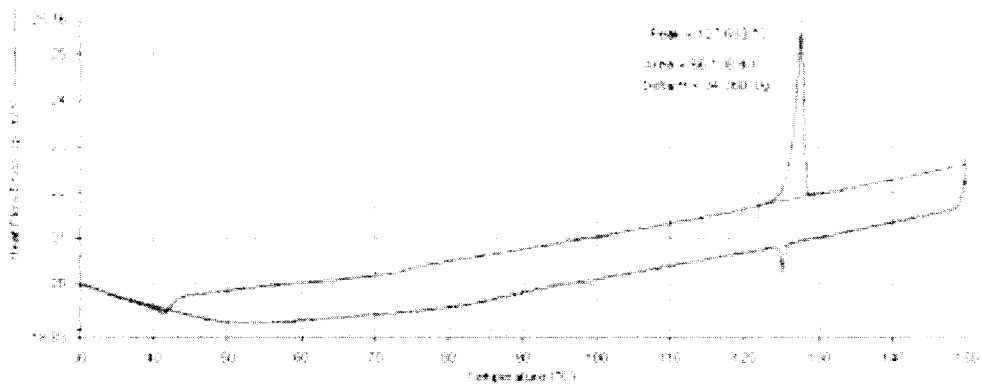

Figure 3-9. DSC trace of (*S*)-**3.8** of the second heating cycle.

3.3.2.2. Pitch measurements

The helical pitch of the chiral nematic phase formed by (*S*)-**3.8** was determined by absorbance measurements using variable temperature UV-Vis spectroscopy. Unlike the series with an alkoxy benzoate and bicyclo[2.2.2.]octyl group, ((*R*)-**2.16a-e**), the pitch of the N* phase of (*S*)-**3.8** increases with decreasing temperature. The entire visible spectrum is observable over a range of approximately 4 K; the reflection spectra and plot

of wavelength vs. reduced temperature are shown in Figure 3-10 and Figure 3-11, respectively. The temperature dependence of pitch shows approximately a twenty-fold increase from (*R*)-**2.16a-e** to (S)-**3.8.** The temperature dependence of pitch for chiral nematogens with an underlying SmA* phase tend to demonstrate non-linear behaviour near the N*-SmA* transition due to the unwinding of the helix to form a lamellar structure[11], which is consistent with observations for (*S*)-**3.8**. The large increase in the slope of the pitch vs. temperature plot of (*S*)-**3.8**, compared to that of series (*R*)-**2.16a-e**, is likely a function of the strong forces imposing the lamellar structure as opposed to the competition between the intrinsic thermal expansion and k_{22}.

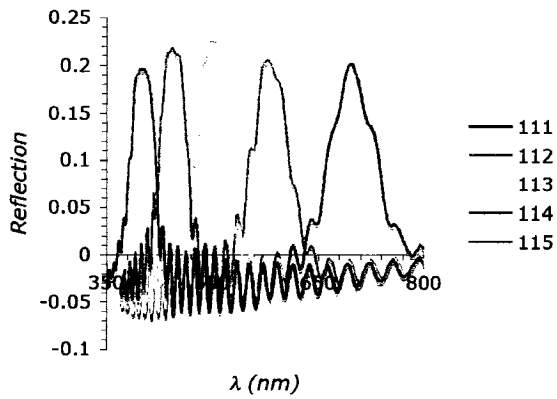

Figure 3-10. UV-Vis reflection spectra of (*S*)-**3.8** in a polyimide coated 4 μm cell.

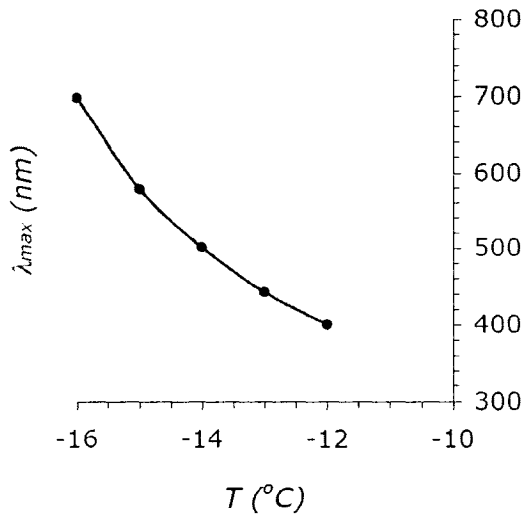

Figure 3-11. Plot of λ_{max} vs. reduced temperature for (*S*)-**3.8**.

As with siloxanes, the occurrence of nematic phases in compounds with highly fluorinated alkyl chains is rare.[7] One example of such a compound comes from a series of metallomesogens from the Tschierske group in Halle, Germany.[12] These compounds (**3.14a-c**) possess a polycatenar aryl group with semiperfluorinated alkyl side-chains, which is bound to both a Pd metal and a second aryl group by a chelating imine linking group. The Pd metal is also bound to a bent core chelating group with decyloxy side-chains at each end.

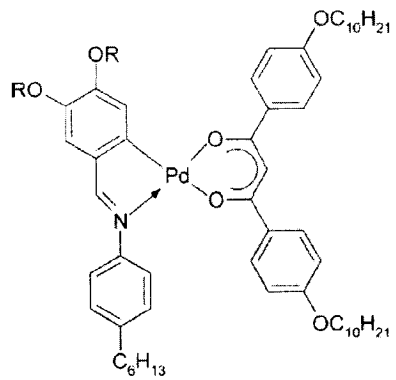

3.14

a: R = $C_{10}H_{21}$ Cr 113 (N 95) I
b: R = $(CH_2)_6(CF_2)_4F$ Cr 104 (SmC 88) SmA 114 N 120 I
c: R = $(CH_2)_4(CF_2)_6F$ Cr 118 (SmC 103) SmA 139 N 141 I

Taken from ref. 12.

3.3.2.3. Polarization measurements

Compound (*S*)-**3.8** was doped into **PhP1** at a mole fraction of $\chi_d = 0.04$ and the induced polarization compared to that induced by its hydrocarbon analogues. The P_o value was determined to be +30.0 nC/cm^2 and the sign of polarization is consistent with other 3,3'-dinitrobiphenyl dopants with the same absolute configuration in **PhP1**. This value is approximately 50% of that induced by the 3,3'-dinitrobiphenyl with two 4-octyloxy benzoate tails, (*S*)-**1.15d** in the same host (+60.8 nC/cm^2).[3] The P_o value for (*S*)-**3.8** is almost twice as large as the P_o induced by the unsymmetrical dopant (*R*)-**2.16** in **PhP1** at the same mole fraction (-17.1 nC/cm^2). The reduction in P_o for (*S*)-**3.8** compared to (*S*)-**1.15d** in **PhP1** is likely due to the reduction in chirality transfer via core-core interactions. This may be due to two factors. The first is the increase in excluded volume of the perfluorinated tail. The second could be a shift in the positional order of

the dopant in the binding site caused by fluorophobic segregation. There may also be a shift in the rotational distribution of the transverse dipole in the binding site towards the tilt plane, as described by Stegemeyer[13], which was observed for another mesogenic form of the 3,3'-dinitrobiphenyl core ((*R*)-**2.16d**) which has a bulky bicyclo[2.2.2.]octyl group closer to the core. The latter case seems less likely as the increased bulk associated with the perfluorinated chain is remote from the core, unlike the bicyclo[2.2.2.]octyl group.

The phase sequence of a mixture of (*S*)-**3.8** in **PhP1** at a mole fraction of χ_d = 0.04 is I 98 N* 93 SmA* 83 SmC* 39 Cr on cooling. These transition temperatures are approximately the same as (*R*)-**3.6** in **PhP1** at χ_d = 0.03 (I 98 N* 93 SmA* 82 SmC* 41 Cr). The temperature range of the SmC* is broader by about 4 K with the octyloxy benzoate side-chain as opposed to the 4-pentylbicyclo[2.2.2.]octyl side-chain due to a reduction of the lateral bulk associated with the core. When comparing the (*S*)-**3.8/PhP1** mixture to a mixture of a mesogenic hydrocarbon analogue (R)-**2.16d/PhP1** at the same dopant mole fraction of χ_d = 0.04 (I 96 N* 90 SmA* 72 SmC* 39 Cr) it is evident that the SmC* phase in the mixture with the semi-perfluorinated dopant is much more stable than with two hydrocarbon chains. Since the stability of the SmC* phase is much greater with perfluorinated side-chains, the phase transitions on heating were determined in order to compare with mixtures of (*R*)-**1.15e** in **PhP1**. The phase transitions of the mixture of (*S*)-**3.8** in **PhP1** at χ_d = 0.04 is Cr 57 SmC* 84 SmA* 94 N* 98 I on heating and the phase transitions for (*R*)-**1.15e** in the same host at a mole fraction of χ_d = 0.04 is Cr 56 SmC* 77 SmA* 90 N* 95 I.[14] The temperature range of the SmC* phase is approximately 5 K larger with mixtures of (*S*)-**3.8** in **PhP1** than in mixtures of (*R*)-**1.15e**

in the same host. Thus, perfluorination may be an alternative to increasing the solubility of the 3,3'-dinitrobiphenyl core in **PhP1**, with less destabilization of the SmC* phase, and with high enough mole fractions to observe non-linear effects.

3.4. References

(1) Mitsunobu, O. *Synthesis* **1981**, 1.

(2) Guillon, D.; Ospirov, M. A.; Méry, S., Siffert, M.; Nicoud, J.-F.; Bourgogne, C.; Sebastião, P. *J. Mater. Chem.* **2001**, *11*, 2700.

(3) Vizitiu, D.; Lazar, C.; Halden, B. J.; Lemieux, R. P. *J. Am. Chem. Soc.* **1999**, *121*, 8229.

(4) Kloess, P.; McComb, J.; Coles, H. J.; Zentel, R. *Ferroelectrics* **1996**, *180*, 233.

(5) Nishiyama, I.; Yamamoto, J.; Yokoyama, H.; Méry, S.; Guillon, D.; Goodby, J. W. *Transactions of the Materials Research Society of Japan* **2004**, *29*, 785.

(6) Alvarez, R.; Mehl, G. *Liq. Cryst.* **2005**, *32*, 469.

(7) Tschierske, C. *J. Mater. Chem.* **1998**, *8*, 1485.

(8) Trabelsi, H.; Szonyi, S.; Geribaldi, S. *J. Fluorine Chem.* **2001**, *107*, 177.

(9) Liu, H.; Nohira, H. *Liq. Cryst.* **1998**, *24*, 719.

(10) Goodby, J. W. *Current Opinion in Colloid and Interface Science* **2002**, *7*, 326.

(11) Gleeson, H. F. Thermography Using Liquid Crystals. In *Handbook of Liquid Crystals*; Demus, D., Goodby, J., Gray, G. W., Spiess, H.-W., Vill, V., Eds.; Wiley-VCH: Weinheim, 1998; Vol. 1, pp 823-838.

(12) Bilgin-Eran, B.; Tschierske, C.; Diele, S.; Baumeister, U. *J. Mater. Chem,* **2006**, *16*, 1145.

(13) Stegemeyer, H.; Meister, R.; Hoffmann, U.; Sprick, A.; Becker, A. *J. Mater. Chem.* **1995**, *5*, 2183.

(14) Hartley, C. S.; Kapernaum, N.; Roberts, J. C.; Giesselmann, F.; Lemieux, R. P. *J. Mater. Chem.* **2006**, *16*, 2329.

Chapter 4. Conclusions and future work

The aim of this project was to induce mesogenic behaviour in a class of non-mesogenic atropisomeric biphenyl dopants with symmetry breaking nitro groups at the 3 and 3' positions (**1.15**). This class of dopant has been shown to induce strong polarization powers in liquid crystalline hosts with a complimentary phenylpyrimidine core (*e.g.* **PhP1**), but tends to destabilize the SmC phase of the LC host.

The introduction of polycatenar motifs onto the 3,3'-dinitrobiphenyl core was unsuccessful in producing mesogenic properties; these materials were either oils (**3.6c-e**) or crystalline solids that are immiscible with **PhP1** at $\chi_d \geq 0.05$ (**3.6a** and **3.6b**). A 4-pentylbicyclo[2.2.2]octyl side-chain was introduced to extend the lateral bulk of the 3,3'-dinitrobiphenyl core and give more rod-shaped molecules. Although these compounds did not form smectic phases, we observed the formation of chiral nematic phases with a helical pitch that increases with increasing temperature. **2.16d** was chosen as a representative of this series in order to investigate the ability of this class to compounds to induce electroclinic (SmA*) and ferroelectric (SmC*) behaviour in the host **PhP1**. In this host, the electroclinic coefficient of **2.16d** is greater than that of **1.15e** despite a 50% reduction in polarization power. Interestingly, **2.16d** destabilizes the SmC phase of **PhP1** despite having mesogenic properties.

Another approach to mesogenic derivatives of the 3,3'-dinitrobiphenyl core is to harness microphase segregation to promote smectic liquid crystalline phases. Siloxane-

terminated compounds **3.2** and **3.3** were synthesized with the intent of controlling the degree of core-core interactions between the atropisomeric core and the siloxane-terminated phenylpyrimidine host, **3.9**, via the formation of a *virtual siloxane backbone.* Unfortunately both **3.2** and **3.3** are immiscible with **3.9** at $\chi_d \geq 0.05$. The mesophases formed by the siloxane dimer **3.4** suggest that oligomeric siloxanes can be used as a means of promoting mesogenic behaviour in molecules possessing the 3,3'-dinitrobiphenyl core.

Finally, a series of compounds with semiperfluorinated alkyl side-chains were synthesized to harness the fluorophobic effect to promote smectic phases. Compounds **3.5** and **3.6**, which feature a 4-pentylbicyclo[2.2.2.]octyl side-chain at one end and a semiperfluorinated alkoxybenzoate side-chain at the other, form a SmA* phase, with the stability of this phase increasing with increasing degree of fluorination. Compound **3.11**, with a 4-octyloxybenzoate side-chain, instead of a bicyclo[2.2.2.]octyl side-chain, forms N*, TGBA* and SmA* phases on cooling only.

The results of these investigations point to three strategies that may be pursued in the future to promote the formation of SmC* phases in compounds with the 3,3'-dinitrobiphenyl core. i) The extent of fluorination may be increased to a fully perfluorinated alkyl side-chain. ii) Based on the observation of mesogenic properties with the siloxane dimer **3.4** the use of a benzoate linking group (instead of ethereal linking group in **3.2** and **3.3**) with a terminal oligomeric siloxane (*e.g.* **4.1**) may produce mesogenic compounds suitable as dopants in phenylpyrimidine hosts with a terminal

siloxane group such as **3.9**. iii) The use of bicyclo[2.2.2.]octyl groups with longer aliphatic chain at the 4-position should also promote smectic phases. The synthesis of 4-hydroxy-bicyclo[2.2.2.]octane-1-carboxylic acid (**4.2**) is reported in the literature.[1] This compound is an important precursor to a series of carboxylic acids (**4.3**) which can be coupled to the 3,3'-dinitro core. In addition, alkylation of **4.2** with groups promoting microphase segregation (*e.g.* oligomeric siloxanes and perfluorinated alkyl chains) could yield a variety of interesting materials.

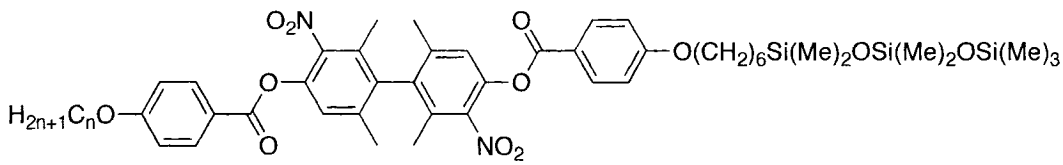

4.1

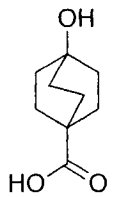

4.2

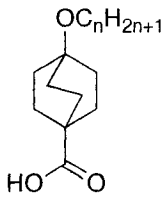

4.3

4.1. References

[1] Grob, C. A.; Rich, R.; *Helv.* **1979**, *62*, 2802.

Chapter 5. Experimental

5.1. Synthesis and characterization

5.1.1. General

^{1}H and ^{13}C NMR spectra were recorded on a Bruker Avance 400 MHz spectrometer using deuterated chloroform or deuterated acetone as solvent. The chemical shifts are reported in δ (ppm) and are relative to tetramethylsilane. Low-resolution and high-resolution ESI mass spectra were recorded on an Applied Biosystems/MDS Sciex QSTAR XL QqTOF mass spectrometer. Low-resolution LDI mass spectra were recorded on an Applied Biosystems Voyager MALDI-ToF mass spectrometer in reflection mode except for (*R*)-**2.14b**, which was obtained in linear mode. Differential Scanning Calorimetery (DSC) analyses were performed on a Perkin Elmer DSC7 Differential Scanning Calorimeter coupled to a Perkin-Elmer TAC 7/DX Thermal Analysis Controller with a scan rate of 5 K/min. Melting points were obtained on a Fisher-Johns melting point apparatus and are uncorrected. Flash chromatography was performed using 60 Å silica gel (Silicycle Inc., Quebec) as the adsorbent. Semi-preparative chiral stationary phase HPLC separations were performed on a Daicel Chiralpak AS column (250 mm x 4.6 mm i.d.) using mixtures of hexanes/EtOH as eluent at a flow rate of 3 mL/min. Preparative chiral stationary phase scale HPLC separations were performed on a Daicel Chiralpak AS column (50 cm x 5 cm i.d.) using mixtures of Hexanes/EtOH as eluent at a flow rate of 50 mL/min.

5.1.2. Materials

All solvents, reagents and the liquid crystal hosts **NCB76** and **PHP1** were obtained from commercial sources and were used without further purification unless otherwise noted. Methylene chloride was purified using a Solv-Tek, Inc. solvent purification system. THF was distilled from sodium/benzophenone under argon. All 4-, 3,4-, 3,5-, and 3,4,5-alkoxybenzoic acids and 6-(1,1,3,3,5,5,5-heptamethyltrisiloxanyl)-hexan-1-ol and 11-(1,1,3,3,5,5,5-heptamethyltrisiloxanyl)-undecan-1-ol were synthesized by members of the Lemieux group. 4-(5,5,6,6,7,7,8,8,9,9,10,10,10-trideccafluoro)decyloxybenzoic acid and bis-[1,5-(4-hexyloxybenzoic acid)1,1,3,3,5,5-hexamethyl]siloxane were synthesized by literature procedures.[1,2] 4-(3,3,4,4,5,5,6,6,7,7,8,8,9,9,10,10,10-heptadecafluoro)decyloxybenzoic acid was synthesized by the reaction of methyl 4-hydroxy benzoate with (3,3,4,4,5,5,6,6,7,7,8,8,9,9,10,10,10-heptadecafluoro)-1-iodo-decane followed by deprotection with NaOH in 1:1 EtOH/H_2O. The key intermediate 4,4'-dihydroxy-2,2',6,6'-tetramethyl-3,3'dinitrobiphenyl (**2.13**) was synthesized according to the method reported by Hartley and showed to have the expected physical and spectral properties.[3] The liquid crystal hosts **PhBz**, **DFT** were synthesized by members of the Lemieux group according to literature procedures and shown to have the expected physical and spectral properties.[4,5] The siloxane-terminated phenylpyrimidine host **3.9** was synthesized by Li Li of the Lemieux group.

5.1.3. Synthetic procedures

(*S*)-4'-{[6-(1,1,3,3,5,5,5-heptamethyltrisiloxanyl)hexyl]oxy}-4-Hydroxy-2,2',6,6'-tetramethyl-3,3'-dinitrobiphenyl](3.1)

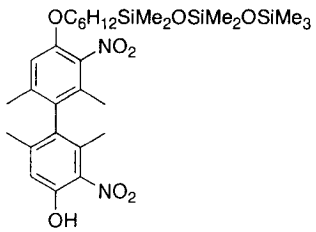

To a solution of (*S*)-**2.13** (170 mg, 0.51 mmol) in dry THF (20 mL) was added triphenylphosphine (262 mg, 1.24 mmol) and 6-(1,1,3,3,5,5,5-heptamethylsiloxanyl)-hexan-1-ol (198 mg, 0.61 mmol). DIAD (267 mg, 1.24 mmol) was then added and the mixture was stirred for 16 hours. The reaction mixture was concentrated to a yellow oil and purified by flash chromatography on silica gel (7:1 hexanes/EtOAc) to give 113 mg (35%) of (*S*)-**3.1** as yellow oil: ^{1}H NMR ($CDCl_3$, 400 MHz) δ 0.00 (s, 6H), 0.05 (s, 6H), 0.06 (s, 9H), 0.52 (t, J = 7.5 Hz, 2H), 1.34 (m, 2H), 1.75 (m, 2H), 1.77 (m, 2H), 1.81 (s, 3H), 1.87 (s, 3H), 1.89 (s, 3H), 2.11 (s, 3H), 4.04 (t, J = 6.3 Hz, 2H), 6.80 (s, 1H), 6.95 (s, 1H), 9.98 (s, 1H).

(*S*)-4-{[6-(1,1,3,3,5,5,5-heptamethyltrisiloxanyl)hexyl]oxy}-2,6-dimethyl-4'-(octyloxy)-3,3'-dinitrobiphenyl (3.2)

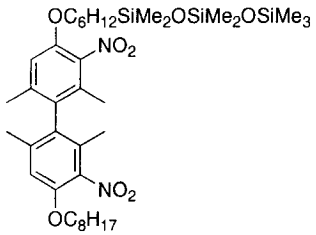

To a mixture of (*S*)-**3.1** (52 mg, 0.08 mmol) and Cs_2CO_3 (53 mg, 0.16 mmol) in anhydrous DMF (2 mL) was added 1-bromooctane (31 mg, 0.16 mmol). The mixture was stirred at room temperature for 16 hours then poured over H_2O (50 mL) and extracted with EtOAc (4x20 mL). The combined organic layers were washed with H_2O, brine, then dried ($MgSO_4$) and concentrated to give a yellow oil. Purification by flash chromatography on silica gel (9:1 hexanes/EtOAc) gave 52 mg (85%) of (*S*)-**3.2** as a yellow oil: ^{1}H NMR ($CDCl_3$, 400 MHz) δ 0.01 (s, 6H), 0.05 (s, 6H), 0.07 (s, 9H), 0.53 (t, J = 7.7 Hz, 2H), 0.88 (t, J = 6.6 Hz, 3H), 1.34 (m, 16H), 1.77 (m, 4H), 1.82 (s, 3H),

1.91 (s, 3H), 4.04 (t, J = 6.3 Hz, 4H), 6.80 (s, 2H). ^{13}C NMR ($CDCl_3$, 100 MHz) δ 0.2, 1.3, 1.8, 14.1, 14.5, 18.2, 20.6, 22.6, 23.1, 25.5, 25.8, 28.9, 28.9, 29.2, 29.3, 31.7, 33.0, 69.3, 112.6, 129.0, 130.4, 139.6, 141.2, 149.4. MS(ESI) *m/z* 771 ([M + Na]$^+$, 17), 605 (77), 528 (94), 186 (100). HRMS (ESI) calc'd for $C_{37}H_{64}N_2NaO_8Si_3$: 771.3868; found: 771.3882.

(*R*)-4'-{[6-(1,1,3,3,5,5,5-heptamethyltrisiloxanyl)hexyl]oxy}-2',6'-dimethyl-4-[4-(octyloxybenzoyl)oxy]-3,3'-dinitrobiphenyl (3.3)

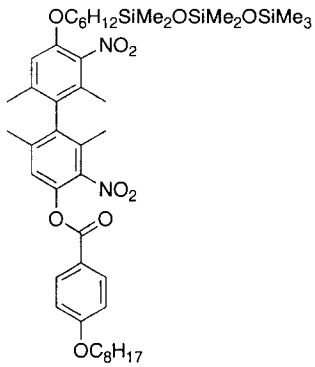

To a mixture of (*R*)-**3.1** (57 mg, 0.09 mmol) DMAP (30 mg, 0.25 mmol) and 4-octyloxybenzoic acid (59 mg, 0.23 mmol) in CH_2Cl_2 (2 mL) was added solid DCC (49 mg, 0.24 mmol) under an argon atmosphere. The reaction mixture was stirred for 20 hours then diluted with CH_2Cl_2 and filtered. The filtrate was diluted with EtOAc and washed with 5% aq. HCl (2x), H_2O and brine. The organic layer was then dried ($MgSO_4$) and concentrated. The residue was purified by flash chromatography on silica gel (12:1 hexanes/EtOAc) to give 60 mg (44%) of (*R*)-**3.2** as a yellow oil: ^{1}H NMR ($CDCl_3$, 400 MHz) δ 0.02 (s, 6H), 0.06 (s, 6H), 0.08 (s, 9H), 0.54 (t, J = 7.7 Hz, 2H), 0.88 (t, J = 6.8 Hz, 3H), 1.36 (m, 16H), 1.79 (m, 4H), 1.86 (s, 3H), 1.94 (s, 3H), 1.95 (s, 3H), 1.97 (s, 3H), 4.05 (m, 4H), 6.83 (s, 1H), 6.96 (d, J = 8.9 Hz, 2H), 7.28 (s, 1H), 8.06 (d, J = 8.9 Hz, 2H). ^{13}C NMR ($CDCl_3$, 100 MHz) δ 0.2, 1.3, 1.8, 14.1, 14.6, 15.1, 18.2, 20.4, 20.6, 22.6, 23.1, 26.0, 28.9, 29.0, 29.2, 29.3, 31.8, 33.0, 68.4, 69.4, 112.8, 114.5, 120.0, 123.3, 128.7, 129.9, 130.1, 132.6, 136.7, 139.2, 140.5, 141.7, 143.3, 149.6, 163.6, 164.1. MS (ESI) *m/z* 892 ([M + Na]$^+$, 10), 365 (54), 186 (100). HRMS (ESI) calc'd for $C_{44}H_{68}N_2NaO_{10}Si_3$: 891.4080; found 891.4071.

(*R*)-4,4'-Bis[3,4-bis-decyloxybenzoyl)oxy]-2,2',6,6'-tetramethyl-3,3'dinitrobiphenyl (2.14a)

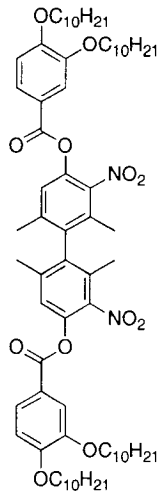

To a solution of (*R*)-**2.13** (35 mg, 0.11 mmol), DMAP (40 mg, 0.33 mmol) and 3,4-bis-decyloxybenzoic acid (31.4 mg, 0.32 mmol) in CH_2Cl_2 (5 mL) was added solid DCC (66 mg, 0.32 mmol) under an argon atmosphere. The reaction was stirred for 20 hours, then diluted with CH_2Cl_2 and filtered. The filtrate was diluted with EtOAc and washed twice with 5% aq. HCl (2x), H_2O and brine. The combined organic layers were dried ($MgSO_4$) and concentrated. The white residue was purified by flash chromatography on silica gel (6:1 hexanes/EtOAc) to give 98 mg (72%) of (*R*)-**2.14a** as a white solid, which was subsequently recrystallized from hexanes after passing through a 0.45 μm PTFE filter: m.p. 88-89 °C. ^{1}H NMR ($CDCl_3$, 400 MHz) δ 0.87 (m, 12H), 1.26 (m, H), 1.48 (m, 8H), 1.85 (m, 8H), 1.98 (s, 6H), 2.02 (s, 6H), 4.06 (m, 8H), 6.92 (d, J = 8.5 Hz, 2H), 7.33 (s, 2H), 7.58 (s, 2H), 7.74 (d, J = 8.5 Hz, 2H). ^{13}C NMR ($CDCl_3$, 100 MHZ) δ 14.0, 14.1, 15.1, 20.4, 22.7, 25.9, 28.9, 29.0, 29.1, 29.3, 29.4, 29.5, 29.6, 29.6, 31.9, 69.1, 69.3, 112.0, 114.6, 119.9, 123.5, 134.9, 129.7, 136.1, 140.0, 142.0, 143.4, 148.8, 154.8, 154.5, 163.6. MS (LDI) *m/z* 1188 ($[M + Na]^+$, 1), 560 (60), 58 (59), 39 (100).

(*S*)-4,4'-Bis[3,4-bis-dodecyloxybenzoyl)oxy]-2,2',6,6'-tetramethyl-3,3'dinitrobiphenyl (2.14b)

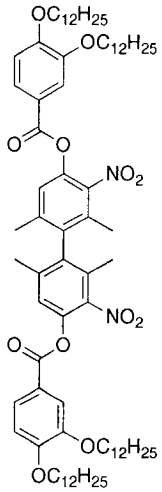

The procedure used in the synthesis of (*R*)-**2.14a** was repeated with 35 mg (0.11 mmol) of (*S*)-**2.13**, 39 mg (0.32 mmol) and 3,4-bis-dodecyloxybenzoic acid to give 88 mg (66%) of (*S*)-**2.14b** as a white solid, which was recrystallized from hexanes after passing through a 0.45 μm PTFE filter: m.p. 93-94 °C. ^{1}H NMR ($CDCl_3$, 400 MHz) δ 0.87 (t, J = 6.6 Hz, 12H) 1.25 (m, 64H), 1.48 (m, 8H), 1.86 (m, 8H), 1.98 (s, 6H), 2.02 (s, 6H), 4.05 (t, J = 6.8 Hz, 4H), 4.08 (t, J = 7.4 Hz, 4H), 6.93 (d, J = 8.6 Hz, 2H), 7.33 (s, 2H), 7.58 (s, 2H), 7.74 (d, J = 8.6 Hz, 2H) . ^{13}C NMR ($CDCl_3$, 100 MHz) δ 14.1, 15.1, 20.4, 22.7, 25.9, 26.0, 29.0, 29.1, 29.3, 29.6, 29,6, 29.7, 31.9, 69.1, 69.3, 112.0, 114.6, 119.9, 123.5, 124.9, 129.7, 136.1, 140.0, 142.0, 143.4, 148.8, 154.5, 163.7. MS (LDI) *m/z* 1301 ([M + Na]$^+$, 1), 562 (55), 308 (89), 139 (100).

(*R*)-4,4'-Bis[3,5-bis-decyloxybenzoyl)oxy]-2,2',6,6'-tetramethyl-3,3'dinitrobiphenyl (2.14c)

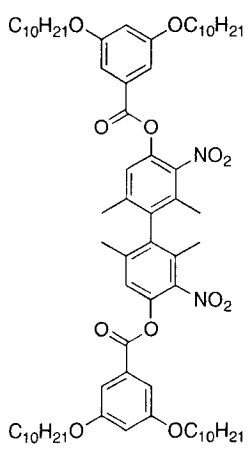

The procedure used in the synthesis of (*R*)-**2.14a** was repeated with with 35 mg (0.11 mmol) of (*R*)-**2.13**, and 143 mg (0.33 mmol) 3,5-bis-decyloxybenzoic acid to give 66 (54%) mg of (*R*)-**2.14c** as a colourless oil: ^{1}H NMR ($CDCl_3$, 400 MHz) δ 0.87 (t, J = 6.7 Hz), 1.27 (m, H), 1.46 (m, 8H), 1.79 (m, 8H), 1.99 (s, 6H), 2.02 (s, 6H), 3.99 (t, J = 6.5 Hz, 8H), 6.72 (2H), 7.23 (s, 4H), 7.31 (s, 2H). ^{13}C NMR ($CDCl_3$, 100 MHz) δ 14.1, 15.2, 20.4, 22.7, 26.0, 29.1, 29.3, 29.4, 29.5, 31.9, 68.4, 107.9, 108.4, 123.4, 129.6, 129.9, 136.4, 140.2, 141.9, 143.3, 160.4, 163.8. MS (LDI) *m/z* 1188 ([M + Na]$^+$, 1), 561 (68), 560 (96), 546 (45), 39 (100).

(*S*)-4,4'-Bis[3,5-bis-dodecyloxybenzoyl)oxy]-2,2',6,6'-tetramethyl-3,3'dinitrobiphenyl (2.14d)

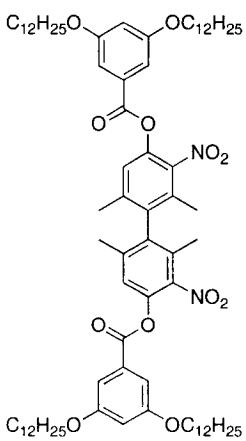

The procedure used in the synthesis of (*R*)-**2.14a** was repeated with 34 mg (0.10 mmol) of (*S*)-**2.13**, 40 mg (0.33 mmol) and 156 mg (0.32 mmol) 3,5-bis-dodecyloxybenzoic acid to give 71 mg (55%) of (*S*)-**2.14d** as a colourless oil: ^{1}H NMR ($CDCl_3$, 400 MHz) δ 0.87 (t, J = 6.8 Hz, 12H), 1.26 (m, 64H), 1.46 (m, 8H), 1.79 (m, 8H), 1.99 (s, 6H), 2.03 (s, 6H), 3.99 (t, J = 6.5 Hz, 8H), 6.72 (s, 2H), 7.24 (s, 4H), 7.32 (s, 2H). ^{13}C NMR ($CDCl_3$, 100 MHz) δ 14.1, 15.1, 20.4, 22.7, 26.0, 29.1, 29.3, 29.4, 29.6, 29.6, 29.6, 29.6, 31.9, 68.4, 108.4, 123.4, 129.6, 129.9, 136.3, 140.1, 141.9, 143.3, 160.4, 163.8.

(*S*)-4,4'-Bis[3,4,5-tris-decyloxybenzoyl)oxy]-2,2',6,6'-tetramethyl-3,3'dinitrobiphenyl (2.14e)

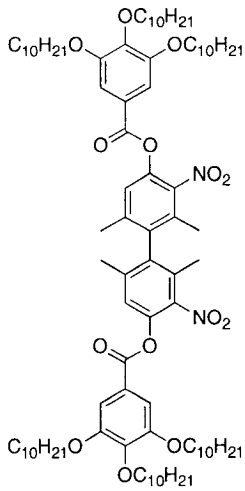

The procedure used in the synthesis of (*R*)-**2.14a** was repeated with 33 mg (0.10 mmol) of (*S*)-**2.13** and 187 mg (0.33 mmol) 3,4,5-tris-decyloxybenzoic acid to give 94 mg (64%) of (*S*)-**2.14e** as a colourless oil: ^{1}H NMR ($CDCl_3$, 400 MHz) δ 0.87 (m, 18H), 1.28 (m, 72H), 1.49 (m, 12H), 1.76 (m, 4H), 1.83 (m, 8H), 1.99 (s, 6H), 2.03 (s, 6H), 4.03 (m, 12H), 7.34 (s, 6H). ^{13}C NMR ($CDCl_3$, 100 MHz) δ 14.1, 15.1, 20.4, 22.7, 26.0, 26.1, 29.2, 29.3, 29.4, 29.5, 29.6, 29.6, 29.7, 29.7, 30.3, 31.9, 31.9, 69.2, 73.6, 108.8, 122.3, 123.4, 129.8, 136.2, 140.1, 142.0, 143.4, 143.7, 153.0, 163.7. MS (LDI) *m/z* 1477 (M^+, 1), 325 (33), 152 (40), 62 (100).

(*R*)-4-Hydroxy-2,2',6,6'-tetramethyl-4'-[(4-pentylbicyclo[2.2.2]octan-1-oyl)oxy]-3,3'dinitrobiphenyl (2.15)

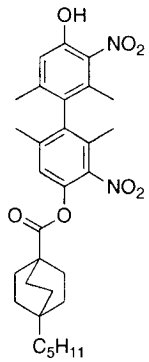

To a mixture of (*R*)-**2.13** (781 mg, 2.35 mmol), 4-pentylbicyclo[2.2.2]octane-1-carboxylic acid (571 mg, 2.55 mmol) and DMAP (575 mg, 4.72 mmol) in CH_2Cl_2 (15 mL) was added solid DCC (982 mg, 4.76 mmol) under an argon atmosphere. After stirring for 20 hours, the reaction mixture was filtered, diluted with EtOAc and washed with 10% aq. HCl (2x), H_2O and brine. The organic layer was dried ($MgSO_4$) and concentrated to a yellow oil, which was purified by flash chromatography on silica gel (7:1 hexanes/EtOAc) to give 689 mg (54%) of (*R*)-**2.15** as a yellow solid: m.p. 59-61 °C. ^{1}H NMR ($CDCl_3$, 400 MHz) δ 0.86 (t, J = 7.2 Hz), 1.19 (m, 10H), 1.43 (m, 6H), 1.89 (m, 12H), 1.92 (s, 3H), 2.14 (s, 3H), 6.99 (s, 1H), 7.07 (s, 1H), 10.00 (s, 1H). ^{13}C NMR ($CDCl_3$, 100 MHz) δ 14.0, 15.0, 18.0, 20.2, 20.9, 22.6, 23.3, 28.4, 30.2, 30.4, 32.7, 39.5, 41.2, 118.7, 123.3, 129.8, 131.4, 133.9, 134.8, 136.7, 140.2, 141.6, 143.3, 145.2, 154.0, 175.5. MS (ESI) *m/z* 577 ($[M + K]^+$, 64), 430 (65), 429 (100), 409 (75), 381 (67), 140 (53). HRMS (ESI) calc'd for $C_{30}H_{38}KN_2O_7$: 577.2316; found: 577.2340.

(*R*)-4'-[(4-hexyloxybenzoyl)oxy]-2,2',6,6'tetramethyl-4-([4-pentyl-bicyclo[2.2.2.]octan-1-oyl)oxy]- 3,3'-dinitrobiphenyl (2.16a)

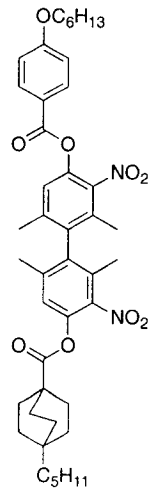

To a solution of (*R*)-**2.15** (31 mg, 0.06 mmol), DMAP (17 mg, 0.14 mmol) and 4-hexyloxybenzoic acid (26 mg, 0.12 mmol) in CH_2Cl_2 (3 mL) was added solid DCC (24 mg, 0.12 mmol) under an argon atmosphere. The reaction mixture was stirred for 20 hours and then filtered. The filtrate was taken up in EtOAc and washed twice with 10% aq. HCl (2x), H_2O and brine. The organic layer was dried ($MgSO_4$) and concentrated to a white solid, which was purified by flash chromatography on silica gel (9:1 hexanes/EtOAc) to give 29 mg (74%) of (*R*)-**2.16a** as a white solid. Further purification was achieved via recrystallization from IPA after passing through a 0.45 μm PTFE filter: ^{1}H NMR ($CDCl_3$, 400 MHz) δ 0.87 (m, 6H), 1.11 (m, 2H), 1.20 (m, 4H), 1.29 (m, 2H), 1.35 (m, 4H), 1.43 (m, 8H), 1.81 (m, 2H), 1.88 (m, 6H), 1.94 (s, 6H), 1.97 (s, 6H), 4.04 (t, J = 6.5 Hz, 2H), 6.96 (d, J = 8.9 Hz, 2H), 7.10 (s, 1H), 7.30 (s, 1H), 8.06 (d, J = 8.9 Hz, 2H). ^{13}C NMR ($CDCl_3$, 100 MHz) δ 14.0, 14.1, 15.0, 20.3, 20.3, 22.6, 22.7, 23.3, 25.6, 28.5, 29.0, 30.2, 30.4, 31.5, 32.8, 39.5, 41.2, 68.4, 114.5, 119.9, 123.5, 123.5, 129.6, 129.7, 132.7, 136.1, 139.9, 134.0, 141.8, 141.9, 143.3, 143.4, 163.6, 164.1, 175.5. MS (ESI) *m/z* 765 ($[M + Na]^+$, 20), 537 (40), 365 (100). HRMS (ESI) calc'd for: $C_{43}H_{54}NaN_2O_9$: 765.3727; found: 765.3741.

(*R*)-2,2',6,6'tetramethyl-4'-[(4-octyloxybenzoyl)oxy]-4-([4-pentyl-bicyclo[2.2.2.]octan-1-oyl)oxy]-3,3'-dinitrobiphenyl (2.16b)

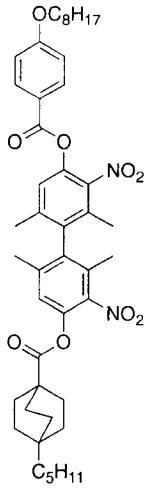

The procedure used in the synthesis of (*R*)-**2.16a** was repeated with 30 mg (0.06 mmol) of (*R*)-**2.15** and 28 mg (0.11 mmol) of 4-octyloxybenzoic acid to give 23 mg (54%) of (*R*)-**2.16b** as a white solid. Further purification was achieved via recrystallization from IPA after passing through a 0.45 μm PTFE filter: ^{1}H NMR ($CDCl_3$, 400 MHz) δ 0.88 (m, 6H), 1.25 (m, 16H), 1.44 (m, 8H), 1.83 (m, 10H), 1.94 (s, 6H), 1.97 (s, 6H), 4.03 (t, J = 6.5 Hz, 2H), 6.96 (d, J = 8.9 Hz, 2H), 7.10 (s, 1H), 7.31 (s, 1H), 8.06 (d, J = 8.9 Hz, 2H). ^{13}C NMR ($CDCl_3$, 100 MHz) δ 14.1, 15.0, 20.3, 20.3, 22.6, 22.7, 23.3, 25.9, 28.5, 29.0, 29.2, 29.3, 29.7, 30.2, 30.4, 31.8, 32.8, 39.5, 41.2, 68.4, 114.5, 119.9, 123.5, 123.5, 129.7, 129.7, 132.7, 136.1, 139.9, 140.0, 141.8, 141.9, 143.3, 143.4, 163.6, 164.1, 175.5. MS(ESI) *m/z* 793 ([M + Na]$^+$, 1), 577 (100), 413 (59), 123 (45). HRMS (ESI) calc'd for $C_{45}H_{58}N_2NaO_9$: 793.4040; found 793.4058

(*R*)-4'-[(4-decyloxybenzoyl)oxy]-2,2',6,6'tetramethyl-4-([4-pentyl bicyclo[2.2.2.]octan-1-oyl)oxy]- 3,3'-dinitrobiphenyl (2.16c)

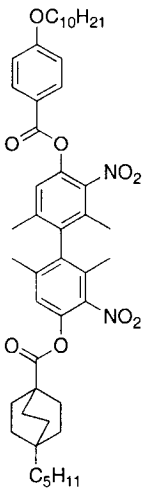

The procedure used in the synthesis of (*R*)-**2.16a** was repeated with 38 mg (0.07 mmol) of (*R*)-**2.15** and 39 mg (0.14 mmol) 4-decyloxybenzoic acid to give 44 mg (78 %) of (*R*)-**2.16c** as a white solid. Further purification was achieved via recrystallization from IPA after passing through a 0.45 μm PTFE filter: ^{1}H NMR ($CDCl_3$, 400 MHz) δ 0.87 (t, J = 7.0 Hz, 6H), 1.27 (m, 22H), 1.43 (m, 8H), 1.81 (m, 2H), 1.88 (m, 6H), 1.94 (s, 6H), 1.97 (s, 6H), 4.03 (t, J = 6.6 Hz, 2H), 6.96 (d, J = 8.8 Hz), 7.10 (s, 1H), 7.31 (s, 1H), 8.06 (d, J = 8.8 Hz, 2H). ^{13}C NMR ($CDCl_3$, 100 MHz) δ 14.1, 14.1, 15.0, 15.1, 20.3,

20.4, 22.7, 23.3, 25.9, 28.5, 29.2, 29.3, 29.3, 29.5, 30.2, 30.4, 31.9, 32.8, 39,5, 41.2, 68.4, 114.5, 119.9, 123.5, 123.5, 129.6, 129.7, 132.7, 136.1, 136.1, 140.0, 140.0, 141.8, 141.9, 143.3, 163.6, 164.1, 175.5. MS (ESI) *m/z* 806 ($[M + Na]^+$, 1), 803 (40), 577 (46), 413 (100), 365 (47). HRMS (ESI) calc'd for $C_{47}H_{62}N_2NaO_9$: 821.4353; found: 821.4361.

(*R*)-4'-[(4-dodecyloxybenzoyl)oxy]-2,2',6,6'tetramethyl-4-([4-pentyl-bicyclo[2.2.2.]octan-1-oyl)oxy]-3,3'-dinitrobiphenyl (2.16d)

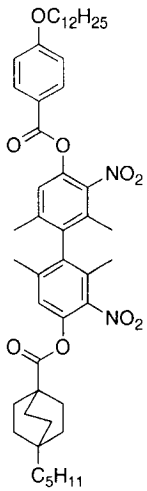

The procedure used in the synthesis of (*R*)-**2.16a** was repeated with 32 mg (0.06 mmol) of (*R*)-**2.15** and 40 mg (0.13 mmol) 4-dodecyloxybenzoic acid to give 38 mg (83%) of (*R*)-**2.16d** as a white solid. Further purification was achieved via recrystallization from IPA after passing through a 0.45 μm PTFE filter: ^{1}H NMR ($CDCl_3$, 400 MHz) δ 0.87 (t, J = 7.1 Hz, 6H), 1.11 (m, 2H), 1.26 (m, 22H), 1.43 (m, 8H), 1.81 (m, 2H), 1.88 (m, 6H), 1.94 (s, 6H), 1.97 (s, 6H), 4.03 (t, J = 6.7 Hz, 2H), 6.96 (d, J = 8.8 Hz, 2H), 7.10 (s, 1H), 7.31 (s, 1H), 8.06 (d, J = 8.8 Hz, 2H). ^{13}C NMR ($CDCl_3$, 100 MHz) δ 14.1, 14.1, 15.0, 20.3, 20.3, 22.7, 23.3, 25.9, 28.5, 29.0, 29.3, 29.5, 29.6, 29.6, 31.2, 30.4, 31.9, 32.8, 39.5, 41.2, 68.4, 114.5, 119.9, 123.5, 123.5, 129.6, 129.7, 132.7, 136.1, 139.9, 140.0, 141.8, 141.9, 143.3, 143.4, 163.6, 164.1, 175.5. MS (ESI) *m/z* 865 ($[M + K]^+$, 10), 381 (100), 313 (60). HRMS (ESI) calc'd for $C_{49}H_{66}KN_2O_9$: 865.4405; found: 865.4399.

(*R*)-2,2',6,6'tetramethyl-4-([4-pentyl-bicyclo[2.2.2.]octan-1-oyl)oxy]-4'-[(4-tetradecyloxybenzoyl)oxy]-3,3'-dinitrobiphenyl (2.16e)

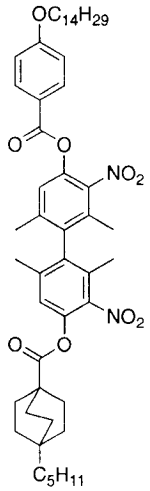

The procedure used in the synthesis of (*R*)-**2.16a** was repeated with 23 mg (0.04 mmol) (*R*)-**2.15** and 30 mg (0.09 mmol) of 4-tetradecyloxybenzoic acid to give 40 mg (88%) of (*R*)-**2.16e** as a white solid. Further purification was achieved via recrystallization from IPA after passing through a 0.45 μm PTFE filter: ^{1}H NMR ($CDCl_3$, 400 MHz) δ 0.87 (m, 6H), 1.11 (m, 2H), 1.25 (m, 26H), 1.43 (m, 8H), 1.81 (m, 2H), 1.88 (m, 6H), 1.94 (s, 6H), 1.97 (s, 6H), 4.03 (t, J = 6.6 Hz, 2H), 6.96 (d, 2H, 8.8 Hz, 2H), 7.10 (s, 1H), 7.31 (s, 1H), 8.06 (d, J = 8.8 Hz, 2H). ^{13}C NMR ($CDCl_3$, 100 MHz) δ 14.1, 14.1, 15.0, 15.1, 20.3, 20.4, 22.7, 23.3, 25.9, 28.5, 29.0, 29.3, 29.3, 29.5, 30.2, 30.2, 31.9, 32.7, 39.5, 41.2, 68.0, 114.5, 119.9, 123.5, 123.5, 129.6, 129.7, 132.7, 136.1, 136.1, 139.9, 140.0, 141.8, 141.9, 143.3, 163.6, 164.1, 175.5. MS (ESI) *m/z* 893 ([M+ K]$^+$, 100). HRMS (ESI) calc'd for $C_{51}H_{70}KN_2O_9$: 893.4718; found 893.4729.

4'-{[4-(3,3,4,4,5,5,6,6,7,7,8,8,9,9,10,10,10-heptadecafluoro)decyloxybenzoyl]oxy}-2,2',6,6'tetramethyl-4-([4-pentyl-bicyclo[2.2.2.]octan-1-oyl)oxy]-3,3'-dinitrobiphenyl (3.5)

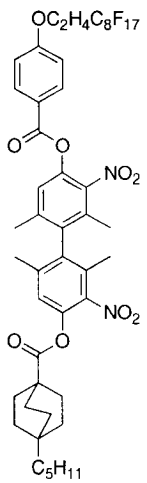

The procedure used in the synthesis of (*R*)-**2.16a** was repeated with 29 mg (0.05 mmol) of (*R*)-**2.15** and 22 mg (0.04 mmol) of 4-(3,3,4,4,5,5,6,6,7,7,8,8,9,9,10,10,10-heptadecafluoro)decyloxybenzoic acid to give 21 mg (51%) of (*R*)-**3.5** as a white solid. Further purification was achieved via recrystallization from hexanes after passing through a 0.45 μm PTFE filter: ^{1}H NMR ($CDCl_3$, 400 MHz) δ 0.87 (t, J = 7.1 Hz), 1.11 (m,

2H), 1.24 (m, 6H), 1.43 (m, 6H), 1.88 (m, 6H), 1.94 (s, 6H), 1.97 (s, 6H), 2.68 (tt, J_{H-F} = 18.4 Hz, J_{H-H} = 6.7 Hz, 2H), 4.36 (t, J = 6.7, 2H), 6.99 (d, J = 8.9 Hz), 7.10 (s, 1H), 7.31 (s, 1H), 8.10, (s, 2H). ^{13}C NMR ($CDCl_3$, 100 MHz) δ 14.1, 15.0, 15.1, 20.3, 20.4, 22.7, 23.3, 28.5, 30.2, 30.5, 31.2, 32.8, 39.6, 41.2, 60.3, 114.5, 121.1, 123.5, 123.5,129.6, 129.8, 132.8, 136.1, 136.3, 139.9, 140.1, 141.8, 141.9, 143.3, 162.8, 163.4, 175.5. MS (LDI) *m/z* 1127 ([M + Na]$^+$, 6), 280 (60), 155 (73), 39 (100).

(*R*)-4'-{[4-(5,5,6,6,7,7,8,8,9,9,10,10,10tridecafluoro)decyloxybenzoyl]oxy}-2,2',6,6'tetramethyl-4-[(4-pentyl-bicyclo[2.2.2.]octan-1-oyl)oxy]-3,3'-dinitrobiphenyl (3.6)

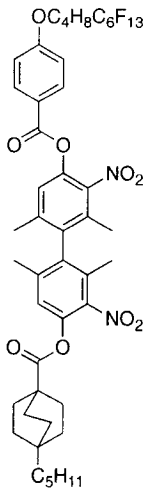

The procedure used in the synthesis of (*R*)-**2.16a** was repeated with 40 mg (0.07 mmol) of (*R*)-**2.15** and 84 mg (0.15 mmol) 4-(5,5,6,6,7,7,8,8,9,9,10,10,10-tridecafluoro)decyloxybenzoic acid to give 37 mg (48%) of (*R*)-**3.6** as a colourless solid. Further purification was achieved via recrystallization from hexanes after passing through a 0.45 μm PTFE filter: ^{1}H NMR ($CDCl_3$, 400 MHz) δ 0.87 (t, J = 7.2 Hz, 3H), 1.12 (m, 2H), 1.24 (m, 6H), 1.29 (m, 2H), 1.43 (m, 6H), 1.86 (m, 8H), 1.94 (s, 6H), 1.97 (s, 6H), 2.16 (m, 2H), 4.09 (t, J = 5.7 Hz, 2H), 6.97 (d, J = 8.9 Hz, 2H), 7.10 (s, 1H), 7.31 (s, 1H), 8.07 (d, J = 8.9 Hz, 2H). ^{13}C NMR ($CDCl_3$, 100 MHz) δ 14.1, 15.0, 15.1, 17.2, 20.3, 20.4, 22.7, 23.3, 28.5, 28.5, 30.2, 30.4, 32.8, 39.6, 41.2, 67.5, 114.5, 120.4, 123.5, 129.6, 129.7, 132.7, 136.1, 136.2, 136.2, 139.9, 140.0, 141.8, 141.9, 143.4, 163.5, 163.7, 175.5. MS (ESI) *m/z* 1071 ([M + K]$^+$, 26), 429 (100), 381 (72). HRMS (ESI) Calc'd for $C_{47}H_{49}F_{13}KN_2O_9$: 1071.2867; found: 1071.2863.

(*R,R*)-{4-[6-(1,1,3,3,5,5 hexamentyl trisiloxanyl) bis-hexyloxybenzoyl]oxy}-2,2',6,6'tetramethyl-4-([4-pentyl bicyclo[2.2.2.]octan-1-oyl)oxy]- 3,3'-dinitrobipheny (3.4)

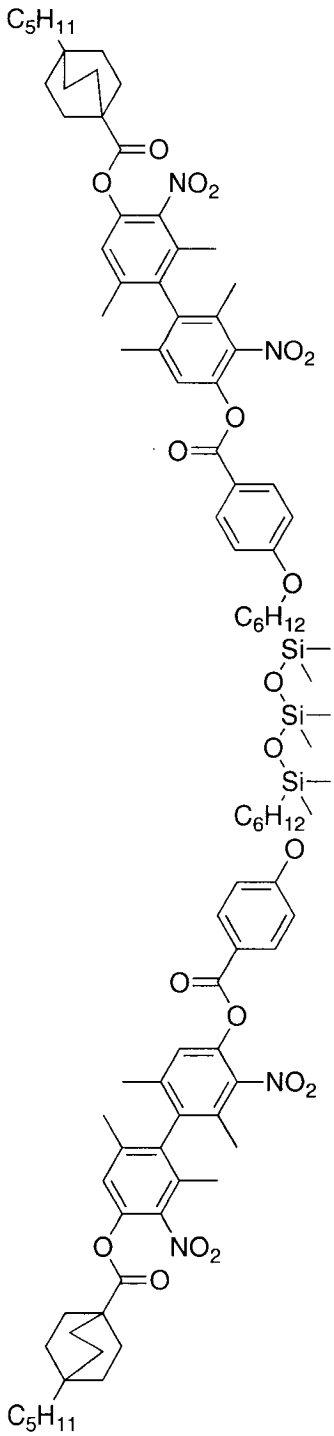

To a solution of (*R*)-**2.15** (75 mg, 0.14 mmol), 4-[6-(1,1,3,3,5,5 hexamethyl trisiloxanyl)-bis-hexyloxy]benzoic acid (31 mg, 0.05 mmol), and DMAP (17 mg, 0.14 mmol) in CH_2Cl_2 (5 mL) was added solid DCC (31 mg, 0.15 mmol) under an argon atmosphere. The reaction mixture was stirred for 20 hours then filtered. The filtrate was diluted with EtOAc and washed with 10% aq. HCl (2x), H_2O and brine. The organic layer was dried ($MgSO_4$) and concentrated to a white solid, which was purified by flash chromatography on silica gel (5:1 Hexanes/EtOAc) to give 27 mg (33%) of (*R,R*)-**3.7** as a white solid. Further purification was achieved via recrystallization from IPA after passing through a 0.45 μm PTFE filter: ^{1}H NMR ($CDCl_3$, 400 MHz) δ 0.04 (s, 12H), 0.52 (m, 4H), 0.87 (t, J = 7.6 Hz, 6H), 1.24 (m, 26H), 2.43 (m, 6H), 1.81 (m, 4H), 1.88 (m, 6H), 1.94 (s, 12H), 1.97 (s, 12H), 4.03 (t, J = 6.5 H, 4H), 6.96 (d, J = 10.2 Hz, 4H), 7.10 (s, 2H), 7.30 (s, 2H), 8.06 (d, J = 10.2 Hz, 4H). ^{13}C NMR ($CDCl_3$, 100 MHz) δ 0.0, 14.1, 14.1, 15.0, 15.1, 18.3, 20.3, 20.3, 22.7, 23.2, 23.3, 25.7, 28.5, 29.0, 30.2, 30.4, 32.8, 33.1, 39.5, 41.2, 68.4, 114.5, 120.0, 123.5, 123.5, 129.6, 129.7, 132.7, 136.1, 140.0, 140.0, 141.8, 141.9, 143.3, 143.4, 163.6, 164.1, 175.5.

(*S*)-4-Hydroxy-2,2',6,6'-tetramethyl-4'-[(4-octyloxybenzoyl)oxy]-3,3'dinitrobiphenyl (3.7)

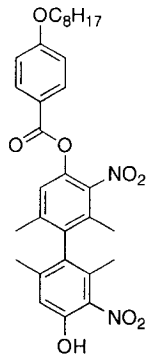

To a solution of (*S*)-**2.13** (100 mg, 0.30 mmol), 4-octyloxybenzoic acid (80 mg, 0.32 mmol) and, DMAP (73 mg, 0.6 mmol) in CH_2Cl_2 (5 mL), was added solid DCC (124 mg, 0.60 mmol) under an argon atmosphere. The reaction mixture was stirred for 20 hours and then filtered. The filtrate was diluted with EtOAc and washed with 10% aq. HCl (2x), H_2O and brine. The organic layer was dried ($MgSO_4$) and concentrated to a yellow oil which was purified by flash chromatography on silica gel (5:1 hexanes/EtOAc) to give 97 mg (57%) of (*S*)-**3.7** as a yellow oil: ^{1}H NMR ($CDCl_3$, 400 MHz) δ 0.88 (t, J = 6.5 Hz, 3H), 1.29 (m, H), 1.46 (m, 2H), 1.81 (m, 2H), 1.93 (s, 3H), 1.93 (s, 3H), 1.97 (s, 3H), 2.19 (s, 3H), 4.04 (t, J = 6.6 Hz, 2H), 6.96 (d, J = 8.5 Hz, 2H), 7.02 (s, 1H), 7.30 (s, 1H), 8.06 (d, J = 8.5 Hz). ^{13}C NMR ($CDCl_3$, 100 MHz) δ 14.1, 15.1, 18.1, 20.4, 21.0, 22.6, 25.9, 29.0, 29.2, 29.3 , 31.8, 68.4, 114.5, 118.7, 119.9, 123.4, 130.0, 131.5, 132.6, 134.0, 134.8, 136.8, 140.4, 141.8, 143.4, 145.3, 154.1, 163.6, 164.1. MS (ESI) *m/z* 587 ([M + Na]$^+$, 76), 365 (100), 332 (79), 186 (91). HRMS (ESI) calc'd for $C_{31}H_{36}N_2NaO_8$: 587.2369; found: 587.2358.

(*S*)-4-{[4-(5,5,6,6,7,7,8,8,9,9,10,10,10-tridecafluoro)decyloxybenzoyl]oxy}-2,2',6,6'tetramethyl-4'-[(4-octyloxybenzoyl)oxy]-3,3'-dinitrobiphenyl (3.6)

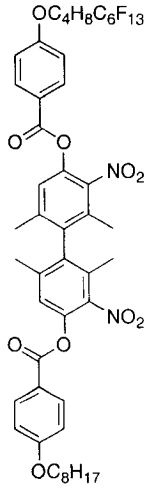

The procedure used in the synthesis of (*R*)-**2.16a** was repeated with 33 mg (0.06 mmol) of (*S*)-**3.7** and 68 mg (0.12 mmol) 4-(5,5,6,6,7,7,8,8,9,9,10,10,10-tridecafluoro)decyloxybenzoic acid to give 42 mg (67%) of (*S*)-**3.8** as a white solid. Further purification was achieved via recrystallization from hexanes after passing through a 0.45 μm PTFE filter: ^{1}H NMR ($CDCl_3$, 400 MHz) δ 0.89 (t, J = 06.7 Hz, 3H), 1.29 (m, 10H), 1.46 (m, 2H), 1.83 (m, 4H), 1.93 (m, 2H), 1.98 (s, 6H), 2.02 (s, 6H), 2.18 (m, 2H), 4.04 (t, J = 6.5 Hz, 2H), 4.09 (t, J = 5.8 Hz, 2H), 6.97 (m, 4H), 7.33 (s, 2H), 8.08 (m, 4H). ^{13}C NMR ($CDCl_3$, 100 MHz) δ 14.1, 15.1, 17.2, 20.4, 22.6, 26.00, 28.5, 29.0, 29.2, 29.3, 30.6, 31.8, 67.5, 68.4, 114.5, 114.6, 119.9, 120.4, 123.5, 123.6, 129.7, 129.8, 132.7, 132.7, 136.1, 136.2, 140.0, 140.1, 141.9, 142.0, 143.4, 163.5, 163.6, 163.7, 164.1. MS (ESI) *m/z* 1097 ([M + K]$^+$, 7), 429 (100), 401 (70). HRMS calc'd for $C_{48}H_{47}F_{13}KN_2O_{10}$: 1097.2660; found: 1097.2680.

5.2. Determination of transition temperatures by polarized microscopy

Phase transition temperatures were obtained by (i) polarized microscopy on thin films in 4 μm polyimide-coated ITO glass cells (E.H.C. Co., Japan) or on untreated glass slides with a cover slip using a Nikon Eclipse E600 POL and a Linkam LTS 350 hot stage or (ii) by DSC. The I-N*, N*-SmA* and SmC*-X transitions were determined, on cooling, by texture changes as observed through cross polarizers while the SmA*-SmC* phase transition was determined either by (i) a texture change between cross polarizers,

(ii) electro-optical response observed when applying an AC triangular wave (6V/μm) across the cell, or, (iii) in cases where the electroclinic response was large, by determining when the tilt angle, θ, was no longer voltage dependant.

5.3. Ferroelectric measurements

5.3.1. Sample preparation

Mixtures were prepared by mixing the appropriate amount of host and dopant in conical glass vials. The mixtures were heated to isotropic liquid to ensure mixing. These mixtures were loaded into rubbed polyimide-coated ITO glass slides (E.H.C., 4 μm x 0.16 cm^2) by capillary action. The cell thickness was determined based on the capacitance measured by an APT-III polarization testbed (Displaytech Inc. Longmont, Colorado). Ferroelectric measurements were performed with the APT-III in conjunction with a Nikon Eclipse E6000 POL and Linkam LTS 350 hot stage. The samples were heated under an AC triangular wave voltage (100 Hz, 6V/μm) into the isotropic liquid phase and held there until air bubbles were no longer visible in the addressed area. Good alignment was obtained by slowly cooling the sample from isotropic, through the N* phase, if present, and into the SmA* phase.

5.3.2. Polarization measurements

The reduced polarization, P_o, was calculated for each mixture at $T-T_{AC}$ = -5 K according to equation 1-2. The spontaneous polarization, P_s, was measured by the triangular wave method (100 Hz, 6V/mm).[6] Tilt angles, θ, were measured as half the

rotation between the two extinction states with applied voltages of +15V and –15V. The sign of polarization was determined from the relative configuration of the electric field and the switching position of the sample according to the established convention.[7]

5.3.3. Electroclinic measurements

The same mixtures used for ferroelectric measurements were cooled, from isotropic, to $T-T_{AC}$ = +1.5, +2.5 and/or +4 K. At these temperatures, the tilt angle, θ, was measured as the half rotation between two extinction states. Electroclinic coefficients were determined by the slope of θ vs. V/μm.

5.4. UV-Vis measurements

UV-Vis spectra were used as a means of determining the pitch of the selective reflection of (*R*)-**2.16a-e** and (*S*)-**3.8**. The mesogens were loaded into Grandjean-Cano wedge cells (E.H.C. Co., Japan), with an angle of 0.48°, by capillary action. An Ocean Optics Mini-D2T deuterium tungsten lamp was employed as a light source and an Ocean Optics ISS-2 Integrated Sampling Detector attached to an Ocean Optics USB2000 Miniature Fiber Optic Spectrometer, which was interfaced with a computer. Spectra were recorded on heating and were processed with the 001Base31 Spectrometer Operating Software (for windows).

The samples were mounted on a vertically aligned Linkam LTS 350 hot stage. For (*R*)-**2.16c-e** the light was passed through the sample at room temperature and was used as the reference. The reference had integration times such that the maximum intensity was ~3000 counts (typically 120-180 ms). The other software parameters used were: average 6, boxcar 6 and F.D. 100 ms. For (*R*)-**2.16a** and (*R*)-**2.16b**, which displayed selective reflection at room temperature, the light was passed through the sample and parameters were set such that the intensity of light was ~500 counts at ~500 nm ((*R*)-**2.16a**) or the maximum intensity of ~3000 counts was observed at ~600 nm ((*R*)-**2.16b**) at room temperature. The sample was then heated to temperatures 20 K above where selective the reflection was no longer evident and a new reference was taken with the predetermined parameters. The samples were then cooled to room temperature, and then reheated. Once references were obtained the software was switched into absorbance mode in which spectra were recorded. Absorbance spectra for (*S*)-**3.8** were obtained as for (*R*)-**2.16c-e**. Spectra were recorded at incremental temperatures with heating at a rate of 5 ^{o}C/min and with an additional 5-10 minutes to allow the sample to equilibrate at the desired temperature before spectra were recorded.

5.5. References:

(1) Cheng, X.; Das, M. K.; Diele, S.; Tschierske, C. *Langmuir* **2002**, *18*. 6521.

(2) Guillon, D.; Osipov, M. A.; Méry, S.; Siffert, M.; Nicoud, J.-F., Bourgognr, C.; Sebastião, P. *J. Mater. Chem.* **2001**, *11*, 2700.

(3) Hartley, S. Ph.D. Thesis, Queen's University, Kingston, 2005

(4) Keller, P. *Ferroelectrics* **1984**, *58*, 3.

(5) Gray, G. W.; Hird, M.; Lacey, D.; Toyne, K. J. *J. Chem. Soc., Perkin Trans. II* **1989**, 2041-2053.

(6) Miyasato, K.; Abe, S.; Takezoe, H.; Fukuda, A.; Kuze, E. *Jpn. J. Appl. Phys.* **1983**, *22*, L661.

(7) Walba, D. M. In *Advances in the Synthesis and Reactivity of Solids*; Mallouck, T. E., Ed.; JAI Press, Ltd.: Greenwich, CT, 1991; Vol. 1, pp 173-235.

Appendix A. ^{1}H NMR of key compounds

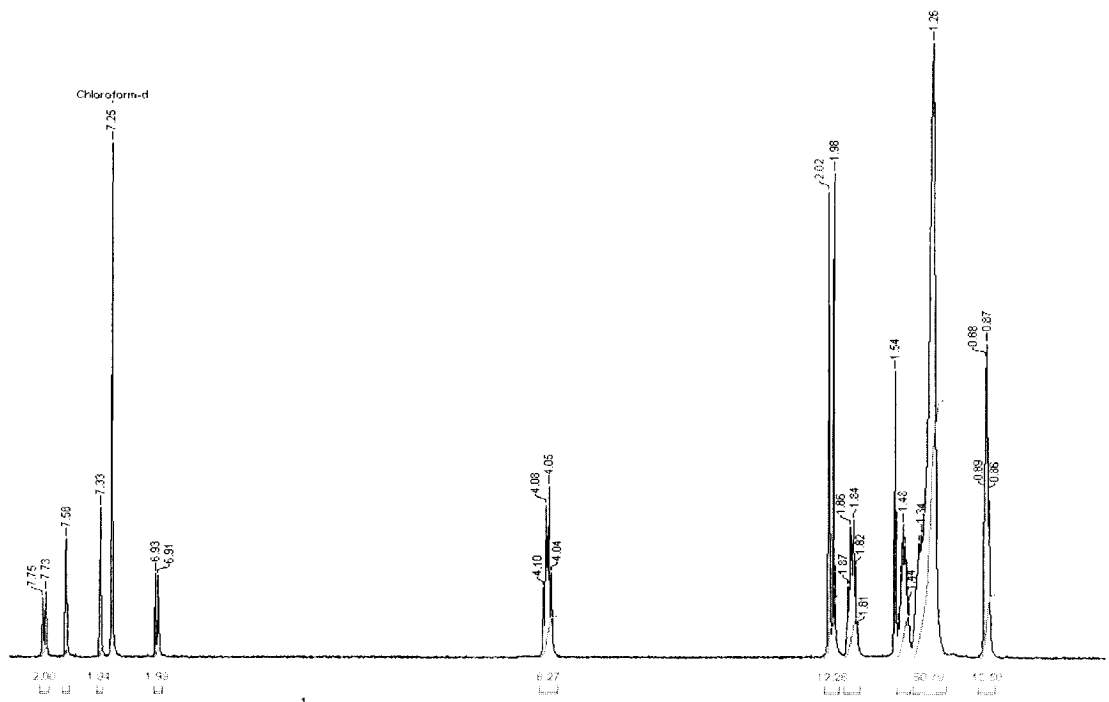

Figure A1-1. 400 MHz ^{1}H NMR spectrum of (*R*)-**2.14a**.

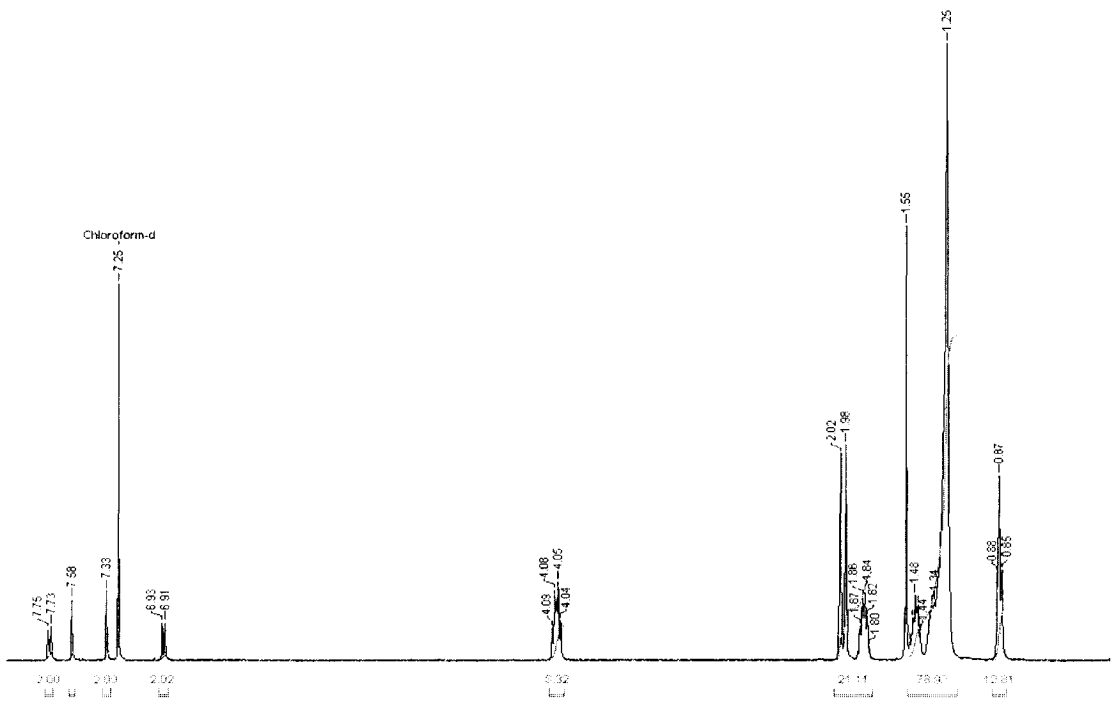

Figure A1-2. 400 MHz ^{1}H NMR spectrum of (*S*)-**2.14b**.

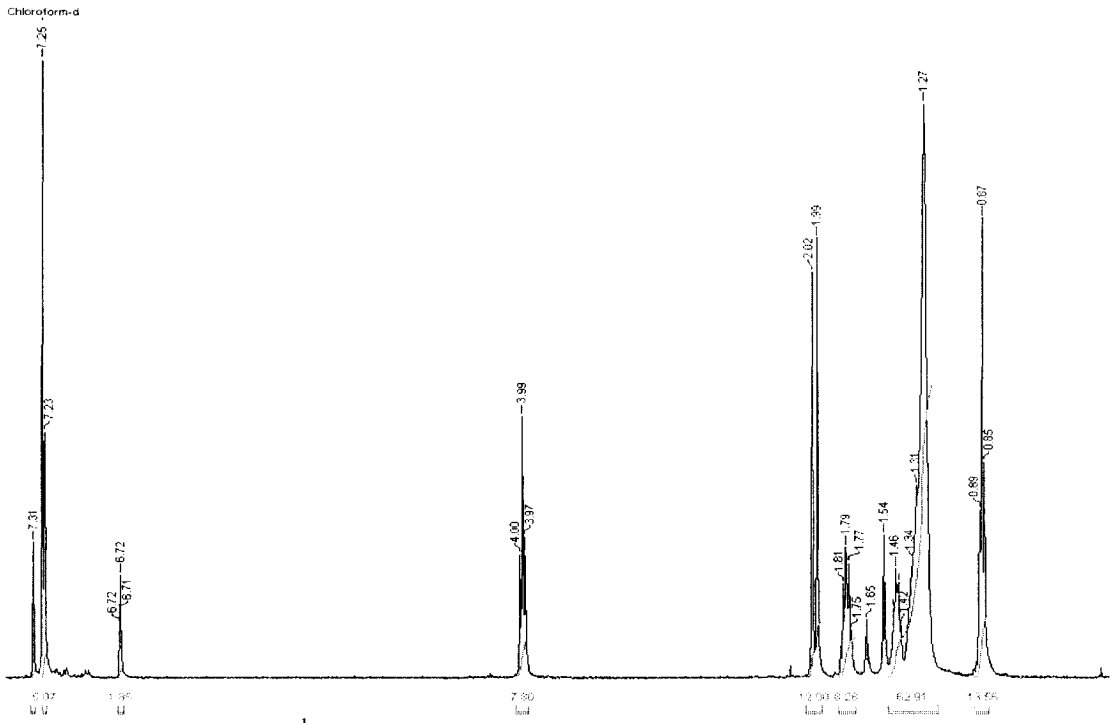

Figure A1-3. 400 MHz ^{1}H NMR spectrum of (*R*)-**2.14c**.

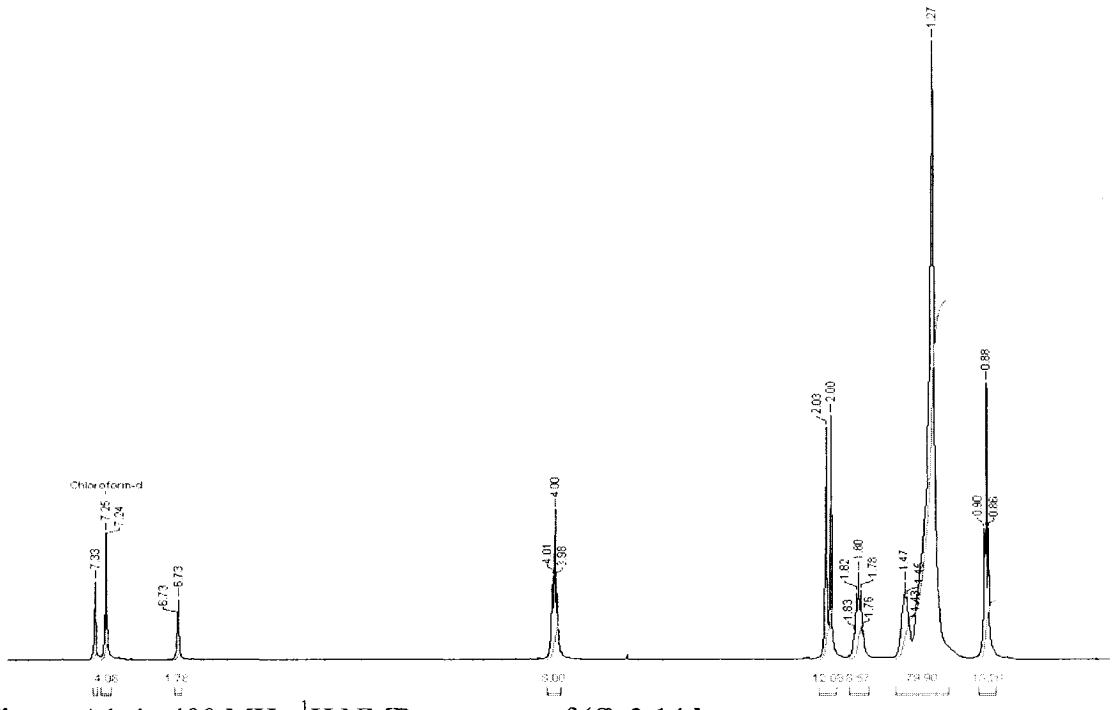

Figure A1-4. 400 MHz ^{1}H NMR spectrum of (*S*)-**2.14d**.

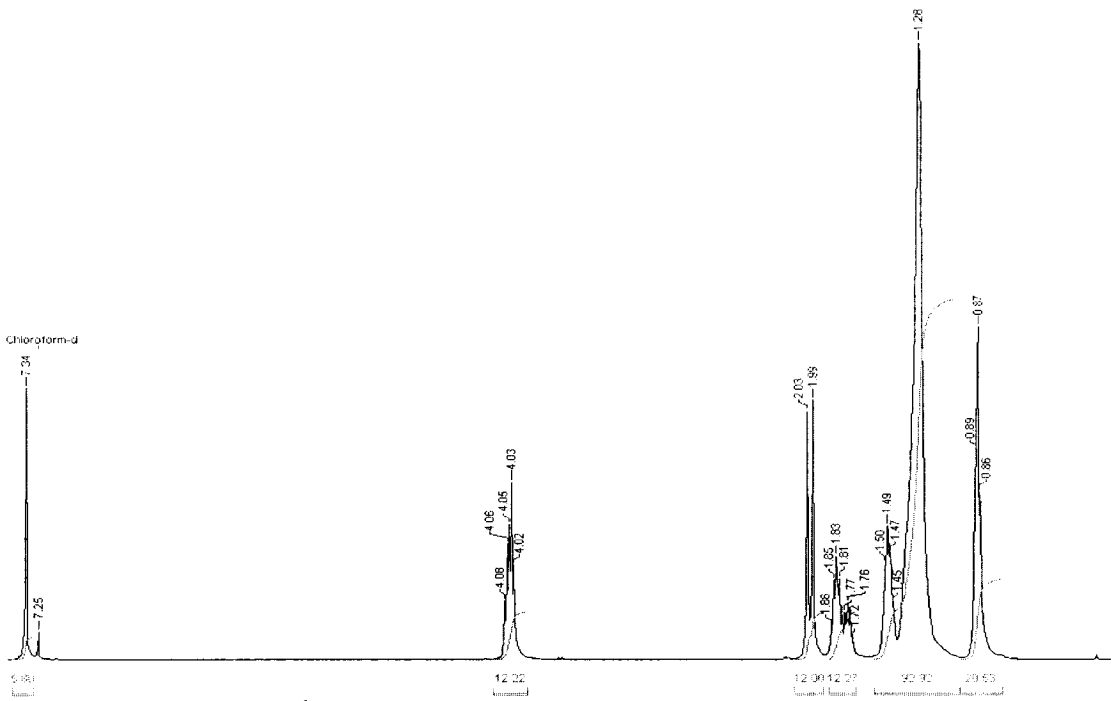

Figure A2-5. 400 MHz ^{1}H NMR spectrum of (*S*)-**2.14e**.

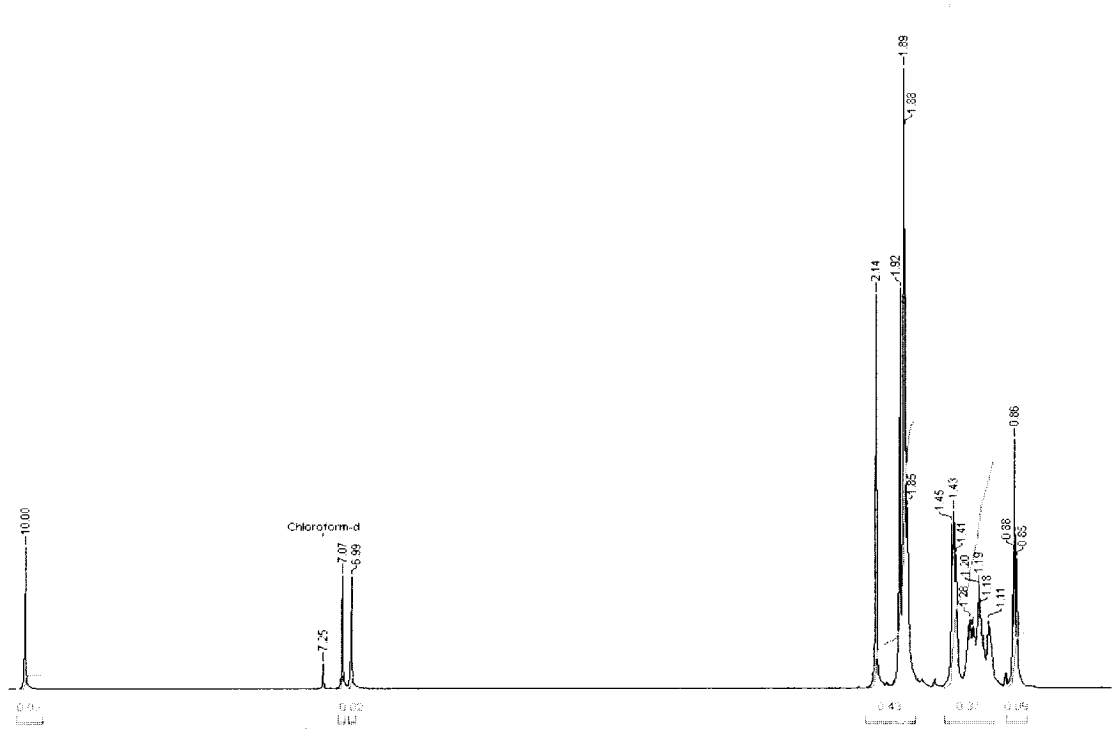

Figure A2-6. 400 MHz ^{1}H NMR spectrum of (*R*)-**2.15**.

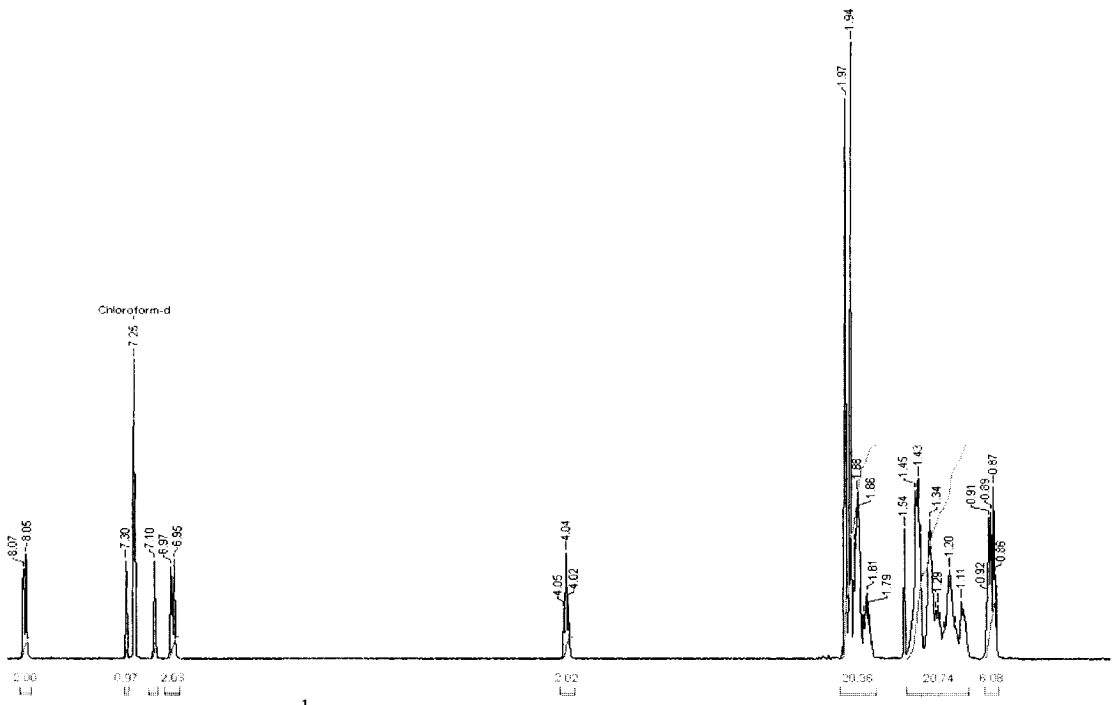

Figure A1-7. 400 MHz ^{1}H NMR spectrum of (*R*)-**2.16a**.

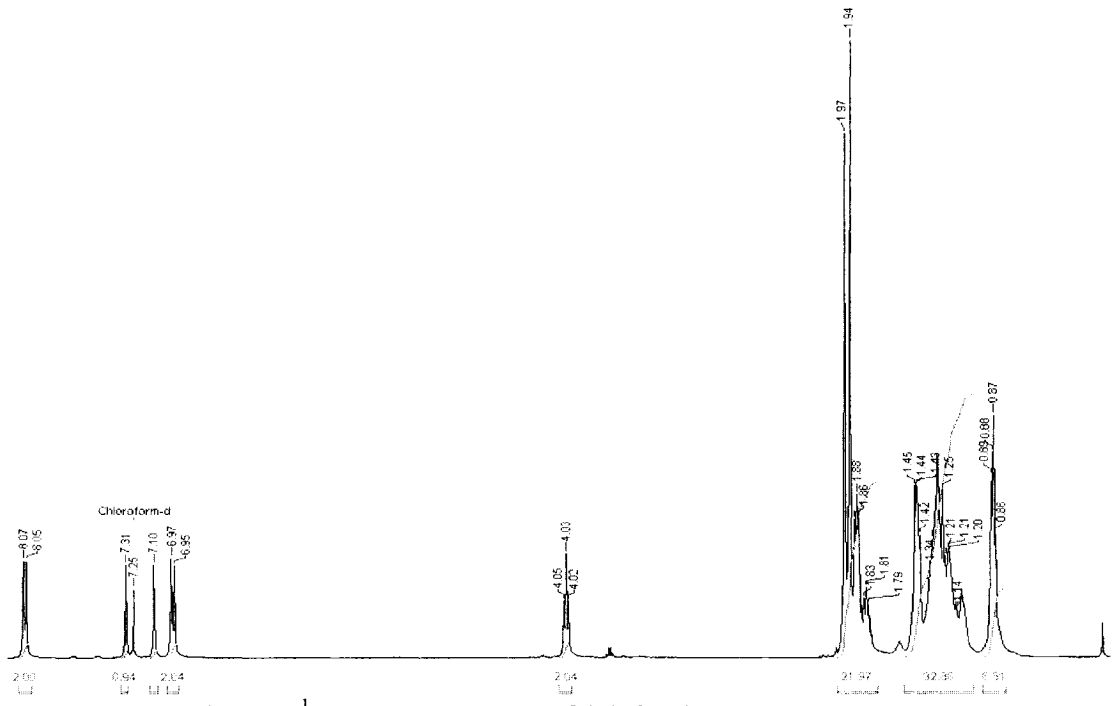

Figure A1-8. 400 MHz ^{1}H NMR spectrum of (*R*)-**2.16b**.

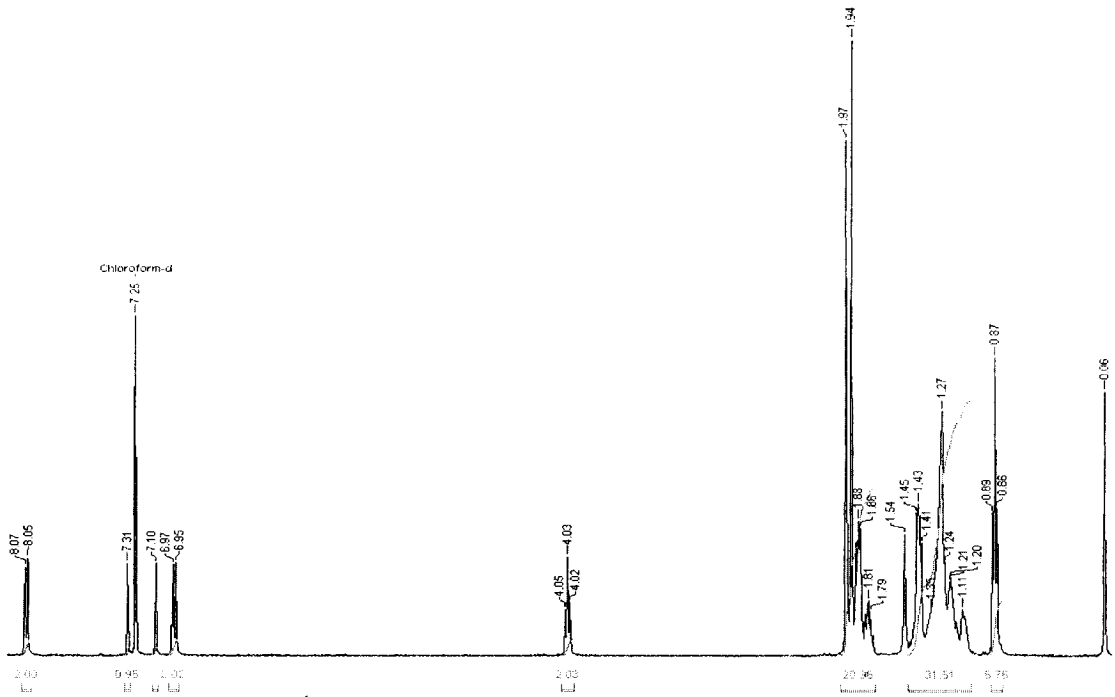

Figure A1-9. 400 MHz ^{1}H NMR spectrum of (*R*)-**2.16c**.

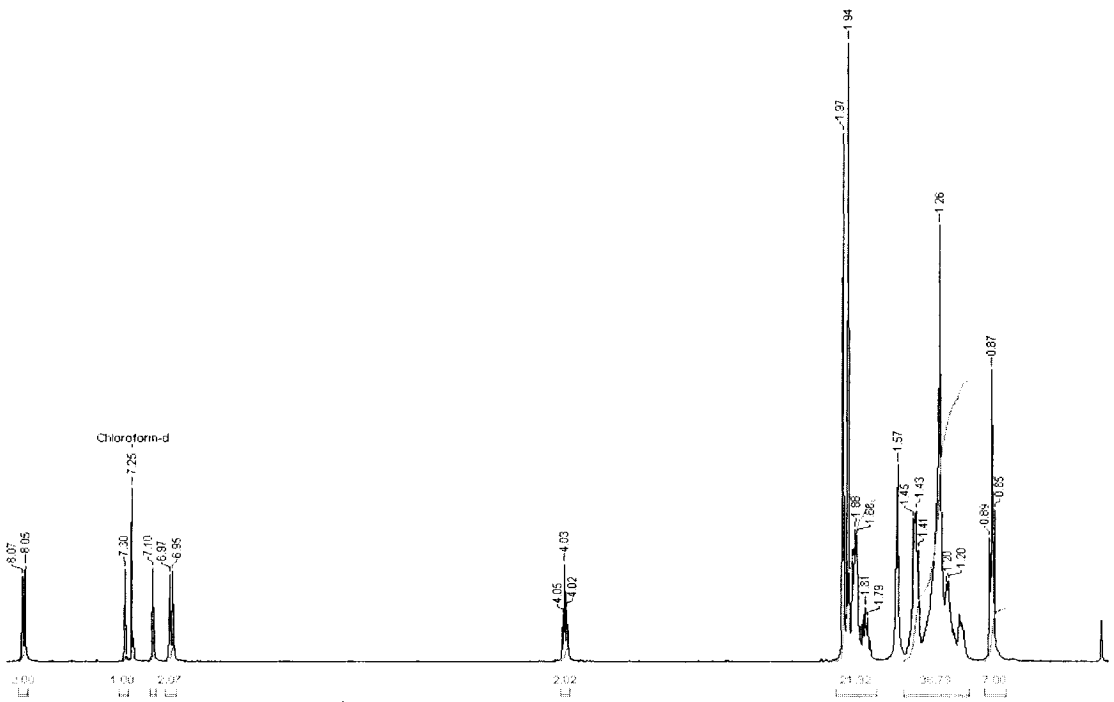

Figure A1-10. 400 MHz ^{1}H NMR spectrum of (*R*)-**2.16d**.

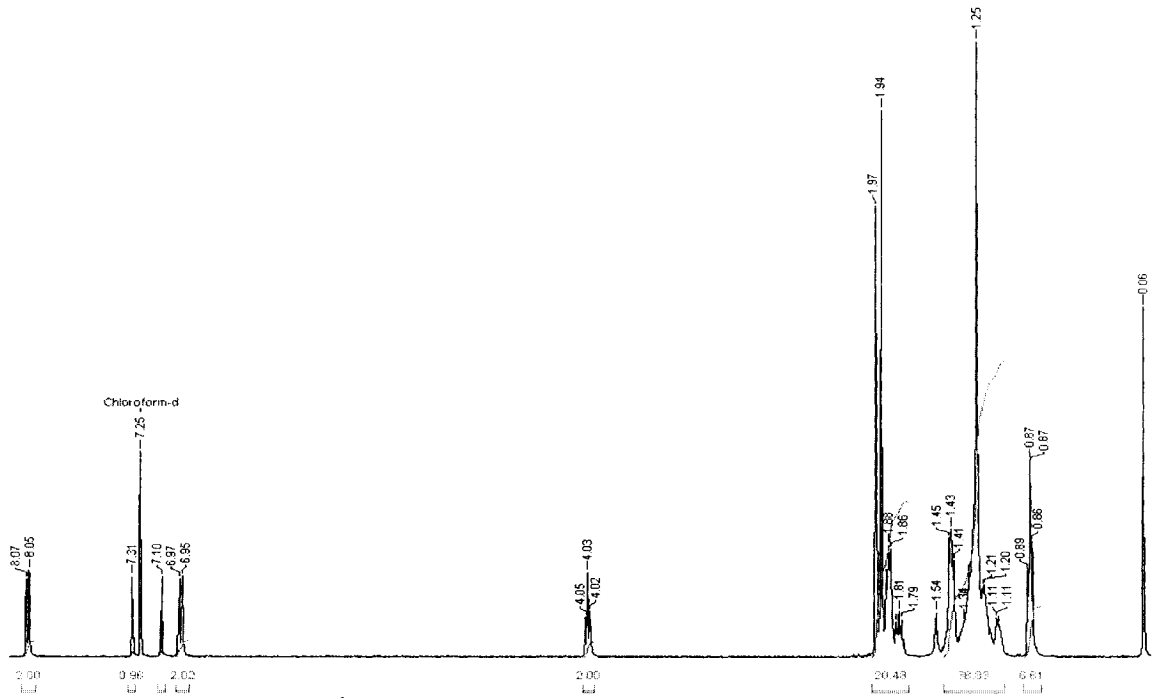

Figure A1-11. 400 MHz ^{1}H NMR spectrum of (*R*)-**2.16e**.

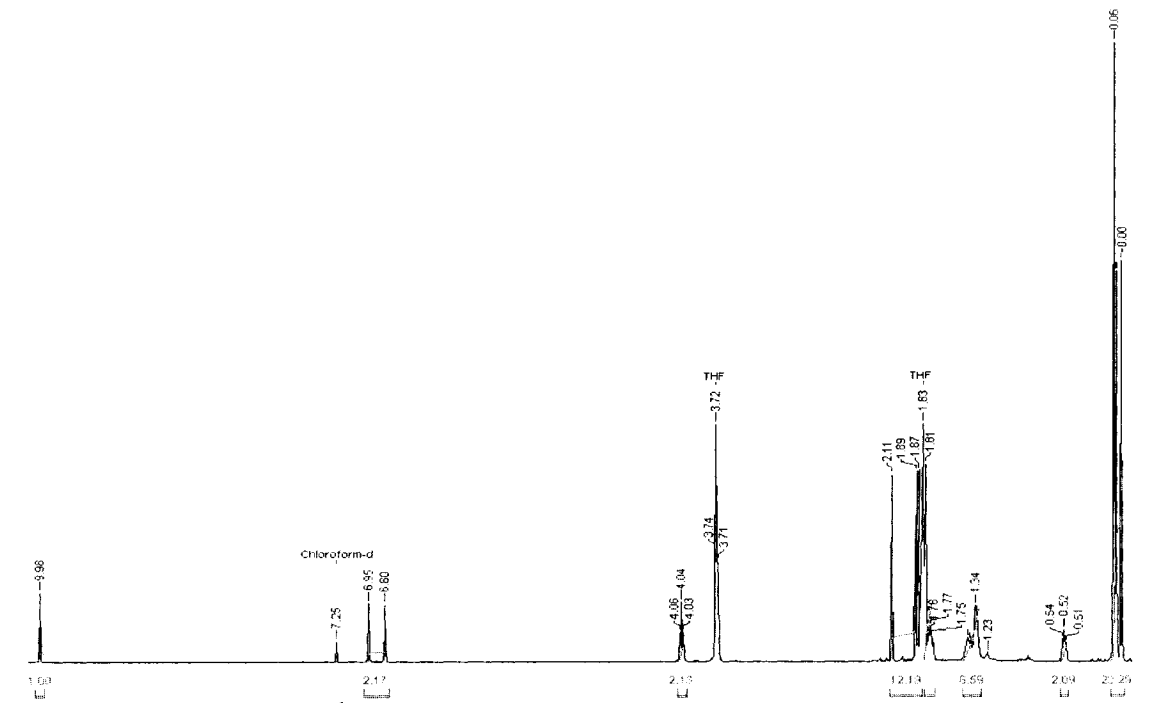

Figure A1-12. 400 MHz ^{1}H NMR spectrum of (*R*)-**3.1**.

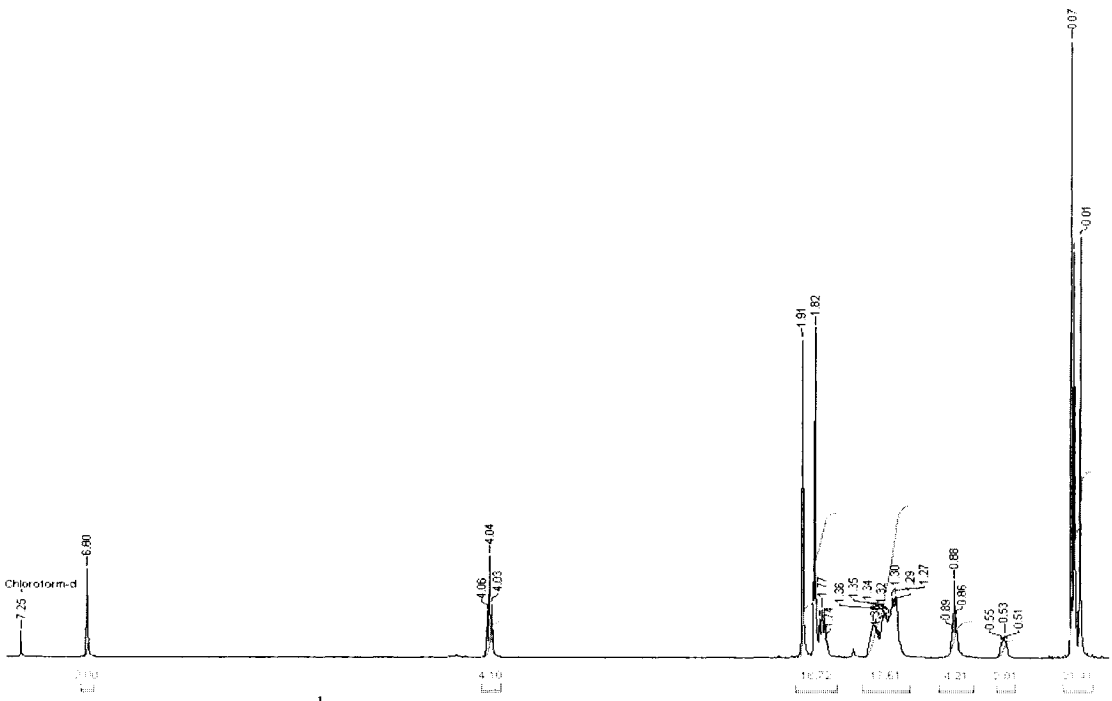

Figure A1-13. 400 MHz ^{1}H NMR spectrum of (*S*)-**3.2**.

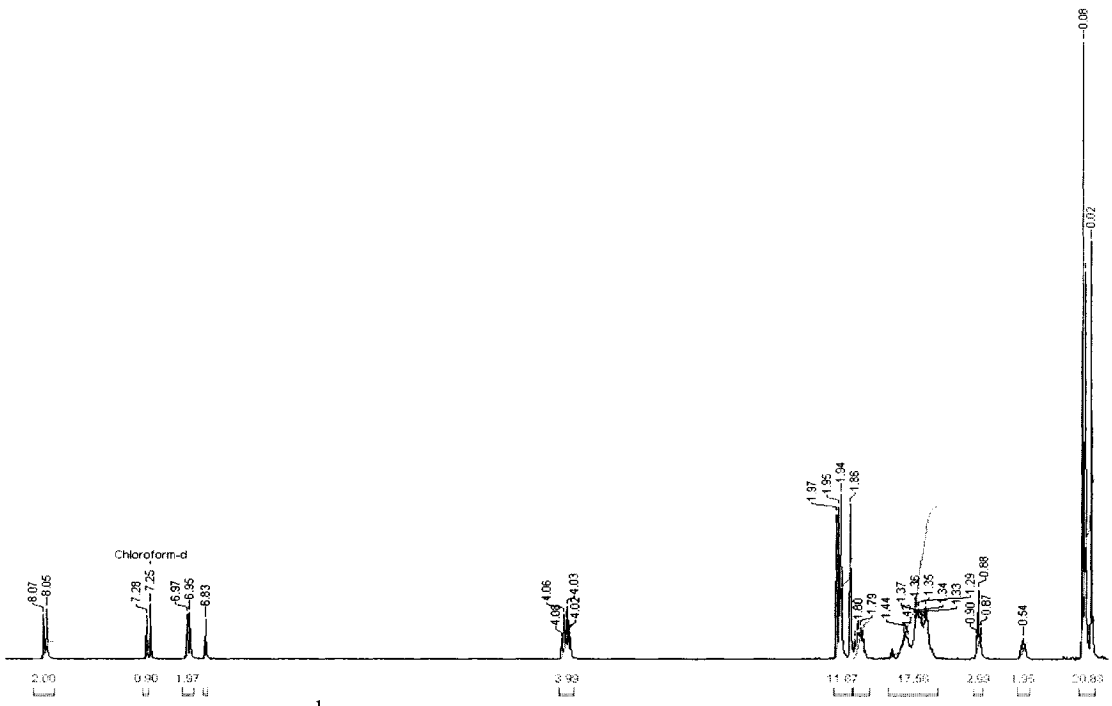

Figure A1-14. 400 MHz ^{1}H NMR spectrum of (*R*)-**3.3**.

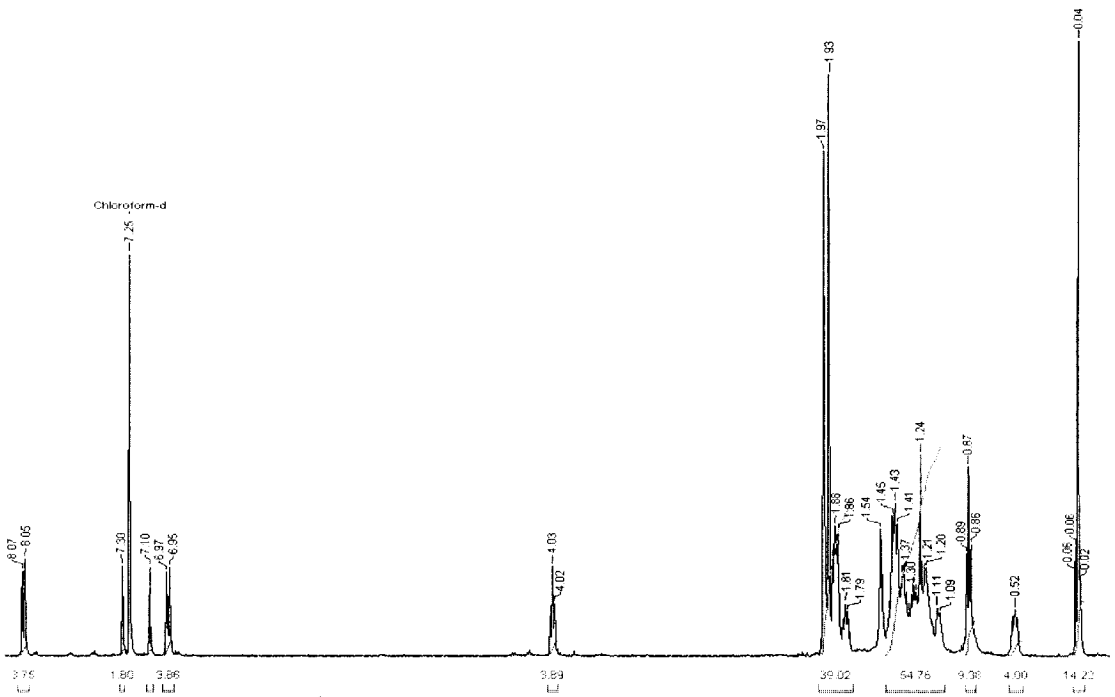

Figure A1-15. 400 MHz ^{1}H NMR spectrum of (*R,R*)-**3.4**.

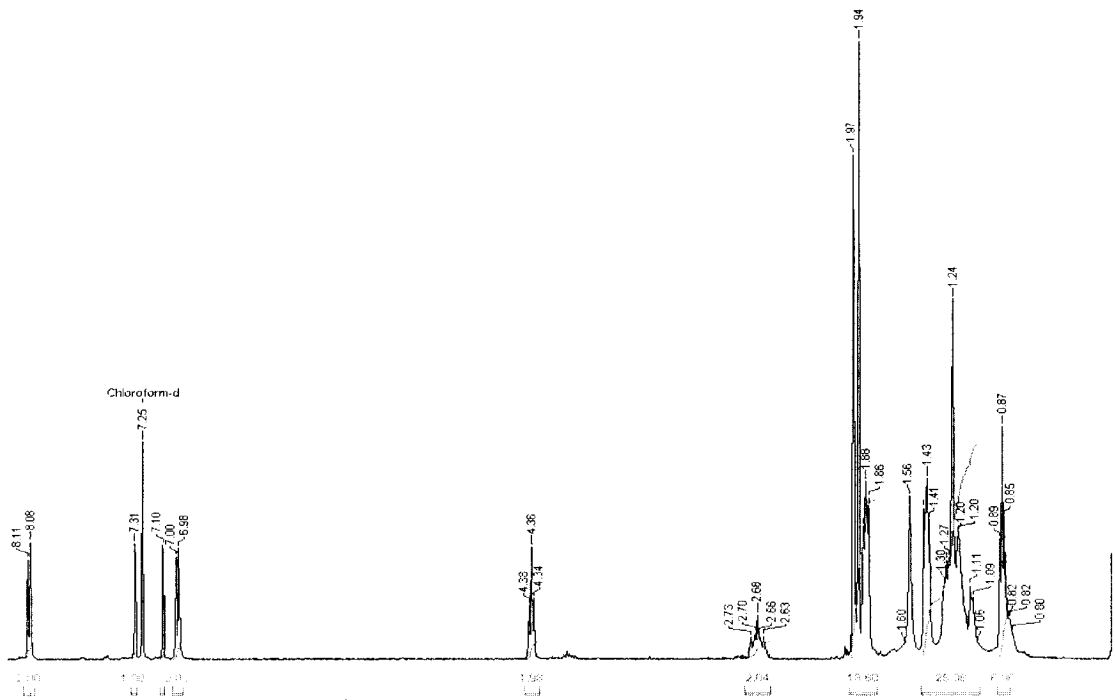

Figure A1-16. 400 MHz ^{1}H NMR spectrum of (*R*)-**3.5**.

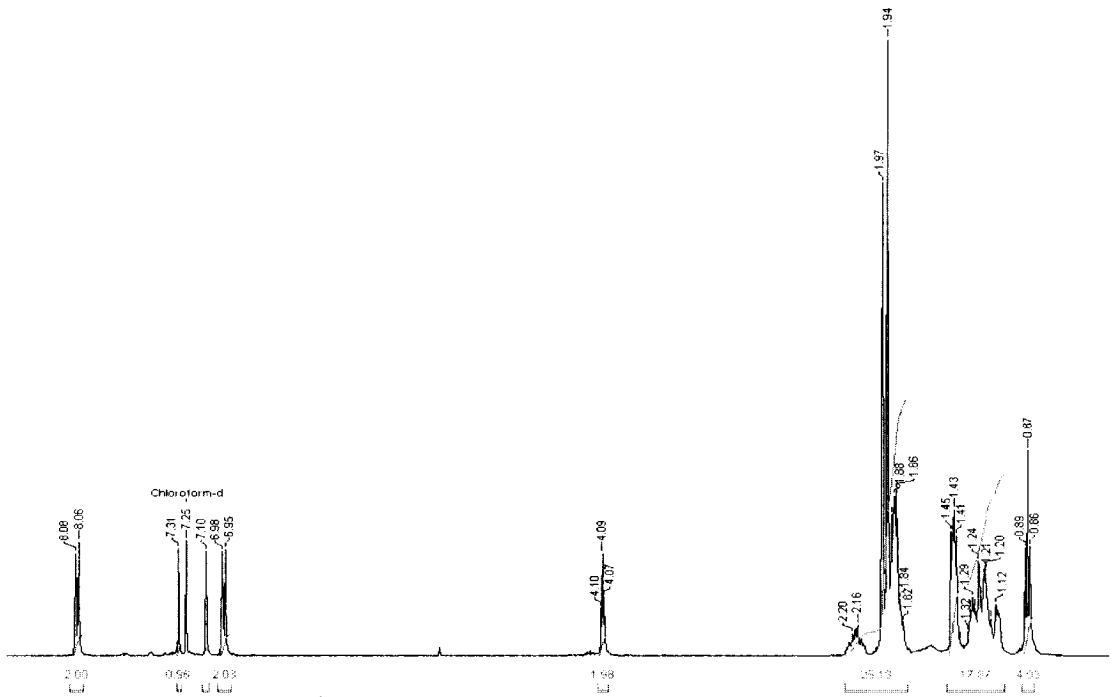

Figure A1-17. 400 MHz ^{1}H NMR spectrum of (*R*)-**3.6**.

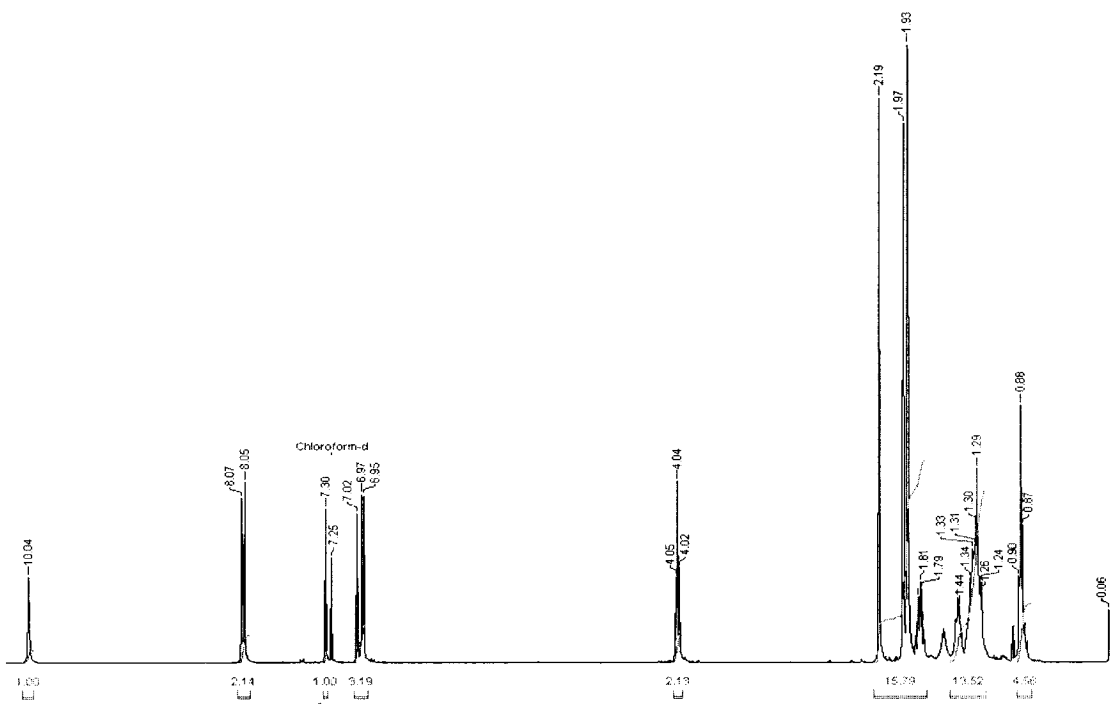

Figure A1-18. 400 MHz ^{1}H NMR spectrum of (*S*)-**3.7**.

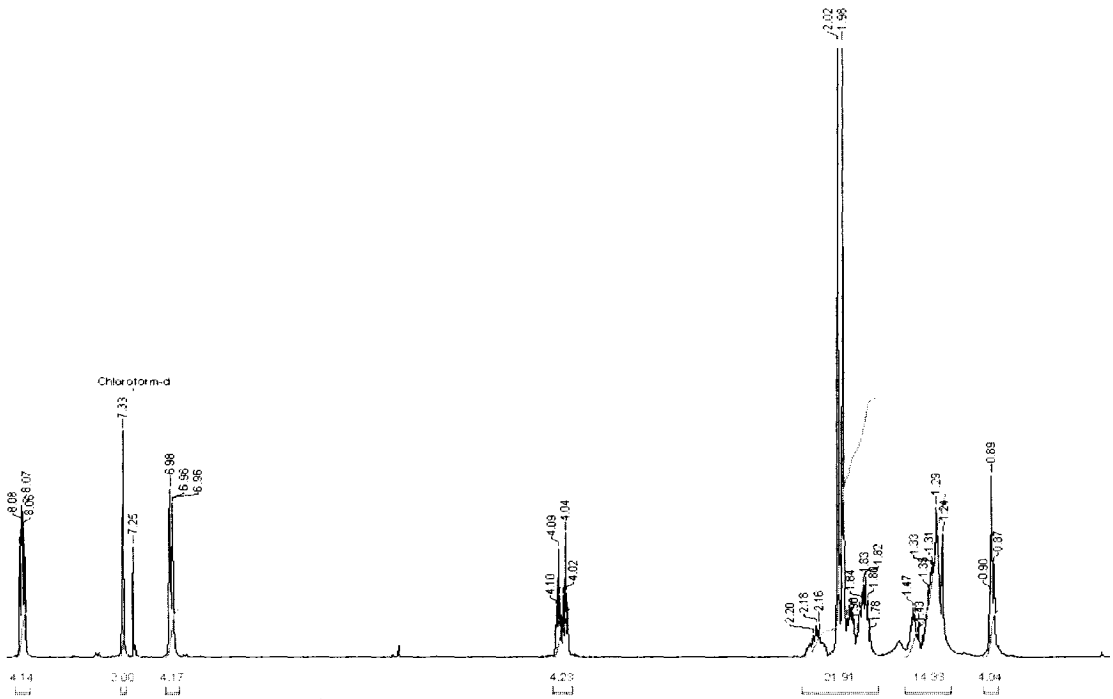

Figure A1-19. 400 MHz ^{1}H NMR spectrum of (*S*)-**3.8**.

Appendix B. DSC of novel mesogens

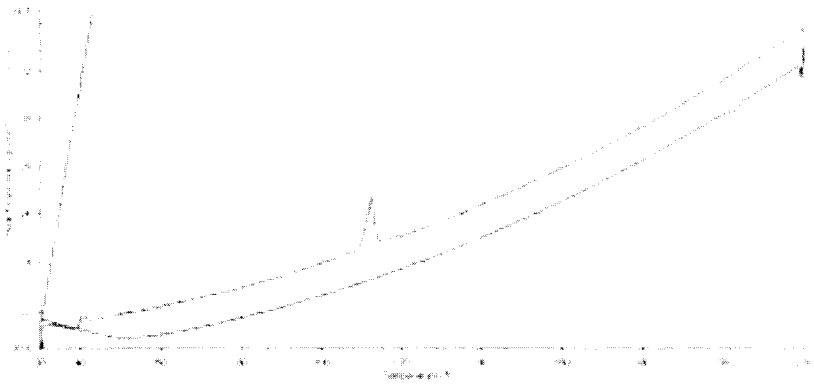

Figure B1-1. DSC trace of (*R*)-**2.16a**.

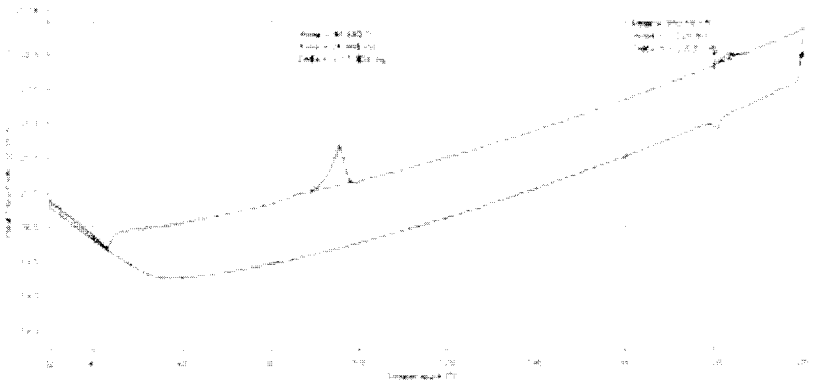

Figure B1-2. DSC trace of (*R*)-**2.16b**.

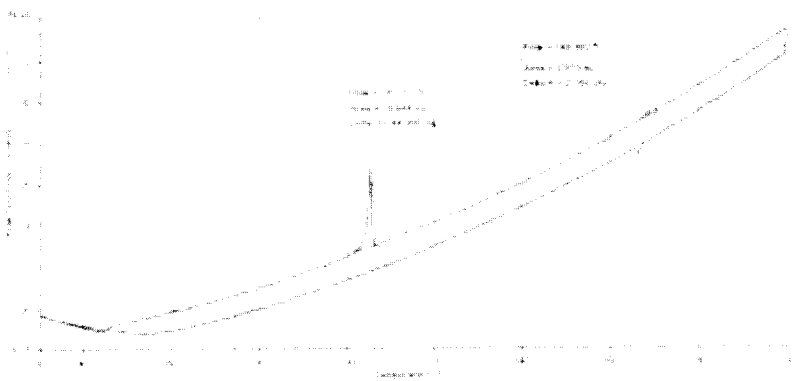

Figure B1-3. DSC trance of (*R*)-**2.16c**.

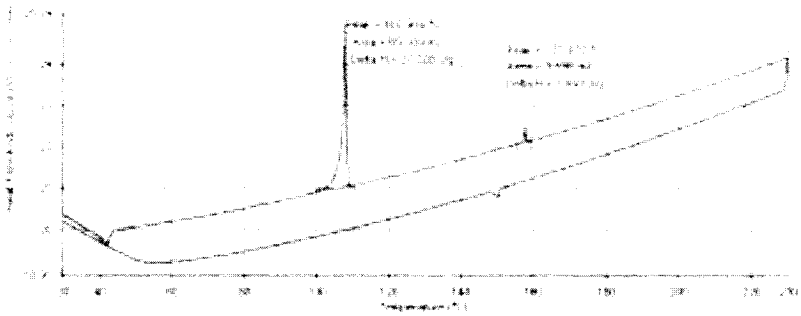

Figure B1-4. DSC trace of (*R*)-**2.16d**.

Appendix C. Textures of novel mesogens

(a) (b)

Figure C1-1. Texture of the N* phase of (*R*)-**2.16a** 400X on a glass slide fitted with a cover slip at 125 °C (a) before and (b) after shearing the cover slip.

Figure C1-2. Texture of the N* phase of (*R*)-**2.16b** 400X on a glass slide fitted with a cover slip at 130 °C (a) before and (b) after shearing the cover slip.

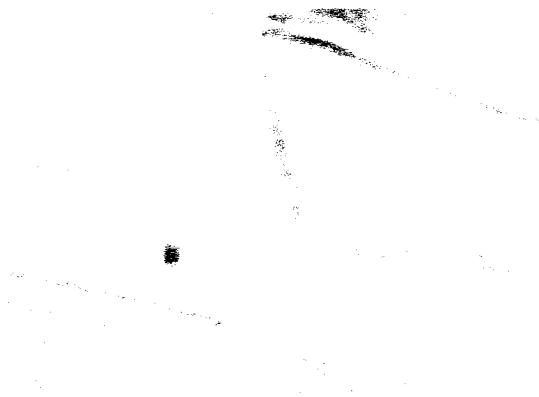

Figure C1-3. Texture of the N* phase of (*R*)-**2.16c** 400X on a glass slide fitted with a cover slip at 135 °C.

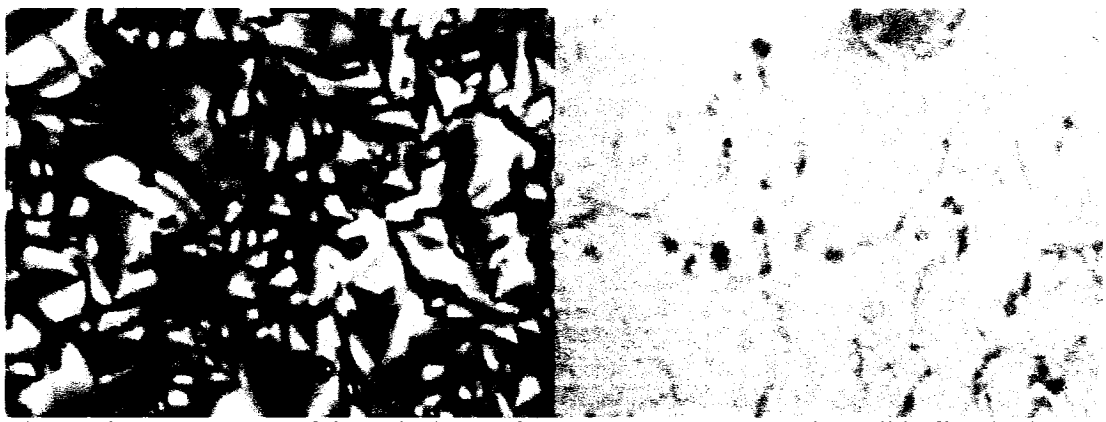

Figure C1-4. Texture of the N* phase of (*R*)-**2.16d** 400X on a glass slide fitted with a cover slip at 140 °C (a) before and (b) after shearing the cover slip.

Appendix D. Experimental data

Table D1-1. Spontaneous polarization, tilt angle, and reduced polarization measurements of chiral dopants containing an atropisomeric 3,3'-dinitrobiophenyl core in achiral liquid crystalline hosts.

dopant	host	χ_d	P_s (nC/cm^2)	θ (°)	P_o (nC/cm^2)
(*R*)-**2.14a**	**PhP1**	0.049	-0.96	17	-3.2
(*S*)-**2.14b**	**PhP1**	0.051	+1.99	9	+13.4
(*R*)-**2.16d**	**DFT**	0.045	-0.08	12	-0.4
(*R*)-**2.16d**	**NCB76**	0.054	-1.10	13	-5.1
(*R*)-**2.16d**	**PhB**	0.048	+3.27	19	+9.8
(*S*)-**3.2**	**3.9**	0.050	+0.14	10	+0.8
(*R*)-**3.3**	**3.9**	0.050	-0.75	14	-3.2
(*R*)-**3.6**	**PhP1**	0.030	-3.03	17	-10.4
(*S*)-**3.8**	**PhP1**	0.036	+9.73	19	+30.0

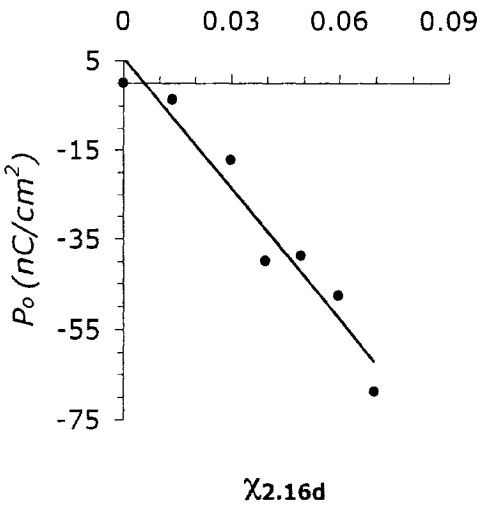

Figure 2-14. Plot of P_o vs. χ_d for (*R*)-**2.16d** in **PhP1** at $T\text{-}T_C$ = -5 K. Solid line indicates least squares best fit.

χ_d (*R*)-**2.16d**	P_s (nC/cm^2)	θ (°)	P_o (nC/cm^2)
0.014	-1.08	18	-3.5
0.030	-4.36	15	-17.1
0.039	-9.44	14	-39.9
0.049	-9.96	15	-38.7
0.060	-11.02	13	-47.6
0.070	-13.69	12	-68.7

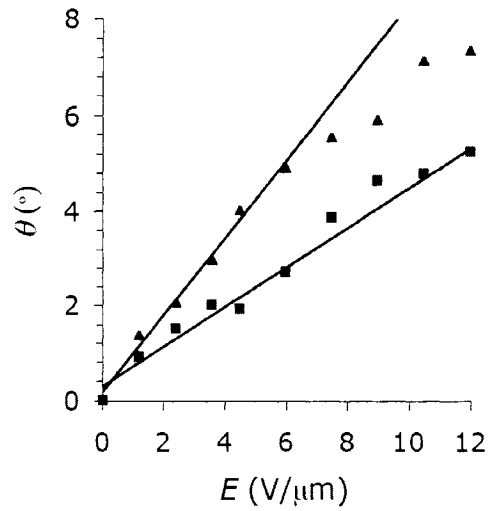

Figure 2-15(a). Induced tilt vs. applied voltage, *E*, for mixtures of (*R*)-**2.16d** in **PhP1** at $\chi_d = 0.06$. $T\text{-}T_C = +2.5$ K as (◆) and $T\text{-}T_C = +1.5$ K as (■). The solid lines represent the least-squares fit used to determine e_c.

	θ (°)	
E (V/mm)	$T\text{-}T_C = +2.5$ K	$T\text{-}T_C = +1.5$ K
0.0	0.0	0.0
1.2	0.9	1.4
2.4	1.5	2.1
3.6	2.0	3.0
4.5	1.9	4.0
6.0	2.7	4.9
7.5	3.9	5.6
9.0	4.7	5.9
10.5	4.8	7.2
12.0	5.3	7.4
13.5	6.0	8.0

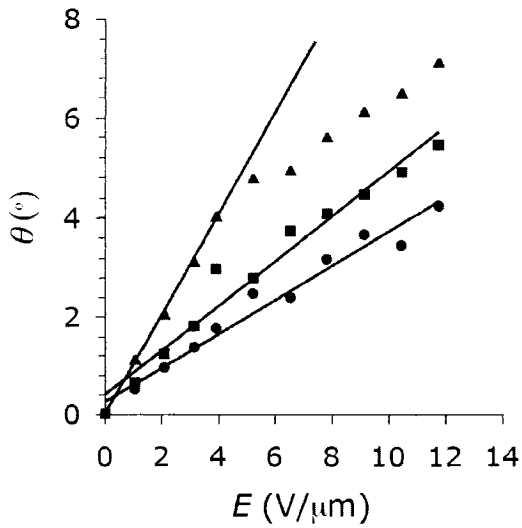

Figure 2-15(b). Induced tilt vs. applied voltage, *E*, for mixtures of (*R*)-**2.16d** in **PhP1** at χ_d = 0.07. $T-T_C$ = +4 K as (●),$T-T_C$ = +2.5 K as (◆) and $T-T_C$ = +1.5 K as (■). The solid lines represent the least-squares fit used to determine e_c.

	θ (°)		
E (V/mm)	$T-T_C$ = +4 K	$T-T_C$ = +2.5 K	$T-T_C$ = +1.5 K
0.0	0.0	0.0	0.0
1.0	0.5	0.7	1.1
2.1	1.0	1.3	2.1
3.1	1.4	1.8	3.1
3.9	1.8	3.0	4.1
5.2	2.5	2.8	4.8
6.5	2.4	3.7	5.0
7.9	3.2	4.1	5.6
9.2	3.7	4.5	6.2
10.5	3.5	4.9	6.5
11.8	4.2	5.5	7.1

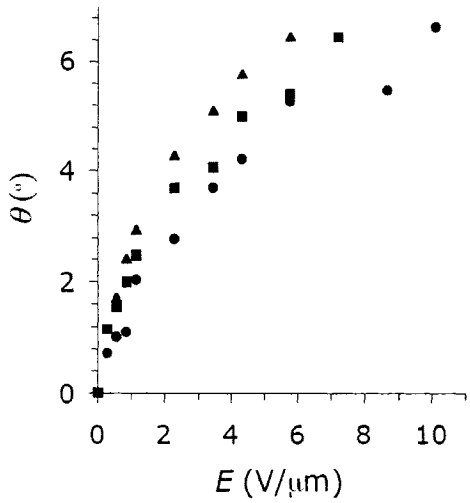

Figure 2-15(c). Induced tilt vs. applied voltage, E, for mixtures of (*R*)-**2.16d** in **PhP1** at $\chi_d = 0.10$. $T\text{-}T_C = +4$ K as (●), $T\text{-}T_C = +2.5$ K as (◆) and $T\text{-}T_C = +1.5$ K as (■).The e_c values were obtained by least-squares analysis on points from $E = 0 - 1.2$ V/μm.

	θ (°)		
E (V/mm)	$T\text{-}T_C$ = +4 K	$T\text{-}T_C$ = +2.5 K	$T\text{-}T_C$ = +1.5 K
0.0	0.0	0.0	0.0
0.3	0.7	1.2	1.2
0.6	1.0	1.6	1.7
0.9	1.1	2.0	2.4
1.2	2.0	2.5	3.0
2.3	2.8	3.7	4.3
3.5	3.7	4.1	5.1
4.3	4.2	5.0	5.8
5.8	5.3	5.4	6.5
7.2	-	6.5	-
8.7	5.5	7.0	-
10.1	6.7	-	-

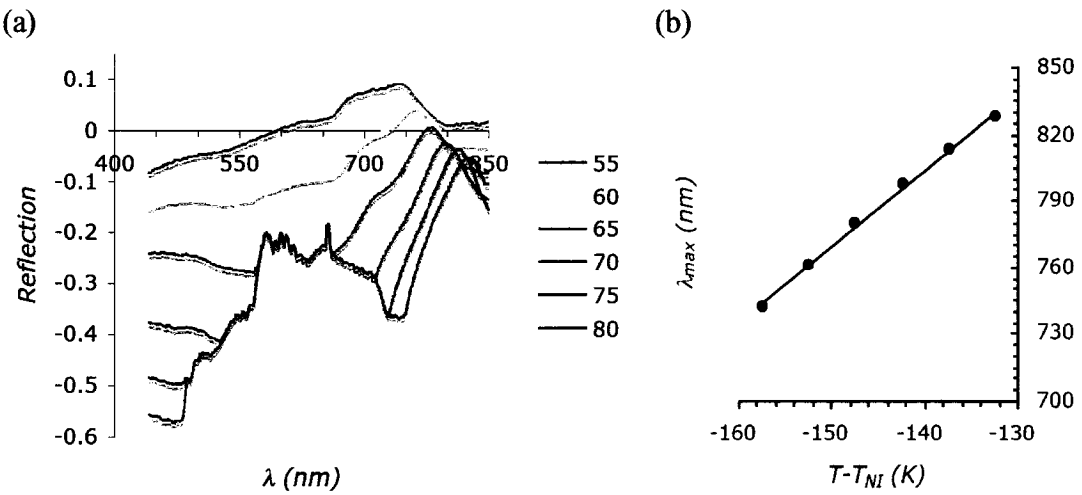

Figure D1-1. (a) Reflection spectrum of (*R*)-**2.16a** at temperatures ranging from 55–80 °C. (b) Plot of the pitch of (*R*)-**2.16a** vs. reduced temperature. Solid line indicates least squares best fit.

$T-T_{NI}$ (K)	λ_{max} (nm)
-157	742
-152	761
-147	780
-142	797
-137	813
-132	828

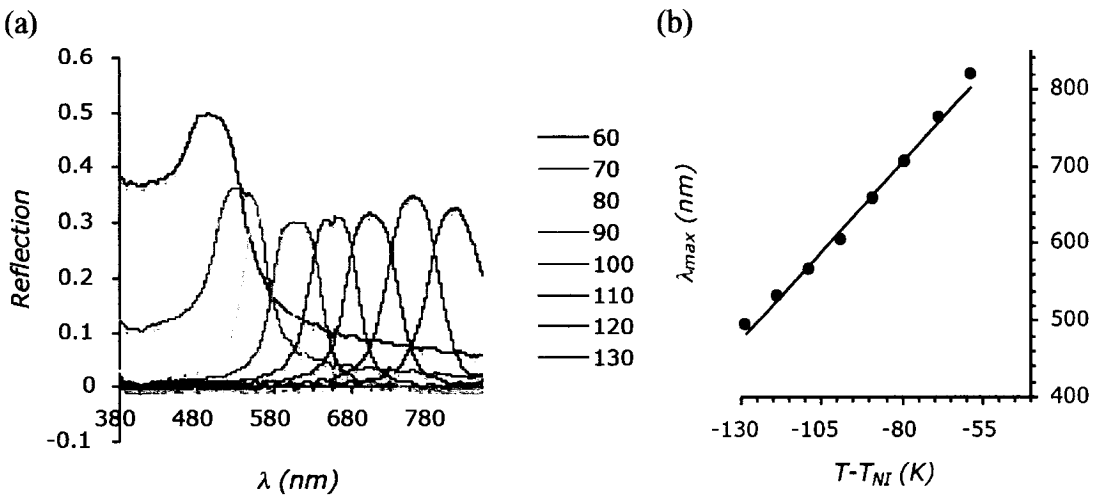

Figure D1-2. (a) Reflection spectrum of (*R*)-**2.16b** at temperatures ranging from 60–130 °C. (b) Plot of the pitch of (*R*)-**2.16b** vs. reduced temperature. Solid line indicates least squares best fit.

$T-T_{NI}$ (K)	λ_{max} (nm)
-129	496
-119	533
-109	566
-99	604
-89	659
-79	705
-69	761
-59	819

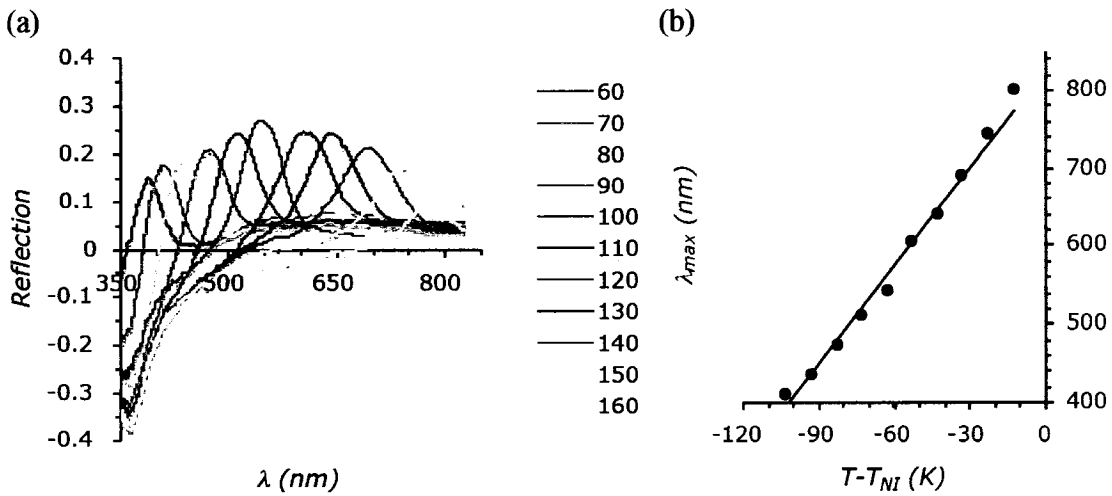

Figure D1-3. (a) Reflection spectrum of (*R*)-**2.16c** at temperatures ranging from 60–160 °C. (b) Plot of the pitch of (*R*)-**2.16c** vs. reduced temperature. Solid line indicates least squares best fit.

$T-T_{NI}$ (K)	λ_{max} (nm)
-113	386
-103	409
-93	435
-83	472
-73	510
-63	542
-53	604
-43	640
-33	689
-23	743
-13	800

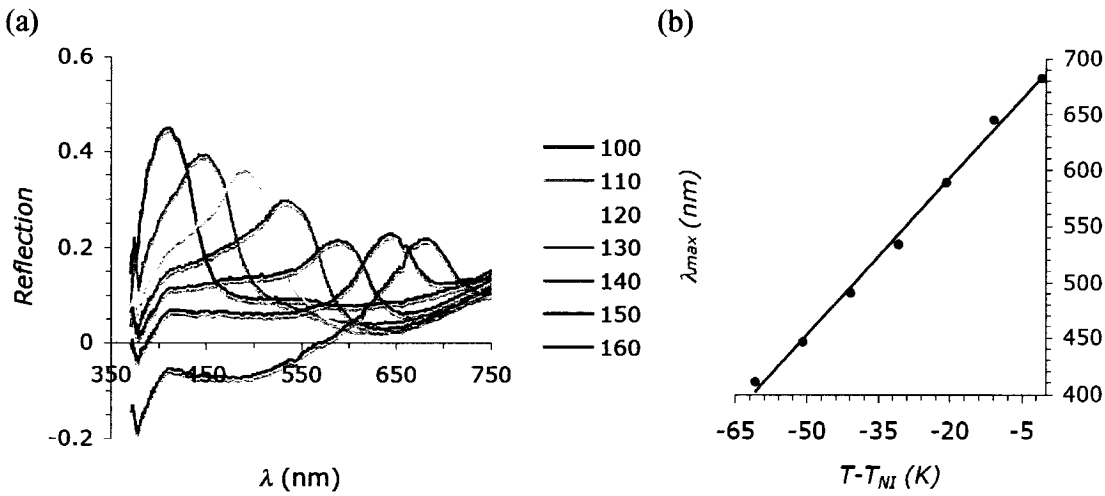

(a) **Figure 2-7.** Reflection spectrum of (*R*)-**2.16d** at temperatures ranging from 100–160°C. (b) **Figure 2-8.** Plot of the pitch of (*R*)-**2.16d** vs. reduced temperature. Solid line indicates least squares best fit.

$T-T_{NI}$ (K)	λ_{max} (nm)
-61	411
-51	447
-41	491
-31	534
-21	589
-11	645
-1	682

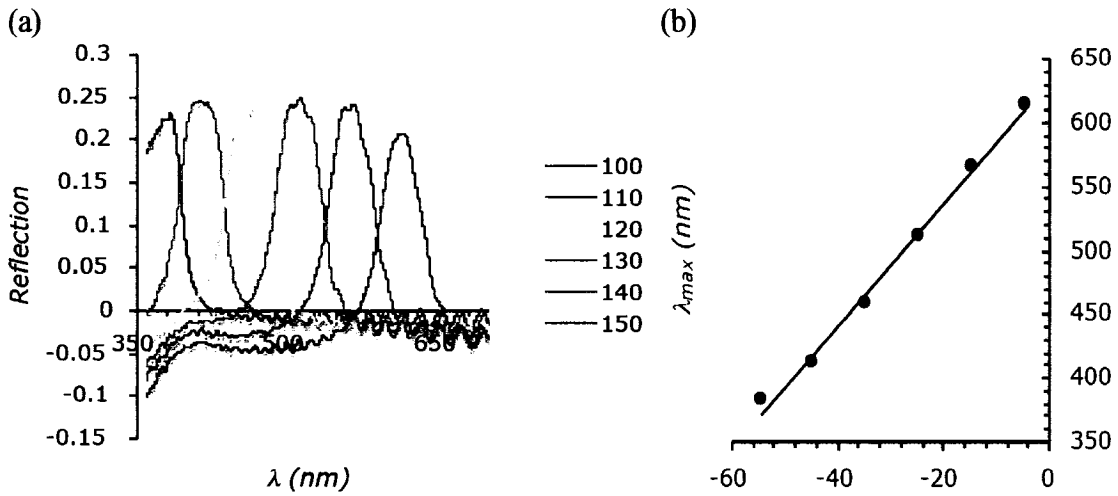

Figure D1-4. (a) Reflection spectrum of (*R*)-**2.16e** at temperatures ranging from 100–150 °C. (b) Plot of the pitch of (*R*)-**2.16e** vs. reduced temperature. Solid line indicates least squares best fit.

$T-T_{NI}$ (K)	λ_{max} (nm)
-55	383
-45	413
-35	459
-25	512
-15	566
-5	614

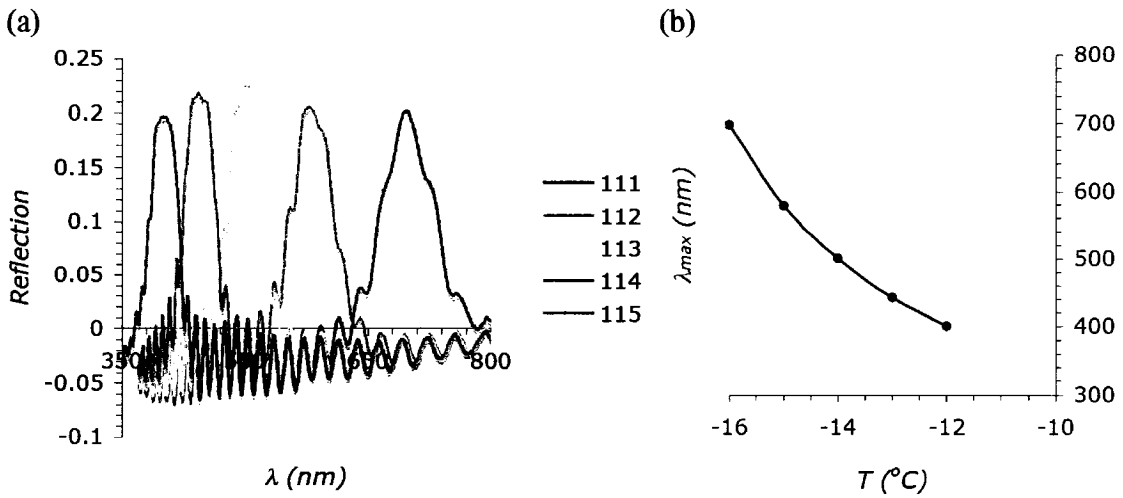

Figure D1-5. (a) Reflection spectrum of (*R*)-**3.8** at temperatures ranging from 111–115 °C. (b) Plot of the pitch of (*R*)-**2.16c** vs. reduced temperature. Solid line indicates least squares best fit.

$T-T_{NI}$ (K)	λ_{max} (nm)
-16	697
-15	578
-14	502
-13	443
-12	401